Proton arc therapy: an assessment of dosimetric potential and investigation of novel strategies towards deliverable treatments

A thesis submitted to The University of Manchester for the degree of Doctor of Philosophy

in the Faculty of Biology, Medicine and Health

YEAR OF SUBMISSION: 2022

YUNZHOU XIA

SCHOOL OF HEALTH SCIENCES, DIVISION OF CANCER SCIENCE

I. List of Contents

Final word count: 46357

II. Other lists

0D	0 dimensional
1D	1 dimensional
2D	2 dimensional
3D	3 dimensional
3DCRT	3D conformal radiotherapy
AMRT	arc modulated radiotherapy
BEV	beam's eye view
BFGS	A computational optimisation algorithm: Broyden-Fletcher-Goldfarb-Shanno
CI	conformality index
CT	computed tomography
CTV	clinical target volume
DNA	deoxyribonucleic Acid
DVH	dose volume histogram
ELEANOR-PAT	Energy Layer sElection bAsed oN cOveRage for Proton Arc Therapy
ELST	energy layer switching time
FPAT	full-energy proton arc therapy
gEUD	generalised equivalent uniform dose
GTV	gross tumour volume
H&N	head and neck
HI	homogeneity index

HU	Hounsfield Unit
ICRU	International Committee for Radiological Units
IDD	integrated depth-dose
IEC	International Electrotechnical Commission
IMAT	intensity modulated arc therapy
IMPT	intensity modulated proton therapy
IMRT	intensity modulated radiotherapy
IPOPT	Interior Point OPTimiser
L-BFGS	limited-memory Broyden-Fletcher-Goldfarb-Shanno
LET	linear energy transfer
MC	Monte Carlo
MFO	multiple field optimisation
MLC	multi-leaf collimator
MRI	magnetic resonance imaging
MU	monitor unit
NTCP	normal tissue complication probability
NTO	normal tissue objective
OAR	organ at risk
PAT	proton arc therapy
PBT	proton beam therapy
PMAT	proton monoenergetic arc therapy* * Bertolet, A, and A Carabe. “Proton monoenergetic arc therapy (PMAT) to enhance LETd within the target.” Physics in medicine

	and biology vol. 65,16 165006. 19 Aug. 2020, doi:10.1088/1361-6560/ab9455
PSPT	passively scattered proton therapy
PTV	planning target volume
QA	quality assurance
QC	quality check
RAM	random-access memory
RBE	relative biological effect
ROI	region of interest
RTOG	Radiation Therapy Oncology Group
SFO	single field optimisation
SOBP	spread out Bragg peak
SPArc	spot-scanning proton arc therapy * * Ding, Xuanfeng et al. “Spot-Scanning Proton Arc (SPArc) Therapy: The First Robust and Delivery-Efficient Spot-Scanning Proton Arc Therapy.” International journal of radiation oncology, biology, physics vol. 96,5 (2016): 1107-1116. doi:10.1016/j.ijrobp.2016.08.049
TPS	treatment planning software
VMAT	volumetric arc therapy
VOI	volume of interest

III. Abstract

The development of proton therapy is fundamentally about exploiting the property of protons to deliver improved dose distributions to patients compared to conventional radiotherapy. Following the widespread implementation of scanned beam proton therapy, Proton Arc Therapy (PAT) has the capability to further improve proton therapy by overcoming some of the limitations currently associated with proton therapy, which is typically delivered with a small number of beams (less than five). PAT has the potential to become the next-generation proton therapy technology due to its ability of improving the target dose conformality and organs-at-risk (OAR) sparing compared to the current technology, intensity-modulated proton therapy (IMPT). At the time of starting this work in 2017, there were only six papers reporting PAT. Most of the studies were retrospective plan comparisons which reported the improved dosimetric characteristics of PAT compared to IMPT, while only two studies reported the potential ways of delivering PAT, i.e., spot-scanning proton arc therapy or SPArc, and proton mono-energetic arc therapy or PMAT. However, at the time of starting this work, the research on PAT was still early stage (not applied clinically) and needed further evidence of PAT's advantages. The aim of this thesis was to gain fundamental understandings of PAT's dosimetric potential and to investigate ways to achieve practical deliveries in order to be closer to realising clinical PAT delivery.

The work described in this thesis is split into three chapters following an introductory Chapter 1. Chapter 2 compared PAT and IMPT plans for one representative brain and two head and neck cases in order to gain understandings of the dosimetric differences between PAT and IMPT and the intrinsic robustness characteristics of PAT. Chapter 3 described a novel energy selection strategy, ELEANOR-PAT (energy layer selection based on coverage for PAT), which aimed to shorten the theoretical delivery time by strategically selecting energy layers compared to the full-energy PAT (FPAT). The ELEANOR-PAT plans were validated for eight ependymoma cases and assessed against clinical dose criteria. Other energy reduction strategies explored prior to the formation of ELEANOR-PAT were described as a separate section in section 3.2 before the main work on ELEANOR-PAT starting in section 3.3. Chapter 4 explored ways to make the ELEANOR-PAT plans from chapter 3 deliverable, by interpolating the selected energies to one per finer beam angle. An emulator was made to predict the

delivered beam angle for each spot under the assumption of continuous gantry rotation. The interpolated ELEANOR-PAT plans were then compared to their emulated dose distributions to quantify any dose differences between the fixed-angle plan and continuous “delivery”.

FPAT plans were found to improve the physical dose distributions under nominal scenarios, but when the dose distributions were evaluated under uncertainty scenarios the robustness was found to be dependent on individual cases. ELEANOR-PAT was shown to be a reliable energy reduction strategy for the eight ependymoma cases. ELEANOR-PAT not only preserved or improved the dose qualities from the IMPT plans but also reduced the total number of energy layers by 25 - 84% (compared to FPAT) which translated into theoretical delivery times of under three minutes for all eight cases. The interpolated ELEANOR-PAT plans under the continuous gantry rotation assumption agreed well in terms of calculated dose to the fixed-angle plans for all eight cases, as assessed using gamma analyses. Results from Chapter 3 and 4 show that ELEANOR-PAT is a reliable strategy for planning and delivering PAT.

In this thesis, the potential dosimetric and delivery time benefits of PAT have been demonstrated for brain (ependymoma) cases. A novel strategy for practical PAT delivery has also demonstrated dosimetric advantages and generalisability to different ependymoma geometries. Therefore, PAT and ELEANOR-PAT should be developed further to realise clinical PAT delivery.

IV. Declaration

No portion of the work referred to in the thesis has been submitted in support of an application for another degree or qualification of this or any other university or other institute of learning.

V. Copyright statement

VI. Acknowledgement

First and foremost, I have to thank my research supervisors, Dr Michael Merchant, Prof Robert Appleby, Dr Adam Aitkenhead, and Prof Ranald MacKay. Without their assistance and dedicated involvement in every step throughout the process, this thesis would have never been accomplished. I would like to thank you very much for your support and understanding over these past four years.

Secondly, I would like to thank every member in my research group, the Precise research group, and at the Christie NHS Foundation Trust, for their support throughout my study. I would also like to thank the University of Manchester and Cancer Research UK for sponsorship towards my PhD program.

Finally, and most importantly, I must thank my family. Thank you for understanding that my study has been a tough and lonely journey and for your continuous love and encouragement, especially during the time of COVID19. This thesis stands as a testament to your unconditional love and support.

VII. The Author

I started this PhD work in autumn 2017, after receiving MSc in Physics from Imperial College London in the same year.

The work within this thesis has not yet been published in a peer-reviewed journal. I intend to submit Chapters 3 and 4 for review following the submission of the thesis. The work described in Chapter 2 has been presented at Medical Physics and Engineering Conference (MPEC) in 2019 and Particle Therapy Co-operative Group conference in 2019.

Chapter 1. Introduction and literature review

Proton therapy is a type of radiotherapy that uses high energy proton beams for treating cancer. Proton therapy brings many advantages over conventional megavoltage X-ray radiotherapy which include better target coverage and organs at risk (OAR) sparing due to protons' unique depth-dose characteristics, i.e., the Bragg peak. Currently, proton therapy is delivered with fixed beam angles with a number that ranges from 2 to 5 depending on the geometry and complexity of the tumour. If the number of beam angles increases and the angular spacing between the beams becomes so small that proton therapy eventually becomes delivered with continuous beam angles, i.e., in the form of proton arc therapy (PAT), it has the potential to further improve the dose distribution compared to the current proton therapy practice as well as to enable a single treatment session completed in a shorter time frame. These assumptions are learned from the development of conventional radiotherapy – photon arc therapy, i.e., volumetric arc therapy (VMAT) brings advantages over intensity modulated radiotherapy (IMRT) in terms of the dose distribution and treatment efficiency.

PAT has the potential to become the next revolution in proton therapy technology. The potential advantages of PAT also stretch to higher therapeutic ratio, improved robustness to treatment uncertainties, and efficiency in patient throughput. This thesis examines the dose characteristics of PAT and investigates its delivery practicality in a theoretical manner. This introductory chapter will introduce the motivation of PAT and reviews its status at the time of writing this thesis. The introduction firstly gives an overview on the development of conventional radiotherapy and proton therapy in section 1.1, which leads to the motivation of studying PAT. These are followed by two sections on general proton therapy treatment planning techniques and hardware status in sections 1.2 and 1.3, which are important aspects for considerations of PAT development. The links to PAT are throughout the introduction chapter.

1.1 The need for radiotherapy

Today, radiotherapy is a widely used cancer treatment for its high level of precision at targeting the tumour. About 40% of all cancer patients receive some form of radiotherapy throughout their treatment [1]. The aim of radiotherapy is to direct as much radiation as possible inside the tumour and to minimise the radiation outside. Radiotherapy can be broadly classified into conventional radiotherapy (treated with X-rays) and ion radiotherapy.

1.1.1 A brief history of conventional radiotherapy

Conventional radiotherapy has developed a long history since the first discovery of X-rays (photons) by Rőntgen in 1895 [2]. Not long after the discovery, doctors began to treat cancer patients by direct irradiation with X-rays. The first X-ray treatment took place in 1899 [3], but it was soon realised that X-rays caused severe skin reactions, i.e., X-rays not only damage cancerous tissue but also the healthy tissue.

The realisation of X-ray's damaging effect of both cancerous and healthy tissue raised the importance of healthy tissue protection and led to 2-dimensional (2D) radiotherapy in the 1950s. 2D radiotherapy was delivered with fixed-angle radiation fields whose boundaries were defined on a pair of orthogonal X-ray images. The X-ray images were used to capture the extent of the tumour in two orthogonal directions. Since there was no beam shaping at the time, the shapes of the radiation fields were either square or rectangular, which were just large enough to cover the tumour's width and height profiles seen from beam's eye view (BEV) in the two orthogonal directions. However, tumour shapes are unlikely to be perfectly uniform, so a large portion of adjacent healthy tissue or OAR still received ionising radiation, which resulted in severe radiotherapy side effects. Besides, the amount of radiation delivered to the target could be inadequate due to the poor accuracy of dose calculation by hand [4]. For these reasons, 2D radiotherapy is a less effective treatment compared to those that followed.

In pursuit of higher dose conformality, beam shaping devices including wedges, blocks, collimators, and boluses were used to conform the radiation field at the distal edges and the lateral sides. As technology progressed in the 1990s, supported by advanced imaging techniques such as Computed Tomography (CT) and magnetic resonance imaging (MRI), the exact 3D profile of the tumour could be visualised on a computer. Together with the use of beam shaping devices and computerised calculation of the planned dose distribution, it was possible to achieve 3D conformal radiotherapy (3DCRT) [5]. In addition, the invention of rotating gantries allowed 3DCRT to be delivered from a range of beam angle choices. As a result, 3DCRT greatly improved the therapeutic outcome compared to the former 2D rectangular radiotherapy [6] [7].

In the 2000s, advanced computational techniques made inverse dose optimisation possible. Inverse dose optimisation is where the fluence of the radiation field delivered from each beam angle is inversely optimised by computer programs [8] to achieve the treatment goals of radiotherapy. This means that treatment planners set the beam angles and how much dose to put where, and the computer will work out how to achieve these goals, e.g., the intensity level of the radiation field from each beam angle. Inverse dose optimisation is a much easier procedure for treatment planners compared to forward treatment planning.

Inverse dose optimisation enabled intensity modulated radiotherapy (IMRT), where multi leaf collimators (MLC) are used to shape the radiation fields precisely in the lateral directions. Inverse dose optimisation and the use of MLCs reduced the average irradiated volumes and increased the overall survival, depending on the cancer site [9] - [11]. Nowadays, IMRT represents the standard of care of conventional radiotherapy and is widely adopted at radiotherapy treatment centres.

From the mid-1990s to the 2010s, in pursuit of even better dose conformality, much attention was paid to the arc therapy form of conventional radiotherapy. A variety of implementations appeared in the literature and can be broadly classified into arc therapy and helical therapy (Tomotherapy [12]). Implementations of arc therapy included intensity modulated arc therapy published in 1995 (IMAT [13]),

Volumetric Arc Therapy in 2007 (VMAT [14]), and arc modulated radiotherapy in 2008 (AMRT [15]). Eventually VMAT became the chosen practice of conventional (photon) arc therapy.

VMAT allows simultaneous modulations of three parameters during treatment delivery: the gantry rotation speed, the dose rate, and the shaping of MLCs. Intensity modulation is achieved by modulating the rotation speed of the gantry and the dose rate. As the gantry rotates, the MLCs continuously reshape such that the total dose delivered from all beam angles conforms to the target. A VMAT treatment typically takes one or two revolutions of the gantry which can be completed under two minutes. By delivering from a large number of continuous beam angles which are planned with closely spaced discrete control points, VMAT reduces the entrance dose and may also reduce the integral dose on a case-dependent basis compared to IMRT [16] [17]. Compared to IMRT, VMAT not only improved the dose distribution [18] [19] but also the treatment efficiency [17][19]. Moreover, IMRT hardware systems do not need to be entirely replaced to support VMAT, which is an economic solution for developed radiotherapy centres to have access to VMAT as a treatment option. This conveniency can also be applied for PAT delivery, i.e., PAT should be developed in a way that its delivery would not require a complete hardware replacement of the current proton therapy delivery system. This restriction was considered when investigating the PAT delivery strategies in Chapter 3 of the thesis.

1.1.2 A brief history of proton therapy

Protons were firstly proposed for their therapeutic applications by Wilson in 1946 [20], which was almost half a century later than the first X-ray cancer treatment. In his original paper entitled ‘The Radiological Use of Protons’, Wilson described the characteristics of high energy proton beams as nearly straight trajectories and that these high energy proton beams deposit most of their energy in a well-defined Bragg peak region at the end of an energy-dependent range (figure 1-1).

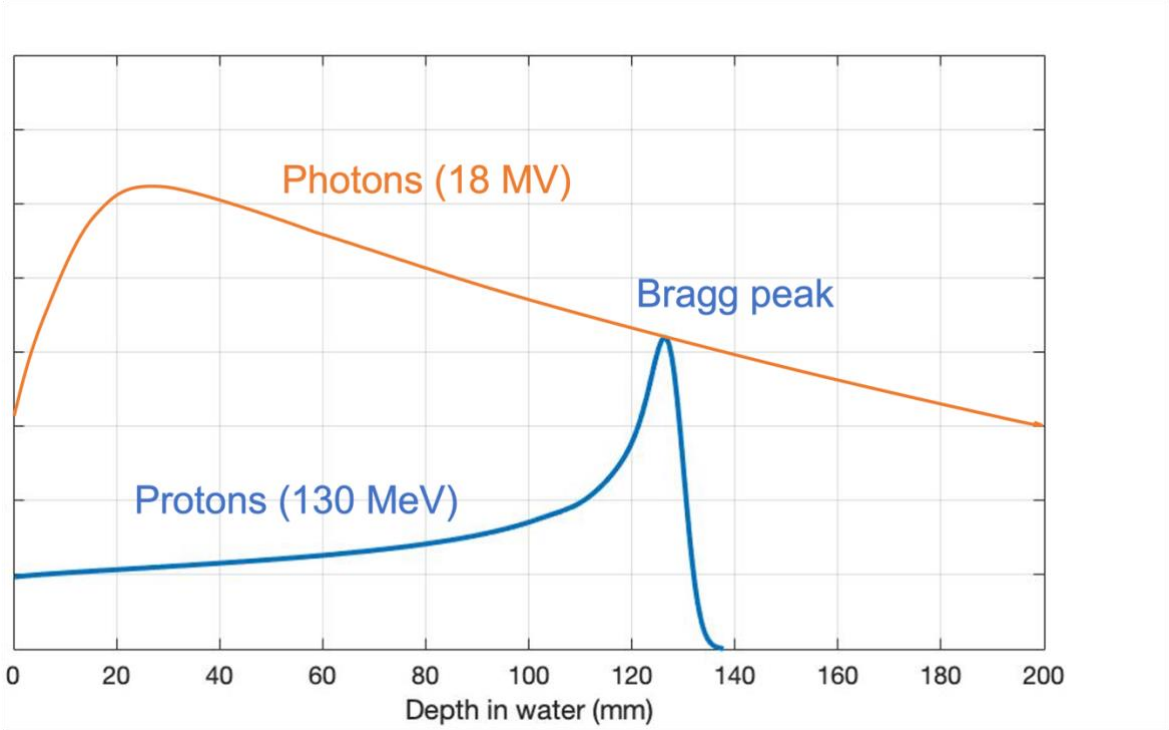

Figure 1-1: Illustration of depth-dose curves of photons and protons shows that protons leave no exit dose which is a fundamental advantage to proton therapy's superior dose conformality and tissue sparing abilities.

The unique depth-dose characteristic of high energy protons brings a few important advantages for cancer treatment:

1. The position of the Bragg peak can be placed precisely within the tumour via means of energy modulation.
2. Proton beams leave no exit dose, i.e., healthy tissue in deeper locations is well protected from radiation.
3. Protons require less integral dose (the total energy received by the patient) to treat the tumour than photons for the same level of prescription dose, i.e., less integral dose is related to less side effects.

On the other hand, protons also bring a few disadvantages. Although a single proton Bragg peak seems to deposit less dose at the entrance than photons (figure 1-1), there usually needs multiple proton energies to cover the tumour with uniform dose (spread-out Bragg peak as shown in figure1-2). Considering the build-up effect of photons up to about 2 centimetres deep in water, the overall entrance dose is not necessarily lower with protons. In addition, protons require

more energy to accelerate as they are about 1800 times more massive than electrons, and due to demand in radiation protection and specialised staff, proton therapy is generally more expensive than conventional radiotherapy in terms of initial investment and operational cost for proton therapy centres as well as treatment cost for patients. Robustness is another concern for proton therapy (explained in more detail in section 1.2) because of the sharp distal fall-off of the Bragg peak, so any treatment uncertainties must be taken extra care when planning a proton therapy treatment.

Following the footsteps of conventional radiotherapy, the first proton beam therapy (PBT) treatment was carried out in 1958 and was already equipped with aperture shaping devices to achieve conformality and tissue sparing [21]. In early-day PBT treatment, the narrow proton beam is scattered into a broad radiation field which is shaped by aperture devices, just like conventional radiotherapy. The technique of delivering PBT with a scattered proton radiation field is called passively scattered proton therapy (PSPT).

Learning from the success of IMRT, the intensity modulation technique was applied to proton therapy which realised intensity modulated proton therapy (IMPT) in the late 2000s [22]. IMPT delivers the proton beam by individual proton spots and switches the beam energy corresponding to the radiologically equivalent depths of the tumour to achieve precise target coverage in 3 dimensions (3D). Intensity modulation in IMPT is achieved by varying the irradiation time at each spot location. Like IMRT, IMPT can be delivered from a variety of beam angles with the use of a rotating gantry or couch. Since IMPT is delivered with individual proton spots, its delivery requires the modern scanned delivery system where the proton beam is directed towards the patient by a pair of orthogonal scanning magnets. IMPT is the most advanced form of proton therapy nowadays and offers superior dose distributions compared to PSPT [23].

1.1.3 Proton arc therapy (PAT)

The histories of conventional radiotherapy and proton therapy share commonalities. Intensity modulation was a revolutionary technique common to

both IMRT and IMPT to achieve superior dose conformality compared to their previous treatment modalities, i.e., 3DCRT and PSPT, respectively. Owing to its longer history, conventional radiotherapy continued to develop into the arc therapy form, i.e., VMAT, which not only offers dosimetric advantages but also faster treatments. It is then natural to proceed to the central question of this thesis - whether proton arc therapy (PAT) will further improve dose conformality compared to IMPT, and whether PAT can bring similar advantages like VMAT, e.g., faster treatment and lower integral dose.

Before the start of this work, there were only 6 published papers on PAT. The first paper was published in 1997 and was the first appearance of the concept of PAT [24]. The paper showed that by irradiating a rotating Rando phantom with PSPT in a continuous arc from a fixed beam line, the volume of irradiated lung was reduced at all dose levels compared to electron arc therapy. Electron arc therapy was used in [24] as the subject of comparison as it was the preferred treatment modality over photons to treat breast cancers at the time [24]. Six years later, a treatment planning study for a lung case compared four treatment modalities, i.e., PSPT, PAT in both PSPT and IMPT techniques, and VMAT [25], and showed that PAT led to 30% reduction in the 95% isodose line volume compared to PSPT, and that PAT planned with the IMPT mode spared the chest wall and ipsilateral lung better than the other three modalities [25]. This first treatment planning study was followed by another paper in 2016 which showed that PAT (planned with the PSPT technique) gave better PTV coverage and lower NTCP than PSPT and IMRT [26]. In the same year, two studies on PAT delivery techniques were published which aimed to achieve PAT's deliverability. These were proton modulated arc therapy (PMAT) [27] and spot scanning proton arc therapy (SPArc) [28] which will be discussed in more detail in section 1.3.

At the time of writing this thesis, a total of 10 more papers were published, with 9 papers being the follow-on papers from the SPArc paper [29] - [36], and 1 paper being the follow-on paper for the PMAT study [37]. The work described in this thesis contributes to a third delivery technique of PAT which shows the improved dose distributions compared to IMPT as well as theoretically faster treatments, assuming continuous gantry rotation.

Currently PAT is still at an early stage of development and is not in clinical use, but preliminary treatment planning studies show great promises for its dosimetric advantages [25] – [37]. However, from the practicality aspect, the arc therapy techniques from VMAT cannot be directly applied to transform IMPT into PAT because VMAT relies on the optimisation of dose fluence through the use of MLCs (a field shaping technique). In contrast, IMPT relies on energy modulation and intensity modulation of individual proton spots, delivered by scanning the beam rather than by shaping a broad field using an MLC. This difference makes the development of PAT practically more challenging.

Section 1.2 of this introductory chapter introduces in detail proton therapy's dose characteristics, treatment modalities and delivery techniques. Section 1.3 then discusses proton therapy's limitations which lead to a detailed description of the state-of-the-art research on PAT in section 1.4. Finally, section 1.5 gives an overall summary of the chapter and describes the research aims of the thesis. Since the work of the thesis relies largely on treatment planning techniques and proton therapy hardware, technical summaries of these topics are covered in sections 1.6 and 1.7 which can be used as background information throughout the entire thesis.

1.2. Proton therapy

1.2.1. Characteristics of proton therapy

1.2.1.1. Physics

As proton beams travel through a medium, they primarily interact with the outer-shell electrons of the atoms in the medium via Coulomb interactions. As a result, the protons continuously lose kinetic energy as they travel further into the medium. As the protons slow down, the interaction cross section increases, so the protons deposit larger amounts of kinetic energy as they travel deeper into the medium.

Eventually, protons deposit a large amount of energy over a narrow range called the Bragg peak and negligible energy beyond it.

The depth of the Bragg peak is energy-dependent, so by means of beam energy modulation (range modulating wheel in PSPT, or the accelerator / energy degrader in scanning / PSPT mode of IMPT delivered with a synchrotron / cyclotron), Bragg peaks can be precisely located within the tumour. Typical therapeutic proton beam energy ranges from 70 MeV (mega electron volts) to 250 MeV, which correspond to water-equivalent depths of 4 centimetres to 30 centimetres. If the target is shallower than 4 centimetres, a range shifter, i.e., a slab of material placed downstream of the treatment head and close to the patient surface to reduce the overall Bragg peak depth, is used.

Delivering proton beams of different energies with suitable intensities, the individual pristine proton beams add up to a flat dose distribution, called the spread-out Bragg peak (SOBP) as illustrated in figure 1-2. The SOBP covers the tumour region precisely in the depth (longitudinal) direction.

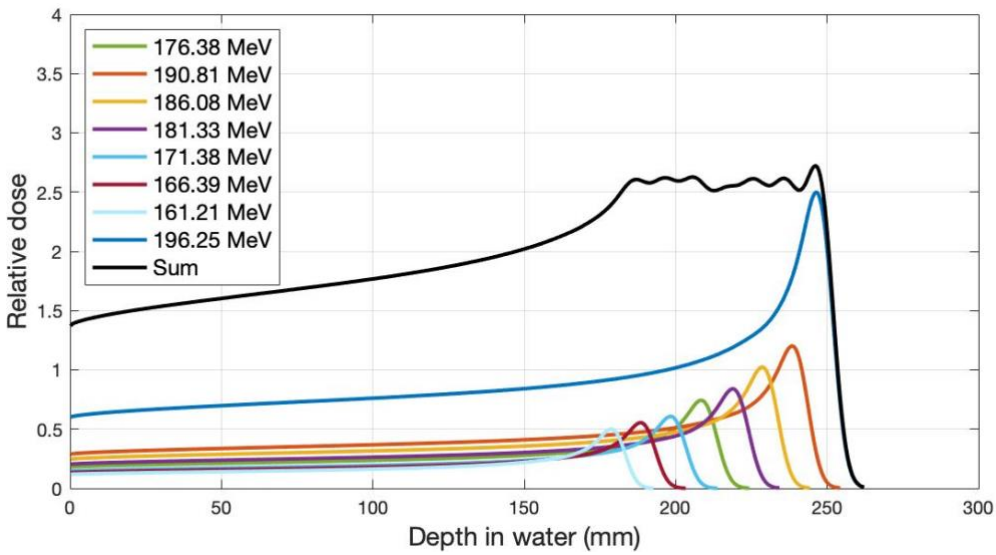

Figure 1-2: Illustration of suitably weighted pristine Bragg peaks sum up to a flat spread-out Bragg peak (SOBP) within the tumour region. Zero dose beyond SOBP and low level of entrance dose give proton therapy its superior dose conformality.

Although the Bragg peaks are advantageous in terms of dose conformality, they have their disadvantageous side. The sharp dose fall-off gradient at the end of the beam range means that if the densities of the medium that the beam travels

through are different to the densities used in a treatment plan, the Bragg peaks will stop in different locations to the treatment plan. This happens when there are treatment uncertainties, e.g., beam range uncertainties and patient set up uncertainties. For example, the beam will overshoot if the overall density becomes lower or undershoot if the overall density becomes higher than planned. As a result, the Bragg peak will stop in a deeper or shallower depth than intended. The resultant shift in SOBP location as illustrated in figure 1-3 is likely to damage the adjacent healthy tissue and OAR and can cause radiation side effects.

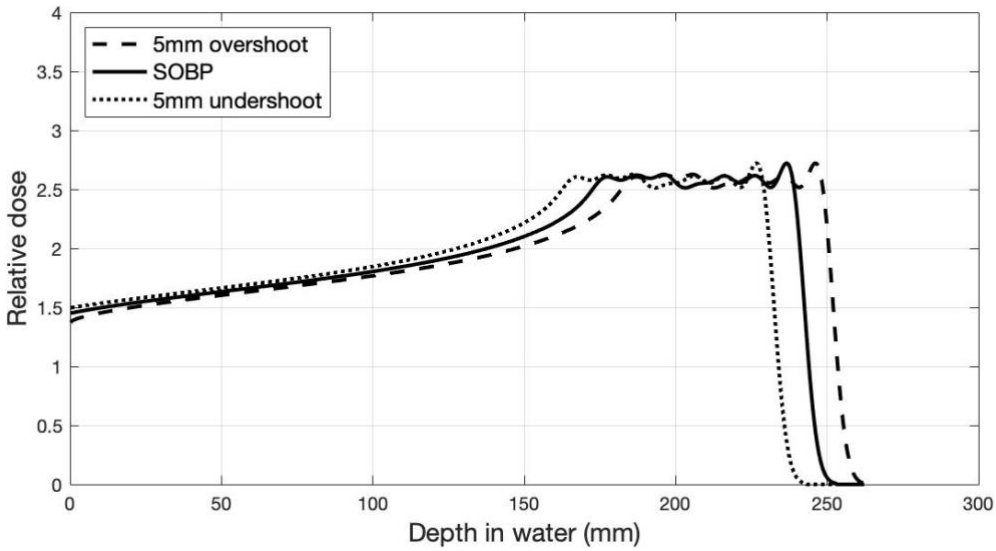

Figure 1-3: Illustration of the shift of SOBP resulting in high dose in healthy tissue and inadequate target coverage due to perturbations in healthy tissue density which can arise due to treatment uncertainties.

The sharp dose fall-off at the distal edge of the Bragg peaks makes proton therapy intrinsically susceptible to treatment uncertainties, i.e., proton therapy is less robust to treatment uncertainties compared to conventional radiotherapy. Robustness is an important topic in proton therapy and can be strengthened via various planning techniques as described in section 1.6. Examples of these planning techniques include delivering the dose to a planning target volume (PTV) which takes into account of the potential treatment uncertainties, and robust optimisation which considers uncertainty scenarios during dose optimisation. However, the improvement of robustness using these techniques increases the total volume irradiated, which is a compromise for the surrounding healthy tissue.

In the case of treatment uncertainties, the delivered Bragg peak locations are different to the planned Bragg peak locations, and so the overall dose distribution will be different to the planned dose distribution. With beams delivered from many more beam angles, the average dose delivered from every beam angle is expected to be lower in PAT than IMPT. The lower dose levels are expected to have less effect on the overall dose differences, and so will improve the robustness compared to IMPT. Prior to the start of this work, there were no publications which compared PAT's intrinsic robustness to IMPT, so it was studied in Chapter 2 of the thesis.

1.2.1.2. Radiobiology

Relative biological effectiveness (RBE) represents the ratio of the doses of two types of ionising radiation that lead to the same biological effect. For example, the RBE of protons relative to photons (X-rays) is given by equation 1-1:

Equation 1-1: Definition of relative biological effectiveness (RBE).

$$RBE = \frac{D_{ref}}{D_R}$$

where D_{ref} is the reference absorbed dose of a standard type of particle (e.g., X-rays), and D_R is the absorbed dose of radiation of type *R* that causes the same amount of biological damage.

The RBE for protons is higher than that of photons due to protons' greater ability at generating lethal DNA damages than photons. Clinically an RBE value of 1.1 is generally used for proton treatment planning as reported ICRU (the International Commission on Radiation Units and Measurements) report 78, which means that protons are 10% more effective biologically than photons.

As protons deposit more energy as they slow down (approach the end of range), the energy deposited per unit track length increases. This means that at the end of the beam range, protons cause more clustered damages to the cell DNA. Most in vitro studies show that the RBE increases rapidly at the distal end of the Bragg

peak to values beyond the clinical use of 1.1. This means that radiation is more damaging at the distal regions considering the potential biological effects. However, the exact values of RBE depend on many factors and are largely derived from cell experiments, so there exist uncertainties in the exact values of RBE [38]. An RBE value of 1.1 is chosen to be a cautious choice which mitigates the risk of under-dosing the target, but this has a corresponding increased risk for normal tissue.

There exists a variety of RBE models to describe the RBE distribution [38] - [40]. Common to all RBE models is the linear energy transfer (LET), which is defined as the average energy deposited per unit track length along the track of ionising particles with the unit being keV/µm (kilo electron volt per micrometre). The LET therefore increases at the end of the proton beam range (figure 1-4). Since the LET quantifies the density of energy deposition of a particular particle type, it largely determines the biological effect.

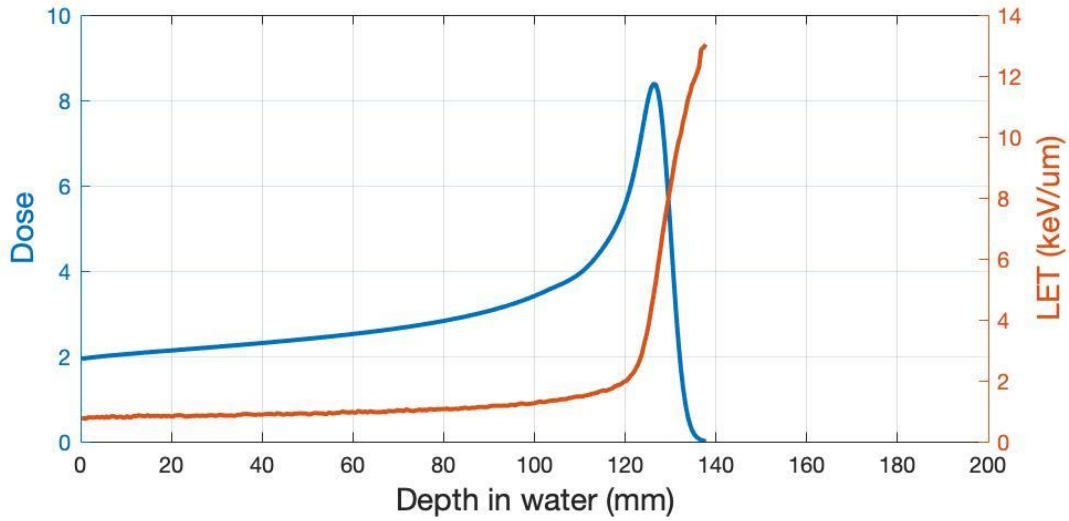

Figure 1-4: Monte Carlo simulated linear energy transfer (LET) of a 130 MeV proton beam in water plotted with its depth-dose curve as a reference for the relative location of high LET at the end of proton beam range, simulated in AutoMC as courtesy of Dr Adam Aitkenhead [41].

Most in-vitro studies report correlations between RBE and LET, so there have been attempts to incorporate LET into proton therapy dose optimisation to reduce the high LET values in healthy tissue [39]. Published approaches include LET-incorporated dose optimisation [42], LET-guided dose optimisation [43] and track-end objectives [44]. Although LET-incorporated dose optimisation offers similar

target coverage, it tends to raise OAR doses as a compromise of migrating the high LET regions. Whether the sacrifice in physical dose is justifiable needs more clinical evidence. For this reason, LET-incorporated dose optimisation is currently not in routine clinical use for proton therapy.

The sacrifice in physical dose could be due to the limited number of beam angles used in IMPT. With potentially many more proton beamlets involved, PAT would allow more flexibility for LET migration, i.e., easier for the optimiser to converge to a treatment plan satisfying both physical and biological dose requirements. LET-incorporated PAT optimisation has been studied in a feasibility study recently which showed PAT's potential of successful LET migration [45]. Despite it being a physical property, the calculation of LET is a complex process. Due to the limited time scope, LET is not considered in the context of this work.

1.3.1. Delivery techniques

Proton therapy can be delivered with two types of techniques, passively scattered proton therapy (PSPT) and intensity modulated proton therapy (IMPT) delivered with the scanned proton therapy system.

1.3.1.1. Passively scattered proton therapy (PSPT)

PSPT involves firstly broadening the proton beam into a radiation field that is large enough to cover the tumour's lateral profile and then shaping the beam with beam modifying devices to achieve dose conformality in lateral and longitudinal directions. A typical PSPT system is illustrated in figure 1-5. The proton beam is directed towards a range modulator wheel, which is a device designed to have varying thickness upon rotation. When the beam passes through sections of different thicknesses, the beam range (or energy) is modulated to form a SOBP which covers the tumour in the longitudinal direction. The scattering system scatters the narrow proton beam into a broad radiation field that is large enough to cover the tumour in the lateral directions. The collimator and compensator, both custom made for each patient and each beam angle, shape the radiation field

laterally and longitudinally, respectively, to conform to the tumour geometry. As a result, the lateral and distal edges of the dose distribution conform well to the tumour geometry. However, the entrance dose cannot be shaped with the PSPT system.

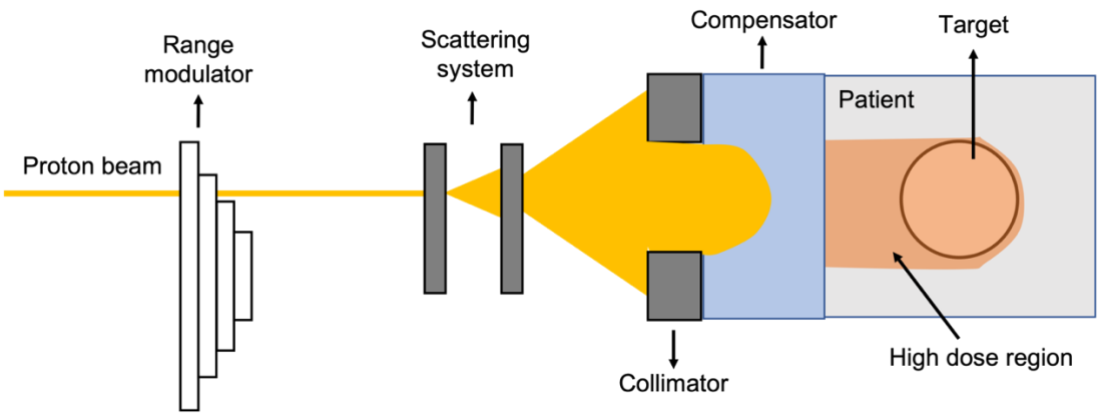

Figure 1-5: Illustration of typical arrangements of a passively scattered proton therapy (PSPT) delivery system. The proton beam's range gets 'pulled back' to form an SOBP by the range modulator wheel and gets scattered into a broad radiation field by the scattering system. The collimator and compensator, both custom made for each patient and each beam angle, shape the radiation field laterally and longitudinally to conform to the tumour geometry.

The advantage of PSPT is that the beam-on time is shorter because the range modulation wheel can rotate very fast (one revolution in one second). This is a major advantage in terms of delivery efficiency which is useful to be applied in PAT [46]. However, collimators and compensators are compulsory in PSPT and they require to be custom made. These would be impractical for continuous PAT delivery. Although there exists the alternative of using combinations of moving range shifters and dynamic MLCs for field shaping to replace fixed devices (3D layer stacking [47]), range shifters move more slowly, and 3D layer stacking introduces more neutron radiation than scanned proton therapy due to the amount of scattering happening at every beam modifying device. In addition, scanned PAT has been shown to improve the dose distribution compared to passively scattered PAT [25]. For these reasons, PSPT is not considered for PAT implementation in this work.

1.3.1.2. Scanned proton therapy

Modern proton therapy centres are equipped with scanned proton therapy equipment as it can achieve higher dose conformality and is simpler in terms of hardware design. Scanned delivery systems are required to deliver IMPT.

Scanned delivery systems deliver proton beams in iso-energy layers (figure 1-6). Starting from the highest energy, the proton beam is scanned towards different directions within the tumour and within one energy layer to deliver dose by proton spots. Once all the spots of the energy layer get delivered, the accelerator (synchrotron) modulates to a lower energy. If a cyclotron is used, an energy degrader at the exit of the cyclotron modulates the energy. The spot scanning process is repeated for every energy layer until all the planned energy layers are delivered.

The advantage of using the scanned modality is the extremely high dose conformality in 3D, which is realised by summing up the dose distribution of individual proton spots with optimised weights. Scanned proton therapy causes less secondary radiation as there are less beam modifying devices. However, the treatment time of scanned proton therapy, i.e., IMPT, is considerably longer than PSPT as the beam energy must be modulated at the accelerator end, which is on the order of seconds and is slower in comparison to PSPT which relies on the modulation wheel (section 1.7).

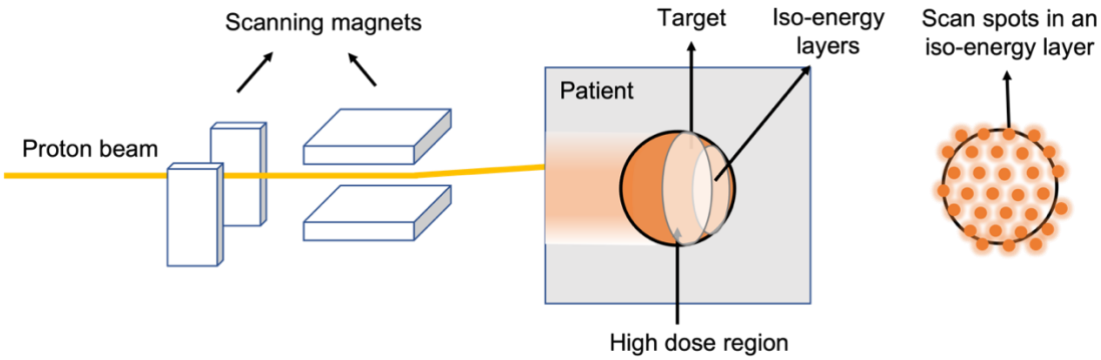

Figure 1-6: Illustration of actively scanned proton therapy delivery system for delivery of IMPT. The accelerated proton beam passes through a pair of scanning magnets which steer the beam into desired directions. The tumour is divided into iso-energy layers and individual spots. By delivering modulated dose to each spot, IMPT achieves superior conformality than PSPT.

1.3.1.3. Comparisons

Table 1-1 summarises the advantages and disadvantages of PSPT and the scanned delivery technique in general and for uses in the context of PAT. The scanned modality is considered to be the better choice for delivering PAT due to its superior dose conformality compared to PSPT. However, the limitation on the treatment delivery time caused by the accelerator becomes an important challenge to solve.

Table 1-1: Summary of the advantages and disadvantages of passively scattered systems and actively scanned delivery systems in general and for the use of PAT delivery.

	Advantages	Disadvantages
Passively scattered proton therapy (PSPT)	• Less susceptible to beam instabilities. • Less susceptible to moving tumours.	• Labour intensive: requires custom made collimators and compensators for each patient. • Low radiation conformality. • Secondary radiation caused by scattering in range shifters, compensators, and collimators etc. • Complex system involving many devices. • Difficult beam modelling within treatment planning system. • Labour intensive if a re-plan is required as new compensators will need to be manufactured.
Scanned proton therapy	• High radiation conformality. • Can realise intensity modulation. • Simple system without compensators.	• Longer treatment time. • Susceptible to moving tumours. • Relies upon beam stability. • More parameters to control. • Longer QA time.

PSPT for PAT	• Shorter beam on time • Easier dose optimisation	• Impractical • More secondary radiation
Scanned proton therapy for PAT	• Superior dose conformality	• Longer beam-on time but can be potentially reduced by strategically removing redundant energy layers.

1.3. Limitations of proton therapy

1.3.1 Treatment time

Currently an IMPT plan usually consists of between 2 and 5 beam angles which are delivered from fixed gantry positions. This leads to a typical treatment time between 15 and 20 minutes. The total treatment time can be longer if the beam switches between treatment rooms which happens at multi-room proton therapy centres where the treatment rooms share a single accelerator. Other factors that increase the treatment time includes the use of range shifters and patient positioning during the treatment. These additional factors can lengthen the treatment time to about 30 minutes or longer which is likely to induce setup uncertainties which proton therapy is sensitive to.

The concept of PAT is for the beam to be delivered with a continuously rotating gantry which is assumed to have a maximum rotation speed of 1 revolution per minute, based on existing technology at the time of investigation. If PAT can be delivered in one or two revolutions like VMAT, it is expected to largely reduce the treatment time and the likelihood of treatment uncertainties compared to IMPT. Chapter 3 and 4 of the thesis show that carefully chosen energy layers can be removed from PAT without hugely affecting the plan quality and that the reduced PAT can be theoretically delivered within about 3 minutes. The magnitude of reduced treatment time is significant compared to how long a typical IMPT treatment takes. The reduced PAT delivery time relies on the assumption that the

IMPT delivery system supports continuous irradiation while the gantry rotates. This could be retrofitted into existing machines without requiring new facilities.

1.3.2 Robustness

The sharp distal fall-off of the Bragg peaks makes IMPT prone to treatment uncertainties which can cause undesired dose changes and damage nearby healthy tissue and OARs. Various methods exist to mitigate the uncertainty effects in IMPT. These mitigation methods include careful choices of the beam angles (section 1.6.1.1), careful designs of the PTV margin (section 1.6.1.2) by considering possible uncertainty effects, and the use of robustness optimisation (section 1.6.3.3). However, the additional PTV margin and robustness optimisation only add to the total volume irradiated, which sometimes is undesirable.

When delivered from many more beam angles in PAT, the dose delivered from each beam angle is expected in general to be lower than that in IMPT. The overall dose deterioration due to treatment uncertainties can be thought of as being spread out over a larger range of beam angles. As a result, the robustness of PAT is expected to improve compared to IMPT. Chapter 2 of the thesis compares the robustness of PAT and IMPT by systematically evaluating the dose distributions under a variety of uncertainty scenarios for a range of tumour geometries.

1.3.3 Beam angles

During clinical treatment planning, sometimes plans planned with more beams offer better OAR sparing and the number of beams could be higher than that specified in the planning protocol. This often happens to cases where the tumour is surrounded by OARs with strict dose requirements. Proton therapy planned with more beams is expected to give better conformality than just 2-5 beams [25] and is investigated in this thesis.

Chapters 2, 3 and 4 of the thesis study PAT and IMPT plans in terms of the target dose conformality and OAR sparing. It is seen that more beams planned in PAT

brought dosimetric advantages including higher dose conformality and better OAR sparing.

1.4 Proton arc therapy (PAT)

1.4.1 Motivation

The limitations of IMPT can potentially be solved by PAT. The treatment time is likely to be significantly reduced with PAT, given that it can be delivered like VMAT in a single arc or two. By irradiating from many beam directions and in one or two arcs in one go, PAT reduces the need for range shifters, beam switching and beam-by-beam verification. PAT may be able to complete one treatment session within 1 – 2 minutes, just like VMAT. By irradiating from a large number of beam angles, PAT delivers a much lower dose from every angle. As a result, the dose deterioration is expected to reduce with PAT, i.e., better robustness. With more proton beamlets involved in dose optimisation, PAT is expected to solve more complex optimisation problems which not only apply to complex tumour geometries, but also the incorporation of LET.

However, PAT will deliver a lower dose to a larger volume, which is an intrinsic property of arc therapies in general. Reduction of low dose baths in IMPT compared to IMRT is predicted to have long-term benefits for paediatric brain patients [48], but the effects of low dose baths in PAT are unknown. Although normal tissue complication probability models could predict these effects, the models themselves require more evidence. Therefore, in this thesis, the effect of low dose baths is only investigated briefly using the integral dose of a PAT plan, which is a quantity related to the risk of secondary cancer [48].

From the practical aspect, proton therapy requires energy modulation which is realised by the accelerator in scanned proton therapy. Energy modulation requires time, and the time limitation must be solved to deliver practical PAT treatment.

1.4.2 Existing PAT strategies

When I began this work, there were very few attempts in making PAT deliverable. The two attempts that existed were spot scanning proton arc therapy or SPArc [28] - [36] and proton monoenergetic arc therapy or PMAT [27] [37] [46]. Both strategies took the approach of reducing the total number of energy layers to be delivered. The motivation is to make PAT practically deliverable, which is backed up by the fact that the large number of energy layers in PAT makes some energy layers redundant, or in other words the removal of some specific energy layers contributes to negligible deterioration in plan quality compared to FPAT. Besides, using all available energy layers from all beam angles would make PAT delivery extremely slow due to the cumulative delay in the multiple energy switching times. The reductions of the energy layers for SPArc and PMAT are carried out via in-house designed algorithm incorporated within the TPS.

Reducing the energy layers is also an economical approach because it does not require a complete hardware upgrade, i.e., PAT will be delivered with the same hardware system as IMPT, although changes must be made to support PAT delivery such as continuous gantry rotation while the beam is active.

1.4.2.1. Spot scanning proton arc therapy (SPArc)

The SPArc algorithm integrates energy layer reduction within the dose optimisation process. Initially, all energy layers from a number of coarsely spaced beam angles are optimised for dose. These energy layers are then distributed to adjacent finer beam angles and optimised again. During the distribution, energy layers with low weightings are removed. This iterative process of energy layer distribution, dose optimisation and energy layer removal is carried out until a desired plan is reached. Eventually, the number of energy layers per finest beam angle ranges between 1 and about 3, which is the direct outcome of the optimisation.

Later, the SPArc algorithm incorporated an energy switching sequence [33]. The motivation was that an energy increase usually takes longer than an energy decrease. The upgraded SPArc algorithm, referred to as SPArc_seq, resulted in a sawtooth shaped relationship when plotting the energy layer selected and the gantry angle position, with 1 or multiple energy layers per beam angle.

The SPArc algorithm has been shown to be clinically satisfactory for a few tumour sites [29] - [32] [34] - [36]. However, the SPArc algorithm is intrinsically time-consuming as it throws additional parameters and processes into the optimisation problem, along with dose optimisation. As reported, the time taken to optimise a lung and an oropharyngeal carcinoma case was 2 and 6 hours respectively on a typical RayStation workstation [28]. This scale of optimisation times might not be ideal as it does not allow iterative planning based on feedback from clinicians and so should be investigated for potential reductions. Another aspect is that SPArc's implementation requires modifications to existing dose optimisation modules within the TPS. Although the algorithm implementation is not a clinical problem, in general TPS should be designed with modular flexibility, so an energy layer preselection algorithm would be a better fit in terms of algorithm compatibility with existing TPS.

1.4.2.2. Proton mono-energetic arc therapy (PMAT)

The PMAT algorithm is based on energy layer selection prior to dose optimisation. PMAT selects a single energy layer corresponding to the middle of the water equivalent thickness of the target seen from every beam angle. As PMAT is a preselection algorithm, the optimisation time it takes is considerably shorter than SPArc. The motivation of PMAT is to place high LET regions within the target, which has been shown successful for cylindrical phantoms [27] [37]. However, whether PMAT applies to general tumour geometries and whether the LET can be migrated in general geometries remain questions to be investigated.

1.4.3 Challenges

A major challenge of PAT development remains to be the energy reduction strategies that solve the practical issues of PAT delivery. This challenge was similarly faced by photon arc therapy in the era where multiple potential strategies were proposed. The two existing PAT strategies both showed their strengths and weaknesses. SPArc completely relies on the computer to work out the maths problem of which energy layers would reduce the value of the objective function. This resulted in long optimisation times. In contrast, PMAT is fast to optimise but its generalisability to tumour geometries is not yet reported.

PAT with full energies should be examined carefully to understand how the increased number of beam angles affects the plan quality. It also represents the most general PAT solution as it is inclusive of any energy-reduced PAT solutions. As energy-reduced PAT has fewer proton spots than full-energy PAT, it is expected to degrade the plan quality in terms of higher (worse) objective function values, although the amount of degradation might not be clinically relevant. This compromise emphasises the importance of strategically reducing the energies in PAT.

Currently PAT is planned with fixed control points but delivered with a continuously rotating gantry, so the actual delivered position of a spot may differ to its planned position. As protons are sensitive to density heterogeneities, a small angular difference to delivery might cause an unacceptable dose deterioration. Given a suitable energy layer reduction strategy, the next question is whether the continuously delivered PAT dose distribution matches the planned dose distribution calculated under the assumption of fixed control points. Smaller angular spacings during planning are expected to reduce the differences between planned and delivered dose, but the scale of the angular spacing for making these differences beyond clinical concerns is unknown.

1.5 Summary and aims

In conventional radiotherapy, VMAT has shown clinical advantages in terms of the delivered dose distribution and the time to deliver a treatment session [17] - [19]. Proton therapy deliveries are currently limited to a small number of fixed angle deliveries. In theory, scanned beam proton therapy could be delivered as an arc but currently arc delivery is not possible. This thesis studies the inherent advantages of PAT and parameters that would make PAT delivery more feasible with the current limitations in proton therapy delivery technology. PAT has the potential to further improve dose conformality, robustness and LET distributions compared to IMPT. This was firstly motivated by the experience learned from VMAT compared to IMRT [17] - [19], and later confirmed in initial plan comparison studies [24] – [36]. Although this observation should be repeated for an extended number of cases, the practicality of PAT delivery became an important challenge to solve and is yet to be solved. The available delivery techniques for proton therapy are PSPT and IMPT. Experience learned from proton therapy delivery suggests that IMPT is the better option for PAT delivery compared to PSPT. However, IMPT relies on the accelerator or energy degraders to modulate beam energy, which is a time-consuming process considering the large number of beam angles and energy layers involved in PAT and FPAT. This problem motivated two existing strategies to remove redundant energy layers in PAT, which are SPArc [28] and PMAT [27]. SPArc relies completely on computational optimisation for energy layer reduction and so takes a long time to optimise a PAT plan. Although the time factor is not a concern for plan quality, it can affect clinical planning workflow and efficiency. In contrast, PMAT is fast to optimise as it preselects energy layers and brings the benefits of LET migration, but whether PMAT can be applied for general tumour geometries is not yet reported.

Other than the challenge of solving the deliverability of PAT, this work is also motivated by PAT's potential of solving some limitations of IMPT, which are the treatment time, robustness, and the number of beam angles (since IMPT delivers the full energies and is delivered from fixed angles, a large number of beam angles will prolong the treatment time). It is important to understand PAT's behaviour on a fundamental level and there was no work that examined this before the start of this work. Therefore, this thesis firstly aims to explore in 2D the plan

characteristics including the robustness of PAT plans compared to IMPT for a variety of cases (Chapter 2). From this, PAT with reduced energy layers is explored in 3D to determine whether the resultant plan quality can be maintained. This is carried out in Chapter 3 which also gives an end-to-end algorithm for PAT energy layer selections. The energy layer selection algorithm has been tested on a group of eight cases representing variations in tumour geometry. Finally, the deliverability of the reduced PAT plans is evaluated in Chapter 4. As the current IMPT delivery system does not yet support PAT delivery, the deliverability in Chapter 4 was assessed via emulation techniques, which showed that the reduced PAT plans in Chapter 3 could theoretically reduce the delivery time significantly compared to IMPT while maintaining dose qualities that are equally or exceedingly competitive compared to the IMPT plans. As the main work in chapters 2, 3 and 4 rely on preliminary knowledge of general proton therapy treatment planning techniques and hardware systems. Introductions to those topics follow in sections 1.6 and 1.7.

1.6 Treatment planning techniques used in proton therapy

The goal of radiotherapy treatment planning is to put the prescription dose into the target and to minimise the dose received by the surrounding healthy tissue. This is achieved via careful choices of plan parameters set by the planner (a clinical scientist responsible for treatment planning within the National Health System in the United Kingdom) and reliable computational algorithms which mainly include the dose calculation engine and dose optimisation algorithms. This chapter introduces the treatment planning techniques used for proton therapy in general which can be applied for PAT planning when appropriate.

1.6.1 Plan parameters

Before a planner makes a treatment plan, the clinician defines the gross tumour volume (GTV), clinical target volume (CTV), and the prescription dose. The planning process then involves the planner making choices for the beam angles, planning target volumes (PTV), uses of any beam modifying devices and treatment planning objectives (if inverse optimisation is used) in order to meet the prescription dose specified by the clinician. Some TPS allow choices made between single field optimisation (SFO) or multiple field optimisation (MFO) and whether to set any dose objective as robust objectives. Suitable settings form the basis of a well optimised treatment plan.

1.6.1.1. Beam angles

Beam angles are selected to avoid passing through a significant amount of healthy tissue and avoid traversing parallel to a tissue boundary due to protons' susceptibility to treatment uncertainties. Factors influencing selections of beam angles contain the following (extracted from proton optimisation strategies at the Christie proton therapy centre):

- Avoid significant normal tissue dose;

- Avoid potential collisions with the patient or hardware devices;
- Avoid high skin dose from overlapping fields;
- Ensure robustness to patient setup uncertainties (avoid traversing parallel to a tissue boundary);
- Avoid beams stopping on critical structures (avoid high LET deposited at the proton beam's track end, and avoid high dose deposited in critical structures in case of range errors);
- Use multiple beams to dilute uncertainties as each beam will deliver a lower dose.

Examples of avoiding significant normal tissue dose are beam arrangements in unilateral H&N cases, where only beams entering from the same side of the tumour are selected (figure 1-7(a)). Examples of avoiding beams stopping on critical structures are tumours situated directly behind the brainstem, in which case two posterior oblique beams as illustrated in figure 1-7(b) can be selected to avoid putting high LET values directly inside the brainstem. A third beam coming from superior-oblique direction can be added to further mitigate the potential effects of range uncertainties.

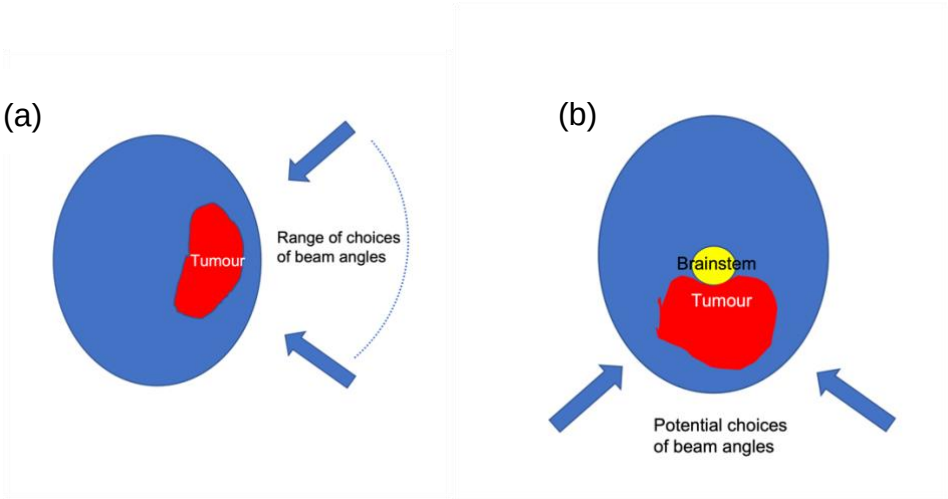

Figure 1-7: Illustrations of potential beam angle choices for (a) a unilateral head and neck, where beams coming from the same side of the tumour are selected to avoid traversing through a large amount of normal tissue, (b) a case where an organ-at-risk (brainstem) is directly adjacent to the tumour, in which case two beams at posterior-oblique angles as illustrated are chosen to avoid high LET values stopping directly inside the brainstem in case of uncertainties.

Currently there are no protocols for determining the angular range for PAT beam angle choices, but learning from IMPT experience, the angular range in general should be on the shallower side of the tumour that goes through less critical structures.

1.6.1.2. Target volumes

A target must be defined for treatment planning. This target is usually the PTV. The PTV is a conceptual structure that contains the following structures (figure 1-8): 1. gross tumour volume (GTV), the tumour volume visible on patient image, 2. clinical target volume (CTV), a margin added to GTV to account for microscopic disease not visible on patient image, 3. sometimes the internal target volume (ITV), a margin added to CTV to account for internal organ motion. While GTV, CTV and ITV are oncological concepts, PTV is a geometrical concept designed for treatment planning purposes to select the appropriate beam arrangements to ensure that the prescription dose is delivered to the CTV.

(the rest of this page intentionally left blank)

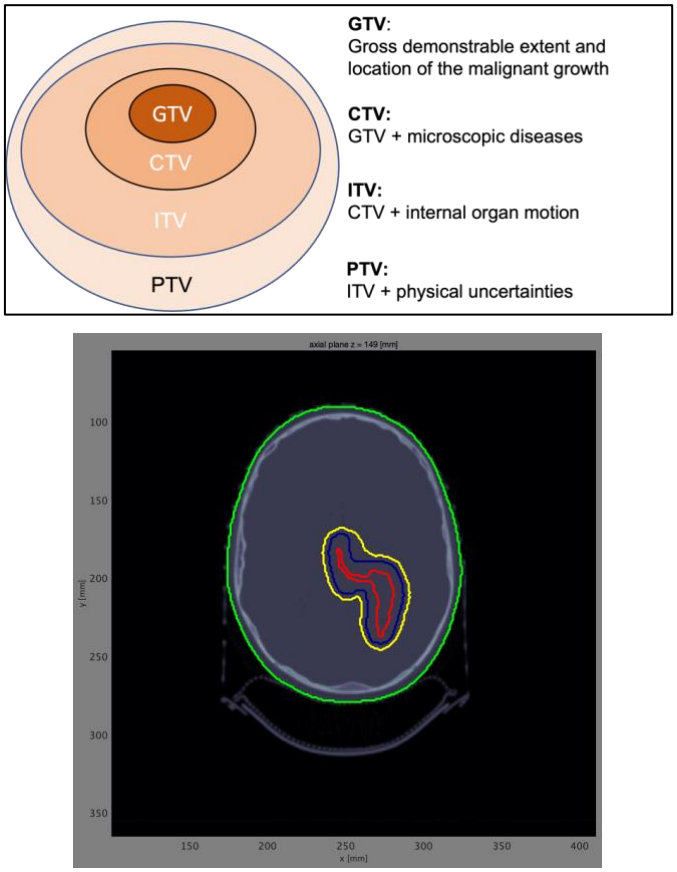

Figure 1-8: Top: definitions of gross tumour volume (GTV), clinical target volume (CTV), internal target volume (ITV), and planning target volume (PTV). Bottom: Examples of contours of the GTV (red), CTV (black), PTV (yellow), and the patient contour (green) displayed on the patient CT visualised within the open-source educational treatment planning software, matRad.

If PAT reduces the effect of physical treatment uncertainties, the extra margin used for PTV might be unnecessary or could be reduced in size. This reduction of PTV margin would reduce the overall volume treated and thus be beneficial in terms of therapeutic outcome.

1.6.1.3. Beam modifying devices

Different proton therapy delivery systems may use different beam modifying devices to increase the radiation conformality. Passively scattered proton therapy (section 1.3.1.1) usually uses a range modulator, a collimator, and a compensator which have been introduced already.

Actively scanned systems do not need these beam modifying devices as high conformality in both lateral and longitudinal directions is achieved by scanning the proton beam. However, if the target is shallower than the range of the lowest possible beam energy, a range shifter is required. The range shifter is attached downstream to the nozzle and is a block of plastic material which absorbs the beam energy and reduces the beam's effective range in patient body. The range shifter must be placed closely to the patient skin as it introduces scattering which results in proton spots of bigger sizes. To avoid patient collisions, the range shifter must move back to its resting position when the delivery of one field is finished. With multiple fields usually used in IMPT delivery, the use of range shifters prolongs the treatment time.

Range shifters are not practical in PAT delivery due to the requirement of it being positioned closely to patient surface. In fact, range shifters might be unnecessary in PAT planning as shallow regions can be covered by beams irradiated from another direction.

1.6.1.4. Single field and multiple field optimisation

When more than one field is used, the planner can choose between single field optimisation (SFO) and multiple field optimisation (MFO) techniques. SFO is where the dose delivered by each beam is optimised individually to meet the dose objectives set by the planner (section 1.6.3.2). The optimised dose distribution of each beam is therefore uniform as it aims to cover the entire target. The relative weighting of each beam can be set to be a fraction of the prescription dose, but in the end all beams add up to the prescription dose (figure 1-9(a)). MFO is where all fields are optimised together to meet the dose objectives, so the optimised dose distributions of individual beams are often heterogeneous (figure 1-9(b)).

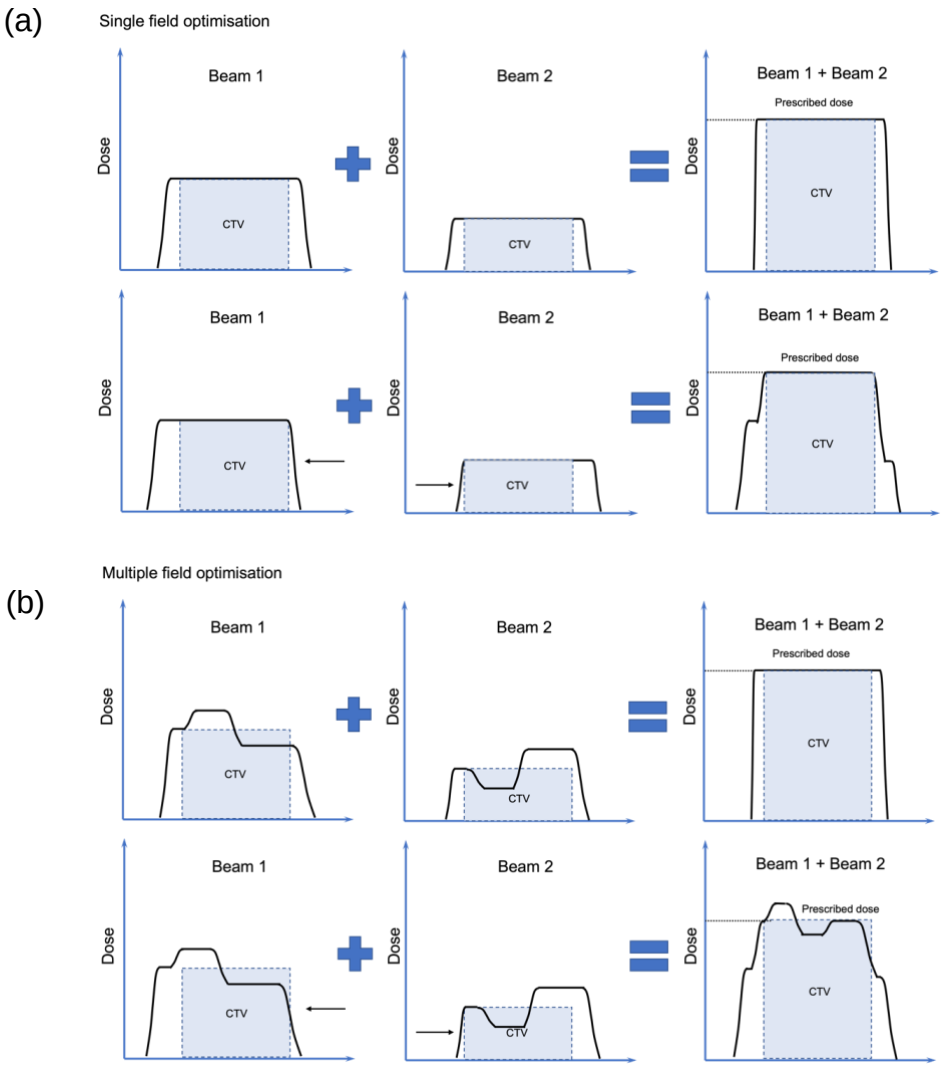

Figure 1-9: (a) Illustration of SFO planning and the effect of uncertainties on the total dose distribution is milder than (b) MFO planning. The top rows illustrate the 1D dose distributions under nominal scenario, and the bottoms rows the same plan re-calculated under setup uncertainties.

The main advantage of SFO is that it tends to be more robust than MFO under uncertainties, but the disadvantage is that SFO could be incapable to achieve complex geometries. The practice taken at the Christie proton therapy centre is that a plan starts with SFO planning, and if it is incapable of meeting clinical dose requirements, MFO planning will be the alternative.

MFO is the choice made for PAT planning in this work as each beam angle in PAT does not need to cover the whole tumour volume.

1.6.2 Dose calculation

The quality of a treatment plan not only depends on the skills of the planner (the ability to manipulate the plan parameters) but also on the accuracy of the dose calculation algorithm. In general, dose calculation algorithms used by commercial TPS can be divided into two categories: pencil beam models and Monte Carlo (MC) algorithms. Pencil beam models are analytical methods, whereas MC algorithms use random sampling of interaction cross sections for a user-defined number of particles to simulate individual particle trajectories which result in statistically variable results depending on the number of particles simulated. Pencil beam models facilitate fast dose calculation but can be less accurate for heterogeneous materials, e.g., lungs and presence of range shifters. On the other hand, MC algorithms can predict accurate dose distributions but take longer to calculate. Therefore, pencil beam models are mostly used for dose optimisation and MC is a choice used for a final dose calculation or quality check (QC).

1.6.2.1. Pencil beam model

Within pencil beam algorithms, a proton beam (an individual spot) is decomposed into many closely spaced mini beams. For a proton beam of a particular energy, the beam model is made up of the longitudinal integrated depth-dose profile (IDD) and the lateral spot's full-width half maximum representing scattering in water. Calculations for the IDDs can be based on the Bortfeld model [49] (the default beam model in matRad) or the Bethe Bloch equation which calculates the average kinetic energy transferred from the protons to the medium (stopping power) (used in Varian's Eclipse treatment planning software and RaySearch Laboratory's RayStation treatment planning software). Another option is to substitute the IDD with commissioned measurements. The lateral profile is often modelled as Gaussian distributions representing scattering of light and heavy ion fragments. With the longitudinal and lateral profiles of proton beams in water described completely by the beam model, the dose deposition in heterogeneous material is then calculated by scaling the profiles according to the relative stopping powers of the material, which is usually a look up table constructed from MC simulations.

1.6.2.2. Monte Carlo (MC)

MC allows detailed tracking of the particles, e.g., protons, photons, through matter by simulations of all types of particle-matter interactions based on large numbers of particle statistics. To simulate a dose distribution, MC needs to model the treatment plan, the patient geometry, and the beam delivery system. Because of the level of details in MC models, MC simulations are considered as the gold standard for dose distribution calculations. On the other hand, analytical models used by commercial TPS for calculating and optimising treatment plans can sometimes differ to the MC results [50][51]. Prior to delivery, a treatment plan can be verified against an MC simulation along with phantom measurements to ensure that the plan would match delivery in reality.

The precision of MC simulations largely depends on the particle statistics modelled. The higher the statistics, the more precise the results are and the longer the calculations take.

1.6.3 Dose optimisation

1.6.3.1. Types of dose optimisation

Forward dose optimisation originates from planning techniques used in early conventional radiotherapy and is used for planning PSPT or for pre-optimisation in scanned proton therapy. In scanned proton therapy, forward optimisation is used to create an approximately flat SOBP inside the target by summing up the dose delivered by spots distributed across each of the energy layers. Within each layer, the weights of the spots are uniform. For scanned proton therapy, forward planning is sometimes used as a pre-optimisation for the inverse dose optimisation. The outcome of the pre-optimisation is uniform spot weights within each energy layer and can serve as good starting conditions for inverse optimisation.

Inverse dose optimisation is found in modern proton TPS which supports actively scanned modality. Inverse optimisation is realised by means of minimising an objective function consisting of dose objectives set by the planner with a suitable optimisation algorithm. Inverse dose optimisation was introduced in the 1990s when computer powers were rapidly developing. The procedure of inverse dose optimisation involves the planner defining the dose objectives or constraints in every ROI and their relative importance factors (relative weight among the dose objectives or constraints). These dose requirements and their importance factors then make up a single dose objective function, which is to be minimised by an optimisation algorithm by adjusting the individual spot weights. The advantage of inverse dose optimisation is that it makes intensity modulation achievable which allows more optimisation possibilities than forward planning.

1.6.3.2. Dose objectives in inverse optimisation

At the user interface of the dose optimisation module in a proton therapy TPS, the planner can choose from a variety of dose objective types and set the desired parameters to meet the prescription dose inside the target and to minimise the dose in healthy tissue. Typical dose objectives include physical dose objectives (maximum dose, minimum dose, mean dose, upper and lower dose objectives as points on a DVH, dose uniformity), biological dose objectives (maximum and minimum generalised equivalent uniform dose, or gEUD), and the fall-off objective. Each structure can be given multiple dose objectives.

For a structure given a maximum dose objective, the optimisation algorithm within the TPS penalises the voxels with dose greater than the value of d_{max} defined by the planner. The mathematical equation of the maximum dose objective is given in equation 1-2:

Equation 1-2: Maximum dose objective function used in proton therapy inverse dose optimisation.

$$f_{max} = \frac{1}{N}\sum_{i=1}^{N} H(d_i - d_{max})\,(d_i - d_{max})^2$$

Where f_{max} represents the objective function for the maximum dose objective, $H(x) = 0$ if $x < 0$, and $H(x) = 1$ if $x >= 0$ is the Heaviside step function, d_i is the dose in the ith voxel within the structure with N voxels, and d_{max} is the maximum dose objective set by the planner. The Heaviside term makes sure that only the voxels within the structure with dose greater than d_{max} are penalised. The extent to which a voxel is penalised is represented by the squared difference term. The contribution of f_{max} towards the total dose objective function is the average of the sum of the squared difference terms over the number of voxels which belong to the structure. The averaging term, $\frac{1}{N}$, makes sure that the constituent objective functions are suitably weighted when multiplied by their importance factors, i.e., avoid situations where the volume of a structure affects the relative importance.

Similarly, for a structure given a minimum dose objective, the optimiser penalises the voxels with dose less than the value of d_{min} defined by the planner. The mathematical equation of the minimum dose objective is given in equation 1-3:

Equation 1-3: Minimum dose objective function used in proton therapy inverse dose optimisation.

$$f_{min} = \frac{1}{N}\sum_{i=1}^{N} H(d_{min} - d_i)\,(d_{min} - d_i)^2$$

Where f_{min} represents the objective function for the minimum dose objective, and d_{min} is the maximum dose objective set by the planner.

The fall-off objective penalises the dose greater than a maximum dose value in a normal-tissue margin outside the PTV, so is sometimes called the normal tissue objective (NTO). The normal-tissue margin used for NTO were chosen to be

uniform (i.e., isotropic) and given as a single distance parameter, m, from the target structure (equation 1-6). The maximum dose values are the greatest at the PTV target border and lowest at some distance (user-defined) away from the PTV border. The maximum dose value in every voxel in the margin, p_i, with the user-defined thickness can be modelled as a sigmoid function given in equation 1-4:

Equation 1-4: Normal tissue objective (NTO) function used in proton therapy inverse dose optimisation as a reference from Varian's Eclipse treatment planning software.

$$p(i) = \frac{(1 + erf(\frac{d(i) + s}{f}))}{2}$$

Where $erf(\,)$ is the error function, $d(i)$ is the distance of voxel i from the PTV border, and s and f are the shift parameter and steepness parameter respectively as defined in equation 1-5 and 1-6:

Equation 1-5: Equation for the shift parameter required in calculating the NTO function.

$$s = erfinv(2D_1 - 1)$$

Equation 1-6: Equation for the steepness parameter required in calculating the NTO function.

$$f = \frac{m}{erfinv(2D_1 - 1) - erfinv(2D_2 - 1)}$$

Where $erfinv(\,)$ is the inverse error function, m is the size of the normal-tissue margin in distance unit, and D_1 and D_2 are the upper and lower dose objective between 0% and 100% relative to the prescription on the PTV border and normal-tissue margin border, respectively.

Within the dose optimisation algorithm of a proton therapy TPS, a single objective function, F_b, is then constructed as a weighted sum of the individual dose objectives, where the weighting to each dose objective is the importance factor defined by the user. The mathematical equation of the objective function is given

by equation 1-7 in the quadratic form. The objective function is then minimised by a selected optimisation algorithm

Equation 1-7: The total objective function as a weighted sum of the individual objective functions.

$$F_b = \sum_j w_j \left(f_j - D_j\right)^2 + w_{margin} \sum_{\substack{i \in margin \\ D(i) > p(i)}} \left(p(i) - D(i)\right)^2$$

where w_j is the importance factor to the jth dose objective with value f_j and objective dose value D_j, p_i is the dose in the ith voxel within the margin with maximum dose objective of $D(i)$, and w_{margin} is the importance factor of the fall-off objective.

1.6.3.3. Robust optimisation

If a dose objective is set to be robust by the planner, the objective function for this dose objective will be considered under uncertainty scenarios, which are situations where a potential treatment uncertainty is likely to occur. Typical uncertainty scenarios considered for robust optimisation are patient setup uncertainties (a shift in the patient position from the position captured in the planning CT images) and beam range uncertainties (or sometimes referred to as CT calibration uncertainties, which cause overshoot or undershoot of the beam range). The goal of robust optimisation is to make sure that the optimised dose distribution would meet clinical dose requirement even under the uncertainty scenarios. There exist a variety of methods of quantifying the objective function considering uncertainties based on worst case uncertainty scenario evaluations. A detailed comparison amongst worst case scenario methods is provided in [52] which compared three typical methods: composite objective function, objective-wise worst case, and voxel-wise worse case.

In the composite objective function method, the uncertainty scenario with the highest total objective function value is considered for dose optimisation upon

each iteration. Objective-wise worst scenario is where the highest values of each constituent objective function are put together to form a total objective function used for dose optimisation. Voxel-wise worst scenario is where the voxel-wise minimum and maximum dose values are calculated to form two new dose cubes, which are then used for dose optimisation. The comparison in [52] found that composite objective function, objective-wise and voxel-wise worst cases all have their advantages and disadvantages (summarised in table 1-2), and that the planner should be aware of the method used by the TPS. For reference, RayStation version 9B's robustness optimisation toolkit uses the composite objective worst case scenario approach, where the scenario (including the nominal scenario) with the highest objective function value is used for optimisation to maintain the physical properties.

Table 1-2: Summary of advantages and disadvantages of worst-case scenario methods used in robust optimisation.

Types of worst-case scenario methods	Advantages	Disadvantages
Composite objective	Gives the lowest objective function values.	Only considers one scenario.
Objective-wise worst-case	Supports multicriteria optimisation.	Gives the highest objective function values out of the three methods.
Voxel-wise worst-case	Considers all scenarios together.	Can be overly conservative.

In general, a plan optimised with robust optimisation has worse dose conformality than nominal optimisation because the dose tries to cover the target under possible uncertainty scenarios. Therefore, robust optimisation must be carefully applied on a case-by-case basis. In addition, robust optimisation is more time-consuming than nominal optimisation as the 'worst case' must be computed from all uncertainty scenarios at every optimisation iteration. The practice taken at the Christie proton therapy centre is that a plan can start without robust optimisation, but its robustness is always evaluated after dose optimisation by evaluating the

resultant dose distributions under uncertainty scenarios against clinical dose requirements. If the plan cannot meet clinical dose requirements under uncertainty scenarios by any means of changing the plan settings, then robust optimisation is an option to achieve robustness goals.

1.6.3.4. Common algorithms used for proton therapy inverse optimisation

Optimisation algorithms have extremely broad applications not only in radiotherapy. In general, an optimisation function runs significantly faster and is easier to compute if the objective function is differentiable, which is fortunately the case for proton inverse optimisation. In fact, the second order derivative of the objective function (Hessian matrix) exists for proton inverse optimisation. A few choices of second derivative optimisation algorithms include: Newton's method, Broyden-Fletcher-Goldfarb-Shanno (BFGS) [53], limited-memory BFGS (Varian's Eclipse treatment planning software, RaySearch Laboratory's RayStation treatment planning software), IPOPT [54] (used in the open-source educational TPS matRad). The optimisation algorithm used for the work in Chapter 2 is limited-memory BFGS, and in Chapter 3 and 4 is IPOPT. These optimisation algorithms were chosen by examining optimiser performance for these cases and selecting the algorithm which converged on a good solution in an acceptable time. Optimiser performance was not a focus of the thesis and optimisation algorithms with better performance for these problems may exist.

1.6.4 Plan evaluation

Once a treatment plan has been optimised, the plan must be evaluated to assess whether it meets clinical dose requirements. The clinical dose requirements consist of criteria on the CTV and OARs under both nominal (error free) scenario and uncertainty scenarios. In general terms, the CTV must receive doses at the prescribed level specified by radiation oncologists, and OAR doses must not exceed certain levels which are specific to each type of OAR. All plan evaluation techniques used for IMPT planning are applicable for PAT plan evaluation.

1.6.4.1. Dose distributions

Various methods exist which evaluate the optimised plan. The optimised dose distribution is displayed in 2D for all three anatomical planes, along with the rendered 3D dose distribution (top right in figure 1-10). An example of this is provided in figure 1-10. The 2D dose distributions are highly informative - the user can scroll through different slices to access the exact dose distribution. The advantage of plan evaluation using these 2D dose distributions is that it presents the spatial dose information.

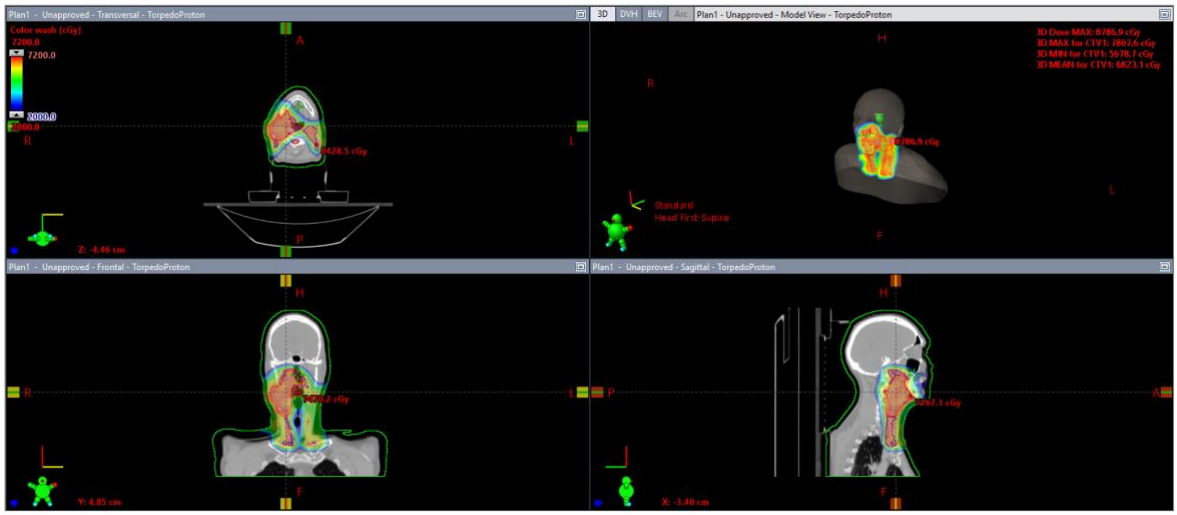

Figure 1-10: Typical layouts for visualising the calculated or optimised dose distribution in a radiotherapy treatment planning system (Varian's Eclipse treatment planning software version 15.6). Three panels display the 2D dose distributions on top of CT images in the three anatomical planes (transversal plan in the top left, coronal plane in the bottom left, and sagittal plane in the bottom right), while a fourth panel (top right) renders the dose distribution in 3D.

1.6.4.2. Dose volume histograms (DVH)

A convenient and extremely common tool to summarise the 3D dose information is a dose-volume histogram (DVH) [55]. A DVH plots the fractional or percentage volume of a region of interest (ROI), which can be a target or an OAR structure, as a function of the dose level. The DVH provides information on dose homogeneity and any hot spots within defined structures. For example, the DVH curve for the target in figure 1-11 shows dose homogeneity as a 'squared' line, and its tail around 100 Gy shows existence of hot spots within PTV. However, the location of

the hot spot is unknown, i.e., DVH does not provide positional information. Therefore, the DVH can be considered as a 1D plan evaluation tool and should be used together with the dose distribution. The advantage of DVH is that it is convenient for comparing different plans (figure 1-12).

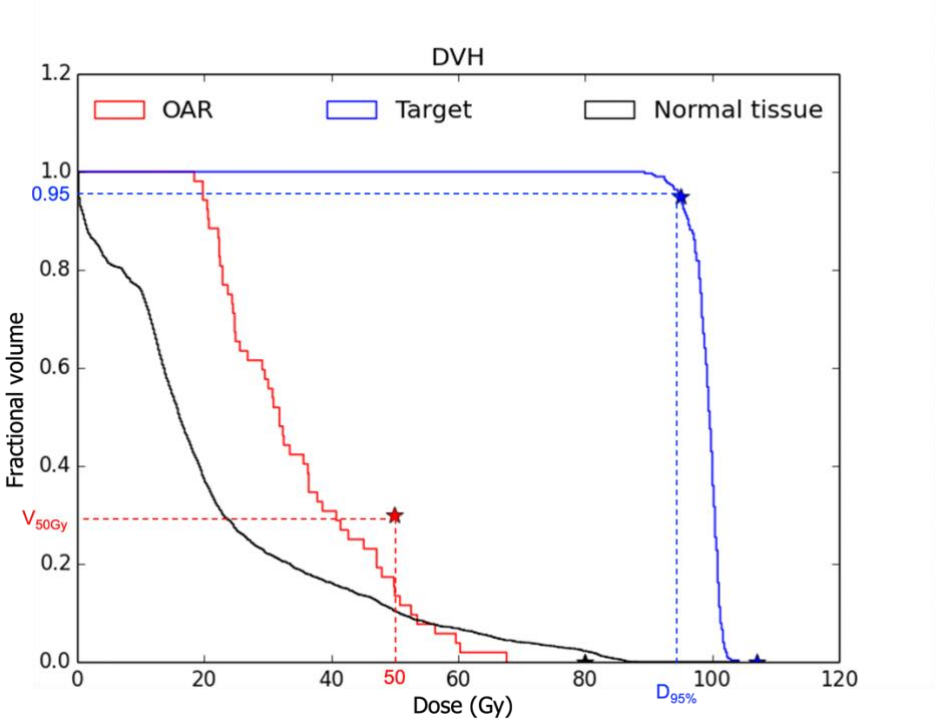

Figure 1-11: A dose volume histogram (DVH) is a 1D plan evaluation tool which provides information on dose uniformity and existence of any hot spots within a defined ROI structure. DVH metrics (e.g., D95%, V50Gy as introduced in section 1.6.4.3) can be used for plan evaluation and dose optimisation

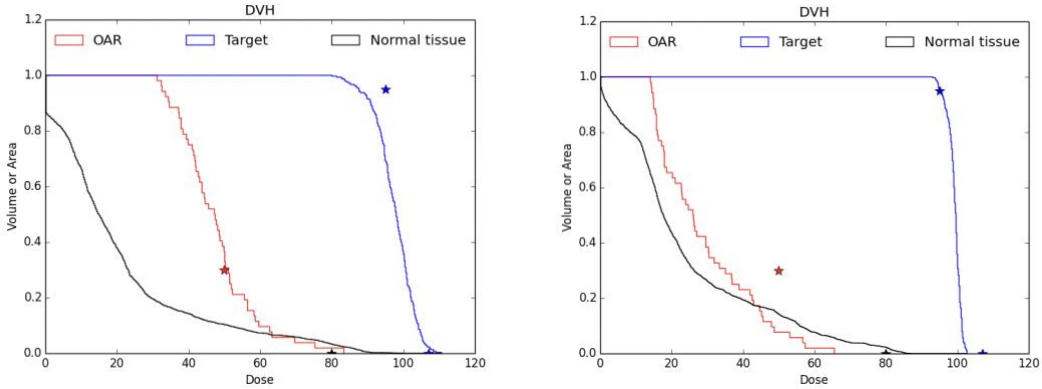

Figure 1-12: Comparison of two sets of DVHs. Left figure is a 5-beam IMPT plan for the RTOG para-spinal phantom, right figure is a 90-beam PAT plan. The sharper edge of the target DVH in the PAT plan means that the dose is more conformed to the target. The OAR DVH being more towards the lower dose levels in the PAT plan means that the OAR is spared better.

1.6.4.3. DVH metrics and clinical assessment sheet

Points on a DVH (DVH metrics) are useful quantification methods to define a specific dose feature of a ROI. Examples of DVH metrics include Dx%, Vx%, maximum, minimum, and mean dose. While the latter three are easy to understand, Dx% represents the dose delivered to x% volume of a structure, and Vx% represents the volume that receives at least x% of the prescribed dose (figure 1-11). DVH metrics are often used in clinical dose assessment criteria and an example of the clinical dose assessment sheet used at the Christie proton therapy centre is provided in figures 1-13 and 1-14. Another usage of DVH metrics is that they can be used to define objectives for dose optimisation (section 1.6.3.2).

Target Volumes

Structure	Volume	Dose required	Dose received /cGy	Min dose under uncertainty* /cGy	Max dose under uncertainty* /cGy	Uncertainty scenario
CTV_High	98%	>90%				
	95%	>95%				
	mean	Reported				
	2%	<110%				
CTV_Low	98%	>90%				
	95%	>95%				
	mean	Reported				
	2%	<110%				

Figure 1-13: Part of the clinical dose assessment sheet for the target volumes for paediatric brain and H&N used at the Christie Proton Therapy Centre.

(the rest of this page intentionally left blank)

Organs At Risk

Structure	Volume	Constraint (Mandatory in bold) (P)= Primary (S)= Secondary	Dose received /cGy	Max dose under uncertainty* /cGy	Uncertainty scenario
Patient	Max	Reported			
Brain	Min	<1800 cGy			
	Max	Reported			
BrainStemCore	0.1 cc	**<5610 cGy**			
BrainStem	0.1 cc	<5660 cGy, **<5800 cGy**			
	D50%	<5240 cGy, **<5400 cGy**			
	D10%	<5540 cGy, **<5600 cGy**			
Cochlea_L	Mean	**< 4500 cGy** if mean to contralateral cochlea >4500 cGy			
	Mean	<2000 cGy (P), <3500 cGy (S)			
Cochlea_R	Mean	**< 4500 cGy** if mean to contralateral cochlea >4500 cGy			
	Mean	<2000 cGy (P), <3500 cGy (S)			
Cornea_L	0.03 cc	**<5000 cGy**			

Figure 1-14: Part of the clinical dose assessment sheet for the OAR volumes for paediatric brain and H&N used at the Christie proton therapy centre.

1.6.4.4. Plan evaluation metrics

Sometimes it is useful to quantify a specific feature of the 3D dose distribution with a single plan evaluation metric. Examples of the specific features include the conformality and homogeneity of the target dose distribution. The plan evaluation metric summarising the dose conformality is called conformality index (CI) which has various definitions (table 1-3) [56]. However, since CI does not contain spatial information, a value of 1.0 does not necessarily mean perfect conformality, i.e., zero dose outside the target. For this reason, CI is commonly used for plan comparisons. Similarly, homogeneity indices quantify the dose homogeneity feature within a target and have various definitions also (table 1-4). All plan evaluation metrics should be used in combination with other higher dimensional evaluation methods to get a complete picture of the dose distribution.

Table 1-3: Summary of definitions of conformality index

Various definitions for conformality index (CI)		
Mathematical definition	Reference	Equation number
$\frac{V_{Rf}}{TV}$	[57]	*Equation 1-8: Definition 1 of conformality index.*
$\frac{TV_{Rf}}{TV}$	[58]	*Equation 1-9: Definition 2 of conformality index.*
$\frac{TV_{Rf}}{V_{Rf}}$	[58]	*Equation 1-10: Definition 3 of conformality index.*
$\frac{TV_{Rf}}{TV_{Rf}} \times \frac{TV}{V_{Rf}}$	[59]	*Equation 1-11: Definition 4 of conformality index.*

V_{Rf}: volume within reference isodose surface.

TV: target volume.

TV_{Rf}: target volume within reference isodose surface.

Table 1-4: Summary of definitions of homogeneity index

Various definitions for homogeneity index (HI)		
Mathematical definition	Reference	Equation number
$\frac{D_{max}}{D_{presc}}$	[25] [27]	*Equation 1-12: Definition 1 of homogeneity index.*
$D_{ref\,low} - D_{ref\,high}$	[26]	*Equation 1-13: Definition 2 of homogeneity index.*
$\frac{D_{min,ref,low}}{D_{min,ref,high}}$	[28]	*Equation 1-14: Definition 3 of homogeneity index.*

D_{max}: maximum dose within the target.

D_{presc}: prescribed dose.

$D_{ref,low}$: dose received by a fraction (e.g. 90%) of the target volume.

$D_{ref,high}$: dose received by a fraction (e.g. 95%) of the target volume.

$D_{min,ref,low}$, $D_{min,ref,high}$: minimum dose in low and high reference isodose regions.

1.6.4.5. Robustness evaluation

Treatment uncertainties can occur and affect the delivered dose, so the optimised plan must be evaluated under various possible uncertainty scenarios to assess the plan robustness. If the dose distribution meets clinical dose requirements under uncertainty scenarios, the plan is considered robust. Different uncertainty scenarios can occur which include uncertainties in patient setup, CT-HU conversion curve (beam range), patient anatomical changes, beam energy, spot position, etc. For evaluating the robustness of treatment plans, usually the first two types of uncertainties are evaluated. Patient setup uncertainties are often modelled as translation of the patient in the six anatomical directions. The extent of the translation is usually 3 mm in H&N patients and 5mm in lung patients [60]. Beam range uncertainties are often modelled as +3.5% and -3.5% changes in the beam range which is realised by scaling the proton stopping power. Each setup and range uncertainty scenario is evaluated independently, which gives eight uncertainty scenarios in total. To summarise the plan robustness in a single figure, DVH curves for the modelled uncertainty scenarios and the nominal scenario can be plotted together, or the voxel-wise maximum and minimum dose can be extracted. The group of DVH curves from all eight uncertainty scenarios form a band, and its width is a straightforward feature for determining the level of robustness.

1.7 Hardware used to deliver scanned proton therapy

The hardware required to deliver scanned proton therapy treatments differs from centre to centre, but they all share some common features. No matter the size of the proton therapy centre, any proton therapy delivery system requires a particle accelerator (cyclotron or synchrotron), a beam transport system, an optional rotating gantry, and a nozzle. For dose quality reasons, the scanned delivery system is considered to be the better choice for PAT delivery than PSPT.

1.7.1 Accelerator

After the protons are separated from hydrogen atoms and exit an injector (for pre-acceleration), they enter an accelerator to be accelerated to the required energy for treatment. The range of proton energy for therapeutic purposes is between about 70 MeV and 250 MeV, which correspond to proton ranges between about 4 centimetres to 30 centimetres in water. If a target is shallower than 4 centimetres, a range shifter is used.

The most common choices for proton therapy accelerators are cyclotrons and synchrotrons. Cyclotrons are often the choice if the ion species are protons or light ions, whereas synchrotrons are more often used for supporting heavy ion therapy as otherwise a large magnetic field is required in cyclotrons to contain heavy ions. Cyclotrons are designed to accelerate the beam to a single potential for one type of particle, but synchrotrons are able to output variable energy beams for a range of particle species by ramping the electromagnetic fields used to confine the beam inside the accelerator.

As cyclotrons have fixed energy output, energy modulation is performed with a wedge-shaped energy degrader which moves into the beam path to let more material block the beam path (figure 1-15). This means that the cyclotron energy output is the highest it can be because energy will always be degraded downwards. Precise control of the energy degrader means that cyclotrons are time-consuming to change the beam energy, with a time to achieve an energy

modulation on the order of seconds, which is about three orders of magnitude longer than the time spent on delivering the proton spots. Moreover, an energy increase takes longer than an energy decrease due to hysteresis of the magnetic optics required to transport the beam.

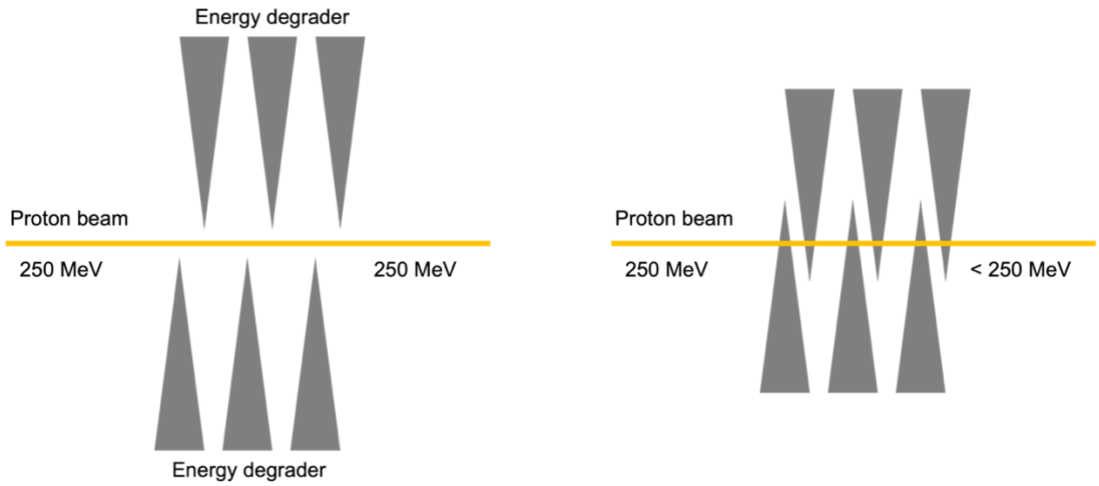

Figure 1-15: Illustration of how energy degraders (wedge-shaped low Z material) at the exit of a cyclotron move in and out of beam path to modulate the beam energy.

Synchrotrons are ring accelerators where the electromagnetic fields synchronise with the particles as they accelerate. The beam extracted from a synchrotron is not continuous, unlike a cyclotron. As PAT delivery requires a continuously active beam with gantry rotation, synchrotrons are not considered for PAT delivery. Instead, a superconducting cyclotron model from the Varian ProBeam system (used at the Christie proton therapy centre) is considered for this work. Detailed investigations of accelerators for PAT delivery are outside the scope of this thesis.

1.7.2 Rotating gantry

Gantries consist of a frame holding a series of magnets to bend and direct the beam so that the beam can irradiate the patient from different directions (beam angles). Proton gantries are considerably larger and heavier than photon gantries as magnets of higher strengths which require larger masses are needed to bend protons' trajectories. A typical proton gantry has a diameter of about 9 metres [61]. Once installed, it will be difficult to replace. Some centres without gantries choose to design rotating treatment pods or chairs to increase the flexibility of beam angle

choices [62]. Due to the proton gantry's heavy mass, there is limitation on the maximum rotation speed to ensure accuracy. The maximum rotation speed is chosen to be 6 degrees per second as it is also the upper speed limit of a conventional radiotherapy gantry.

Proton therapy system manufacturers do not typically state whether their systems support continuous irradiation while the gantry rotates, since proton arc delivery is not yet supported for clinical use. This must be verified and enabled for practical development of PAT. Chapter 4 of this thesis investigates the theoretical delivery time and dose distribution under continuous gantry rotation, but it relies on the assumption that each spot is delivered instantaneously at a unique beam angle, such that the dose calculation can be performed based on the individual spot profile. The spot profile under continuous gantry rotation should be measured to assess any potential profile deformation (outside the scope of this work), although the time spent at each spot should be too short to cause any clinically important differences.

1.8 References

[1] Mee, Thomas. Monte Carlo applications for local treatment healthcare usage simulations. University of Surrey (United Kingdom), 2015.

[2] Tubiana, M. “Wilhelm Conrad Röntgen et la découverte des rayons X” [Wilhelm Conrad Röntgen and the discovery of X-rays]. Bulletin de l'Academie nationale de medecine vol. 180,1 (1996): 97-108.

[3] Martins, Paulo Nuno. "A brief history about radiotherapy." International Journal of Latest Research in Engineering and Technology 4 (2018): 8-11.

[4] Benveniste, Marcelo F., et al. "Recognizing radiation therapy–related complications in the chest." Radiographics 39.2 (2019): 344-366.

[5] Schlegel, Wolfgang, and Andreas Mahr. 3D conformal radiation therapy: Multimedia introduction to methods and techniques. Springer Berlin, 2007.

[6] Gupta, V., et al. "A Comparison of Two-Dimensional and Conformal Radiotherapy for Post-Operative Treatment of Non-Small Cell Lung Cancer (NSCLC)." International Journal of Radiation Oncology, Biology, Physics 63 (2005): S227-S228.

[7] Zhang, Binglan, et al. "Intensity-modulated radiation therapy versus 2D-RT or 3D-CRT for the treatment of nasopharyngeal carcinoma: a systematic review and meta-analysis." Oral oncology 51.11 (2015): 1041-1046.

[8] Webb, Steve. Intensity-modulated radiation therapy. CRC Press, 2015.

[9] Xu, Dandan, et al. "Comparison of IMRT versus 3D-CRT in the treatment of esophagus cancer: a systematic review and meta-analysis." Medicine 96.31 (2017).

[10] Arbea, Leire, et al. "Intensity-modulated radiation therapy (IMRT) vs. 3D conformal radiotherapy (3DCRT) in locally advanced rectal cancer (LARC): dosimetric comparison and clinical implications." Radiation oncology 5.1 (2010): 1-9.

[11] Hermanto, Ulrich, et al. "Intensity-modulated radiotherapy (IMRT) and conventional three-dimensional conformal radiotherapy for high-grade gliomas: does IMRT increase the integral dose to normal brain?." International Journal of Radiation Oncology* Biology* Physics 67.4 (2007): 1135-1144.

[12] Mackie, T. Rock, et al. "Tomotherapy: a new concept for the delivery of dynamic conformal radiotherapy." Medical physics 20.6 (1993): 1709-1719.

[13] Yu, Cedric X. "Intensity-modulated arc therapy with dynamic multileaf collimation: an alternative to tomotherapy." Physics in Medicine & Biology 40.9 (1995): 1435.

[14] Otto, Karl. "Volumetric modulated arc therapy: IMRT in a single gantry arc." Medical physics 35.1 (2008): 310-317.

[15] Wang, Chao, et al. "Arc-modulated radiation therapy (AMRT): a single-arc form of intensity-modulated arc therapy." Physics in Medicine & Biology 53.22 (2008): 6291.

[16] Ślosarek, Krzysztof, et al. "Integral dose: Comparison between four techniques for prostate radiotherapy." Reports of Practical Oncology and Radiotherapy 20.2 (2015): 99-103.

[17] Davidson, Melanie TM, et al. "Assessing the role of volumetric modulated arc therapy (VMAT) relative to IMRT and helical tomotherapy in the management of localized, locally advanced, and post-operative prostate cancer." International Journal of Radiation Oncology* Biology* Physics 80.5 (2011): 1550-1558.

[18] Quan, Enzhuo M., et al. "A comprehensive comparison of IMRT and VMAT plan quality for prostate cancer treatment." International Journal of Radiation Oncology* Biology* Physics 83.4 (2012): 1169-1178.

[19] Rao, Min, et al. "Comparison of Elekta VMAT with helical tomotherapy and fixed field IMRT: plan quality, delivery efficiency and accuracy." Medical physics 37.3 (2010): 1350-1359.

[20] Wilson, Robert R. "Radiological use of fast protons." Radiology 47.5 (1946): 487-491.

[21] Tobias, C. A., et al. "Pituitary irradiation with high-energy proton beams a preliminary report." Cancer research 18.2 (1958): 121-134.

[22] Kooy, H. M., and C. Grassberger. "Intensity modulated proton therapy." The British journal of radiology 88.1051 (2015): 20150195.

[23] Kase, Yuki, et al. "A treatment planning comparison of passive-scattering and intensity-modulated proton therapy for typical tumor sites." Journal of radiation research 53.2 (2012): 272-280.

[24] Sandison, George A., et al. "Phantom assessment of lung dose from proton arc therapy." International journal of radiation oncology, biology, physics 38.4 (1997): 891-897.

[25] Seco, Joao, et al. "Proton arc reduces range uncertainty effects and improves conformality compared with photon volumetric modulated arc therapy in stereotactic body radiation therapy for non-small cell lung cancer." International Journal of Radiation Oncology* Biology* Physics 87.1 (2013): 188-194.

[26] Rah, Jeong-Eun, et al. "A treatment planning study of proton arc therapy for para-aortic lymph node tumors: dosimetric evaluation of conventional proton therapy, proton arc therapy, and intensity modulated radiotherapy." Radiation Oncology 11.1 (2016): 1-10.

[27] Sanchez-Parcerisa, Daniel, et al. "Range optimization for mono-and bi-energetic proton modulated arc therapy with pencil beam scanning." Physics in Medicine & Biology 61.21 (2016): N565.

[28] Ding, Xuanfeng, et al. "Spot-scanning proton arc (SPArc) therapy: the first robust and delivery-efficient spot-scanning proton arc therapy." International Journal of Radiation Oncology* Biology* Physics 96.5 (2016): 1107-1116.

[29] Ding, Xuanfeng, et al. "Improving dosimetric outcome for hippocampus and cochlea sparing whole brain radiotherapy using spot-scanning proton arc therapy." Acta Oncologica 58.4 (2019): 483-490.

[30] Ding, Xuanfeng, et al. "Have we reached proton beam therapy dosimetric limitations?–A novel robust, delivery-efficient and continuous spot-scanning proton arc (SPArc) therapy is to improve the dosimetric outcome in treating prostate cancer." Acta Oncologica 57.3 (2018): 435-437.

[31] Chang, Sheng, et al. "Feasibility study: spot-scanning proton arc therapy (SPArc) for left-sided whole breast radiotherapy." Radiation Oncology 15.1 (2020): 1-11.

[32] Liu, Gang, et al. "Improve the dosimetric outcome in bilateral head and neck cancer (HNC) treatment using spot-scanning proton arc (SPArc) therapy: a feasibility study." Radiation Oncology 15.1 (2020): 1-11.

[33] Liu, Gang et al. “A novel energy sequence optimization algorithm for efficient spot-scanning proton arc (SPArc) treatment delivery.” Acta oncologica (Stockholm, Sweden) vol. 59,10 (2020): 1178-1185. doi:10.1080/0284186X.2020.1765415

[34] Li, Xiaoqiang, et al. "The first prototype of spot-scanning proton arc treatment delivery." Radiotherapy and Oncology 137 (2019): 130-136.

[35] Liu, Gang, et al. "Lung stereotactic body radiotherapy (SBRT) using Spot-scanning Proton Arc (SPArc) therapy: A feasibility study." Frontiers in Oncology 11 (2021): 1245.

[36] Liu, Gang, et al. "Is proton beam therapy ready for single fraction spine SBRS?–a feasibility study to use spot-scanning proton arc (SPArc) therapy to improve the robustness and dosimetric plan quality." Acta Oncologica 60.5 (2021): 653-657.

[37] Toussaint, Laura, et al. "Towards proton arc therapy: physical and biologically equivalent doses with increasing number of beams in pediatric brain irradiation." Acta oncologica 58.10 (2019): 1451-1456.

[38] Wilkens, Jan J., and Uwe Oelfke. "Optimization of radiobiological effects in intensity modulated proton therapy." Medical physics 32.2 (2005): 455-465.

[39] McNamara, Aimee L., Jan Schuemann, and Harald Paganetti. "A phenomenological relative biological effectiveness (RBE) model for proton therapy based on all published in vitro cell survival data." Physics in Medicine & Biology 60.21 (2015): 8399.

[40] Rørvik, Eivind, et al. "Exploration and application of phenomenological RBE models for proton therapy." Physics in Medicine & Biology 63.18 (2018): 185013.

[41] Aitkenhead, Adam H., et al. "Automated Monte-Carlo re-calculation of proton therapy plans using Geant4/Gate: implementation and comparison to plan-specific quality assurance measurements." The British Journal of Radiology 93.1114 (2020): 20200228.

[42] Cao, Wenhua, et al. "Linear energy transfer incorporated intensity modulated proton therapy optimization." Physics in Medicine & Biology 63.1 (2017): 015013.

[43] Unkelbach, Jan, et al. "Reoptimization of intensity modulated proton therapy plans based on linear energy transfer." International Journal of Radiation Oncology* Biology* Physics 96.5 (2016): 1097-1106.

[44] Ödén, J., and E. Traneus. "Introducing proton track-end objectives as a tool to mitigate the elevated relative biological effectiveness in critical structures." International Journal of Radiation Oncology, Biology, Physics 99.2 (2017): E705.

[45] Li, Xiaoqiang, et al. "Linear Energy Transfer Incorporated Spot-Scanning Proton Arc Therapy Optimization: A Feasibility Study." Frontiers in Oncology (2021): 2636.

[46] Sánchez-Parcerisa, Daniel, et al. "Fast range switching of passively scattered proton beams using a modulation wheel and dynamic beam current modulation." Physics in Medicine & Biology 59.7 (2014): N19.

[47] Kanai, Tatsuaki, et al. "Broad beam three-dimensional irradiation for proton radiotherapy." Medical physics 10.3 (1983): 344-346.

[48] T. E. Merchant, C.-h. Hua, H. Shukla, X. Ying, S. Nill, U. Oelfke, Proton versus photon radiotherapy for common pediatric brain tumors: comparison of models of dose characteristics and their relationship to cognitive function, Pediatric blood & cancer 51 (1) (2008) 110–117.

[49] Bortfeld, Thomas. "An analytical approximation of the Bragg curve for therapeutic proton beams." Medical physics 24.12 (1997): 2024-2033.

[50] Rana, Suresh, et al. "Radiobiological and dosimetric impact of RayStation pencil beam and Monte Carlo algorithms on intensity-modulated proton therapy breast cancer plans." Journal of applied clinical medical physics 20.8 (2019): 36-46.

[51] Liang, Xiaoying, et al. "A comprehensive dosimetric study of Monte Carlo and pencil-beam algorithms on intensity-modulated proton therapy for breast cancer." Journal of applied clinical medical physics 20.1 (2019): 128-136.

[52] Fredriksson, Albin, and Rasmus Bokrantz. "A critical evaluation of worst case optimization methods for robust intensity-modulated proton therapy planning." Medical physics 41.8Part1 (2014): 081701.

[53] Wright, Stephen, and Jorge Nocedal. "Numerical optimization." Springer Science 35.67-68 (1999): 7

[54] Nocedal, Jorge, Andreas Wächter, and Richard A. Waltz. "Adaptive barrier update strategies for nonlinear interior methods." SIAM Journal on Optimization 19.4 (2009): 1674-1693.

[55] Drzymala, R. E., et al. "Dose-volume histograms." International Journal of Radiation Oncology* Biology* Physics 21.1 (1991)

[56] Feuvret, Loïc, et al. "Conformity index: a review." International Journal of Radiation Oncology* Biology* Physics 64.2 (2006): 333-342.

[57] Huchet, A., et al. "[Volume-effect and radiotherapy [II]. Part II: volume-effect and normal tissue]." Cancer radiotherapie: journal de la Societe francaise de radiotherapie oncologique 7.5 (2003): 353-362.

[58] Lomax, Nicoletta J., and Stefan G. Scheib. "Quantifying the degree of conformity in radiosurgery treatment planning." International Journal of Radiation Oncology* Biology* Physics 55.5 (2003): 1409-1419.

[59] Van't Riet, Arie, et al. "A conformation number to quantify the degree of conformality in brachytherapy and external beam irradiation: application to the prostate." International Journal of Radiation Oncology* Biology* Physics 37.3 (1997): 731-736.

[60] Xu, Yihang, et al. "Assessment of daily dose accumulation for robustly optimized intensity modulated proton therapy treatment of prostate cancer." Physica Medica 81 (2021): 77-85

[61] Eros Pedroni. “Gantries”. https://www.ptcog.ch/archive/conference_p&t&v/PTCOG49/presentationsEW/18-1_gantries.pdf (PTCOG conference 2010). Accessed [2022 March 19th].

[62] Sheng, Yinxiangzi, et al. "Performance of a 6D treatment chair for patient positioning in an upright posture for fixed ion beam lines." Frontiers in oncology 10 (2020): 122.

Chapter 2. Proton arc therapy: a study of the inherent robustness to treatment uncertainties

Authors

[*,†]Yunzhou Xia

[*,†]Adam H Aitkenhead

[†,‡]Robert Appleby

[*,†,‡]Michael J Merchant

[*,†]Neil G Burnet

[†]Matthew Lowe

[*,†,‡]Karen J Kirkby

[*,†]Ranald I MacKay

Affiliations

[*]Division of Cancer Sciences, Faculty of Biology, Medicine and Health, University of Manchester, United Kingdom

[†]Christie Medical Physics and Engineering, The Christie NHS Foundation Trust, Manchester, United Kingdom

[‡]Cockcroft Institute, United Kingdom

2.1 Rationale and strategy

Proton arc therapy (PAT) has the potential to further improve plan quality compared to intensity-modulated proton therapy (IMPT). However, it was not previously understood whether the robustness would also improve in PAT plans. There was also a lack of evidence for feasibility of PAT treated for brain and head and neck patients at the start of this work. I examined PAT plans optimised with full energies (full-energy PAT or FPAT) for three representative cases, which include one brain and two head and neck cases, and compared to their IMPT plans in terms of the physical dose distributions and robustness under typical range and setup uncertainties. As there was no treatment planning tool available at the time for studying PAT, a 2D dose optimisation program written in Python which was originally used for IMPT investigations [19] was adapted to support the relevant dose optimisation and plan evaluation functions for PAT.

Individual author contributions are as follows. Mathew Lowe provided the 2D dose optimisation program written in Python [19]. The Python code initially supported a simple dose calculation engine in water based on convolution of a pencil beam kernel with every spot location. I upgraded this to calculate dose distribution based on a single Gaussian model (a longitudinal IDD with Gaussian lateral profiles) with IDDs and lateral profiles being the beam commissioning data previously measured at Christie proton therapy centre. I also upgraded the dose engine to support calculations in non-homogeneous material. The Python code originally supported phantoms in .png file format where different colour pixels represented different structures. I extended the code to support calculations on DICOM CT and DICOM structure data. The Python code originally supported calculations for gantry angles of multiples of 90 degrees. I upgraded this to support any gantry angle from 0 – 360 degrees. Initially, the inverse dose optimisation supported minimum dose, maximum dose, and prescription dose objectives. I extended this to additionally cover DVH and normal tissue objectives to mimic clinical objective settings. I also upgraded the speed of dose optimisation by the use of fluence maps rather than full dose reconstruction at every iteration. In addition, I added functions including metric evaluations, robustness evaluation, DVH / DVH band visualisation, and box plots of metrics.

Adam H. Aitkenhead and Matthew Lowe provided medical physics advice including the planning procedures for the patient cases provided by Adam H. Aitkenhead. Michael J. Merchant, Robert Appleby, and Ranald I. MacKay provided physics related advice. Neil H. Burnet provided clinical advice including integral dose evaluation and discussion. Karen J. Kirkby provided the opportunity of project funding. Michael J. Merchant, Adam H. Aitkenhead, Robert Appleby, and Ranald I. MacKay also gave daily supervision over this work. All authors have read and commented on the manuscript.

2.2 Abstract

Purpose: The study aimed to compare the robustness of proton arc therapy (PAT) plans to intensity-modulated proton therapy (IMPT) plans.

Patient and methods: PAT and IMPT plans for one brain and two head and neck (H&N) cases were optimized in the Python environment. The PAT plans were approximated as closely spaced fixed-angle IMPT fields (i.e., unconstrained PAT) and were evaluated in terms of conformality (CI), homogeneity (HI), and sparing of healthy tissue under nominal, range uncertainties and setup uncertainties. Range uncertainties were simulated as ± 3% proton stopping power; setup errors were simulated as a systematic shift of up to ±3 mm with a random shift drawn from a Gaussian distribution of width 2 mm for individual fractions.

Results: In the nominal scenarios for all cases studied, PAT gave similar or better target conformality and homogeneity in comparison to IMPT and reduced the high-dose (> 10 Gy for a prescribed dose of 50 - 60 Gy) volume of organs-at-risk, normal tissue and skin. PAT improved target robustness in terms of CI and HI for the brain case under range and setup uncertainties, and for the H&N cases under range uncertainties: for example, in the brain case, the standard deviation of CI was reduced by 46% in the PAT plan under range errors, and by 41% under setup errors; in the unilateral H&N case, the standard deviation of CI was the same for both plans under range errors, and increased by 0.02 in the PAT plan under setup uncertainties; in the bilateral H&N case, the standard deviation of CI for PTV1 reduced by 81% in the PAT plan under range uncertainties, and increased by 0.02 under setup uncertainties. However, the PAT plans were less robust than the IMPT plans under setup uncertainties for the H&N cases.

Conclusion: PAT intrinsically improved the target robustness compared to IMPT under range and setup uncertainties, but results suggest that this depends on the tumour geometry.

Keywords: proton arc therapy; intensity-modulated proton therapy; range uncertainty; setup uncertainty; robustness.

2.3 Introduction

Since the 1960s, X-ray radiation therapy has developed from rectangular field treatment, through conformal radiation therapy [1] to intensity modulated radiation therapy [2] - [7] and then to arc therapy with many possible implementations [8] - [14]. As can be seen, the direction of X-ray radiation therapy development has been towards increasing conformality through the use of inverse treatment planning, computerized control of multi-leaf collimators and arc therapy which also provides the benefit of faster delivery. The development of proton therapy is unsurprisingly similar, with passively scattered proton therapy analogous to conformal radiation therapy, and intensity modulated proton therapy (IMPT) analogous to IMRT. This analogy between X-ray and proton therapy naturally leads to the question: with proton's advantage in sparing distal tissue, can proton arc therapy (PAT) also improve plan conformality and delivery speed compared to IMPT?

Plan comparison studies have previously shown that PAT plans improve target conformality, homogeneity and planning target volume (PTV) coverage for lung cancer [15] [16] and para-aortic lymph node cancer [17]. Organ-at-risk (OAR) and normal tissue sparing can be superior to IMPT for both oropharyngeal and non-mobile lung cases [16] and is similar to IMPT for para-aortic lymph node cases [17]. Moreover, PAT has been shown to reduce range uncertainty effects in lung cancer [15]. For the stomach, small bowel and liver, the normal tissue complication probabilities in para-aortic lymph node tumours were calculated using the Lyman-Kutcher-Butcher model and found to be lower in the PAT plan than passively scattered proton therapy [17]. These studies agree that PAT offers similar or even improved planned dose distributions as IMPT. In these studies, proton arc plans were approximated as static fixed-angle plans with closely spaced beams and optimized in either commercial or in-house treatment planning software.

The existing literature has demonstrated that PAT provides dosimetric improvements for the targets and OARs, despite the increased low dose volume as a result of arc plans (discussed in section 4). However, proton therapy can be sensitive to treatment uncertainties [18]. With a proton beam delivered from a

larger number of control points (i.e., beam angles), the robustness of PAT is expected to be better. This study aims to test this hypothesis by evaluating PAT plans' robustness to two common treatment uncertainties: range and patient setup uncertainties, by comparing PAT planned dose distributions, dose-volume histograms (DVH) and DVH metrics to clinician-approved IMPT plans for three clinically representative cases.

2.4 Patients and Methods

This study is a retrospective analysis of patient treatment plans. The patients gave consent for their data to be used for research purposes. All data was handled according to the General Data Protection Regulations. The research was approved by the Radiotherapy Related Research committee at the Christie NHS Foundation Trust.

2.4.1 The optimization program

A 2-dimensional (2D) spot-scanning IMPT treatment planning program was developed in Python (version 2.7) in a research environment based on work by Lowe et al [19]. The program was used to optimize both IMPT and PAT plans, where PAT plans were approximated as closely spaced fixed-angle IMPT control points. The angle between adjacent control points in PAT plans was chosen to be 10° [15]. The PAT plans in this study were unconstrained PAT which we define as PAT planned without layer reduction. Unconstrained and constrained PAT will be discussed further in section 2.6.1.

2.4.2 Beam profiles and dose calculation

The beam model was approximated as a longitudinal profile (i.e., Bragg peaks) derived from interpolations of the commissioning measurements in water for a Varian ProBeam system, spread laterally (i.e., perpendicular to the beam direction) by a single Gaussian profile. The technique of interpolation was based on Bortfeld's analytical equations for Bragg curves with the assumption that the

width of energy straggling given as $\sigma = 0.012R^{0.935}$ [20] could be approximated as $\sigma = c^2R$ [21], where σ is the standard deviation of energy straggling in MeV, R is the proton range in centimetres, and c^2 is a constant. Appendix A shows comparisons of the interpolated Bragg peaks of four example energies to Monte Carlo (MC) simulations, showing good agreement within 2% error. The width of the lateral Gaussian profile of a specific beam energy was taken from the MC simulated width at the Bragg peak location of a mono-energetic proton beam in water.

For each beam angle, the energies were chosen such that the depth of the distal 80% of the Bragg peak of one energy coincides with the depth of proximal 80% Bragg peak magnitude of the higher energy [22]. A range shifter with water equivalent thickness of 3 centimetres was used for the H&N IMPT plans; no range shifters were needed for the PAT plans (discussed in section 2.6). Finally, the total dose was calculated by summing up the dose contributions from all beams at all angles.

2.4.3 Optimization

The optimization algorithm used was ‘L-BFGS’ (limited memory Broyden-Fletcher-Goldfarb-Shanno) from SciPy’s (version 0.13.3) optimization library. L-BFGS is an established optimization algorithm used in many studies of ion therapy [23, 24, 25]. Spot weights of all control points were optimized simultaneously to meet DVH objectives. A lower bound of zero was placed on all spot weights to ensure no negative weightings. No minimum MU was used to remove the low-weighted spots as deliverability was not the focus of the paper. We planned to an additional margin to the clinical target volume (CTV), the planning target volume (PTV). As the goal was to investigate the intrinsic robustness of PAT plans, plans were optimized without robust optimization (discussed in section 2.6). The objective function can be expressed as in equation 2-1:

Equation 2-1: Total objective function to be minimised in proton therapy inverse dose optimisation.

$$minimize\ F(w) = F_m(w) + \sum u_c f_c(w),$$

$$subject\ to\ w \geq 0$$

where $F(w)$ is the overall objective function to be minimized, w is the spot weights, and $f_c(w)$ is the individual component of the overall cost function with relative weighting u_c. $F_m(w)$, as defined in equation 2-2, is the cost function for the additional margin outside the PTV to aid a smooth dose fall off at the PTV boundary and so to avoid high doses just outside the PTV,

Equation 2-2: NTO function used for constraining the dose in the vicinity of PTV.

$$F_m = \sum_{i \in margin} (d_i - p_i)^2\ for\ \ d_i > p_i,$$

where d_i is the dose in voxel i and p_i is the upper dose objective for voxel i in the margin.

Quadratic cost functions [26] were used for penalizing overdose or underdose for the target and OARs. Penalty for overdose or underdose is defined in equation 2-3 and 2-4, with $d_i > d_c$ or $d_i < d_c$ respectively,

Equation 2-3: Quadratic form of the dose objective function.

$$A_c = \sum_{d_i > d_c\ or\ d_i < d_c} (d_c - d_i)^2$$

Equation 2-4: Objective function for dose volume histogram objectives.

$$f_c = \begin{cases} \dfrac{p - V_c}{p} A_c & if\ p > V_c \\ 0 & if\ p \leq V_c \end{cases}$$

where f_c is the individual cost function as in equation 2-1, d_i is the dose to a voxel of the structure that receives higher or lower dose than the upper or lower dose objective d_c, V_c is the fractional volume objective, and p is the fractional volume that does not meet the objective.

PAT plans were approximated as many-beam multi-field optimization (MFO) IMPT. MFO was carried out for both IMPT and PAT plans, with a convergence criterion of less than 0.1% change in the cost function, which guaranteed convergence on the cost function in all the plans studied.

2.4.4 Patient selection and treatment planning

Three clinical cases that represent a range of typical brain and head and neck geometries were studied.

1. ependymoma,
2. unilateral head & neck (H&N): left sub-mandibular, and
3. bilateral H&N: oropharynx, left base of tongue.

A transverse slice of each case was selected based on how well the slice represented the three-dimensional case. The Computed-Tomography (CT) scans of the chosen slices, contours of volumes of interests (VOIs), and the planned beam angles are shown in figure 2-1. In all cases, the beam angles were chosen to avoid angles that go through critical organs or that are particularly susceptible to treatment uncertainties, so partial arcs were used to spare the contralateral sides [27, 28]. Spots were placed over the PTV with an additional margin for which the dose objective at the edge of the PTV was 95% of the prescription dose and at the exterior edge of the margin was 5% of the prescription dose. The optimization objectives of all three cases were taken from their original clinical plans and are summarized in Appendix B table A.1 - A.3 respectively.

1. Ependymoma (figure 2-1(a)). This case was planned with 2 beams at [120°, 240°] and couch angles of [0°, 0°], using the IEC (International Electrotechnical

Commission) gantry angle convention, for the IMPT plan to avoid high-dose irradiation of the brainstem in case of treatment uncertainties. PAT was planned with 19 beams at 10° increments between 90° and 270°. The upper half arc was excluded as the target is posterior to the brainstem. The primary OAR of interest was the brainstem as it is dose-limiting. Since the brainstem overlaps the PTV, the dose objective for the non-overlapping part was 54 Gy, and for the overlapping part was 52.8 Gy.

2. Unilateral H&N (figure 2-1(b)). IMPT was planned with 2 beams at [35°, 145°] and couch angles of [0°, 0°] which were chosen as angles between two extremes: two opposite angles (e.g., 5° and 185°) were undesirable as the use of MFO meant that any uncertainties would cause an inhomogeneous dose distribution in the target, while two close angles would deposit a high dose at the proximal edge which could damage healthy tissue under uncertainties. PAT was planned with 19 beams at 10° increment from 5° to 185°. The primary OAR was the left parotid. Skin dose was of interest as the target is shallow. The dose prescription was 60 Gy to the PTV.

3. Bilateral H&N (figure 2-1(c)). The IMPT plan was planned with 5 beams at [0°, 55°, 140°, 220°, 355°] with no couch rotations. The PAT plan was planned with 29 beams at 10° increment from 140° to 220° to avoid radiation traversing the spinal cord. The dose prescription was 65 Gy for PTV1 and 54 Gy for PTV2.

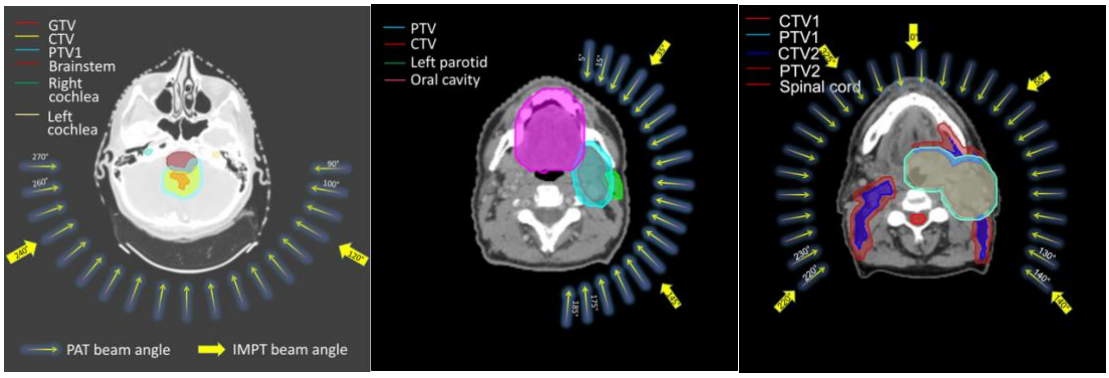

Figure 2-1: Beam angles for IMPT (wide arrows) and PAT plans (thin arrows) are overlaid on the CTs of the three clinical cases studied: (a (left)) ependymoma , (b (middle)) unilateral head & neck and (c (right)) bilateral head & neck visualized in Dicompyler (version 0.4.2). Targets and organs at risk are contoured on top of the CTs.

2.4.5 Plan evaluation

Plan dose distributions were evaluated using a variety of metrics. The evaluation metrics were conformality index ($CI_{95\%}$), homogeneity index (*HI*), OAR $V_{30,60,90\%}$, normal tissue and skin $V_{10,20,30Gy}$, and integral dose (*ID*).

$CI_{95\%}$ was defined as the fraction of the PTV volume receiving at least 95% of the prescription dose, as given in equation 2-5 [15, 16].

Equation 2-5: A definition of the conformality index.

$$CI_{95\%} = \frac{V_{95\%}}{V_{PTV}}$$

where $V_{95\%}$ is the volume of the PTV receiving at least 95% of prescribed dose and V_{PTV} is the volume of PTV. A larger conformality index that is closer to one means a higher target conformality.

The homogeneity index (*HI*) was defined as the ratio of the maximum dose level in the PTV to the prescribed dose, as given in equation 2-6 [15]:

Equation 2-6: A definition of the homogeneity index.

$$HI = \frac{D_{max}}{D_p}$$

where D_{max} is the maximum dose in the PTV and D_p is the prescribed dose for the target. A smaller value that is closer to one indicates a more homogeneous dose in the target.

OAR $V_{30,60,90\%}$ were defined as the fractional volume of OAR receiving at least 30%, 60% and 90% of the upper dose objective of these structures. Skin and

normal tissue $V_{10,20,30Gy}$ were the fractional volume of skin or normal tissue receiving at least 10, 20 and 30 Gy. Smaller values of V_x indicate better sparing at the *x* dose level.

The integral dose within a structure was defined as in equation 2-7 [29]:

Equation 2-7: Definition of the integral dose.

$$ID = \sum_i D_i v_i \rho_i$$

where the integral dose (ID) was the product of the dose D in voxel i (Gy), the volume v (cm^3) and the mass density ρ (kg/cm^3) of voxel i integrated over all voxels in that structure. This gives the integral dose the unit of energy (J). This definition of the integral dose based on the mass integral rather than a volume integral (without the density term) best represents the total energy deposited within the structure. As the dose calculation is carried out in 2D, the integral dose was integrated over a slice of the dose grid with resolution in three directions the same as a CT voxel.

2.4.6 Error scenarios

Two types of error scenarios were simulated independently: a percentage error in the beam range and a patient setup error assuming fractionated treatment.

- Range errors were simulated as −3% to +3% error in the stopping power of protons at an increment of 1% [30].
- Setup errors were evaluated as a systematic setup error of up to 3 mm with fractional setup errors which were drawn randomly from a Gaussian distribution with a standard deviation of 2 mm [31].

For a fair comparison between IMPT and PAT plans, both IMPT and PAT plans were independently reviewed by an experienced clinician at the Christie Hospital NHS, Manchester (N G Burnet) to ensure the plans would be clinically acceptable.

Both IMPT and PAT were pushed equally hard in the optimization process by using identical convergence criteria and optimization objectives.

2.5 Results

Sections 2.5.1 - 2.5.3 give narratives of the results for ependymoma, unilateral H&N and bilateral H&N respectively. Section 2.5.4 gives results on the integral dose. Tables of the complete metric values are provided in Appendix C.

2.5.1 Ependymoma

Figure 2-2(a) and figure 2-2(b) show the nominal IMPT and PAT plans of the ependymoma case. The PTV receives the prescription dose in both plans. In the PAT plan, the 10 to 30 Gy isodose lines are more conformed to the PTV. These two observations are supported by their DVHs shown in figure 2-5(a) where the PTV's DVHs are similarly sharp at the prescription dose level 54 Gy and the normal tissue DVH leans more towards lower doses in PAT. The doses to the brainstem overlapping the PTV and the sparing of the non-overlapping parts are similar in both plans. The DVHs of the left cochlea, normal tissue and skin show sparing with PAT above 3, 10 and 7 Gy respectively compared to IMPT.

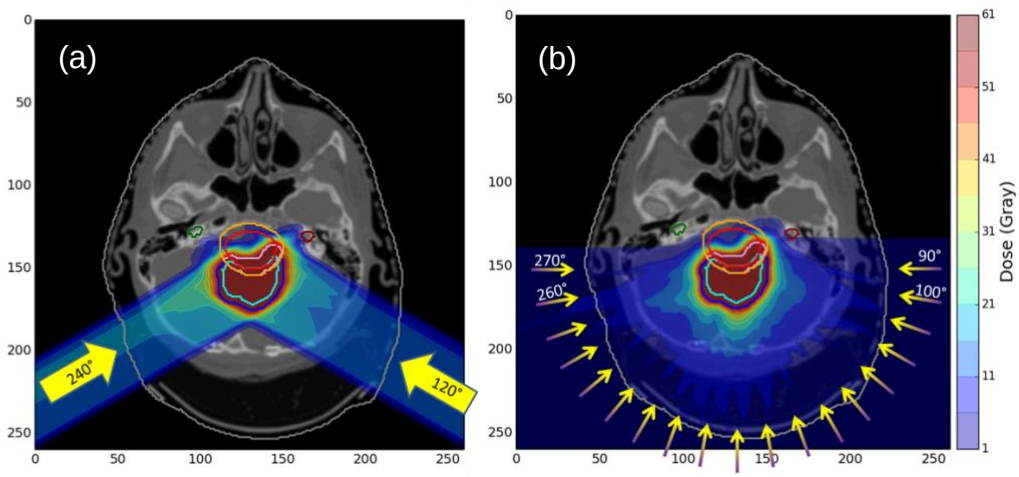

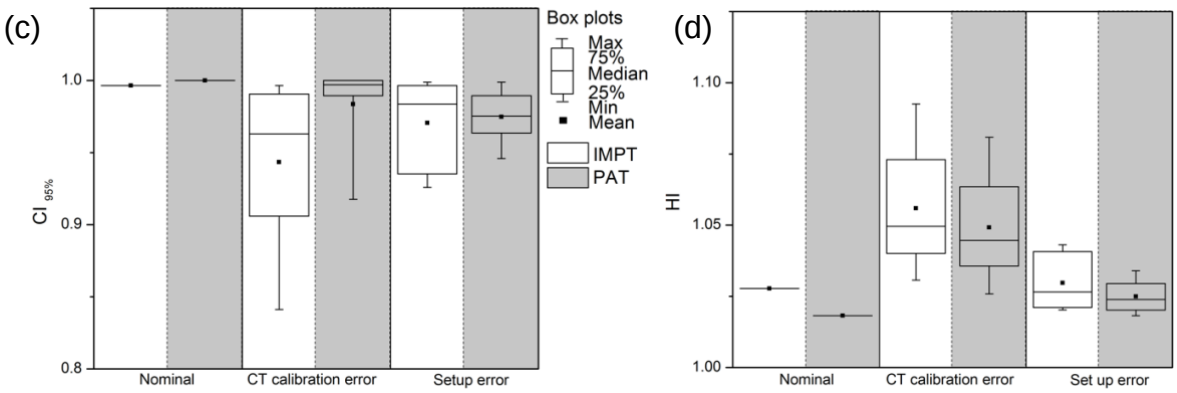

Figure 2-2: Ependymoma case. (a) 2-beam IMPT plan; (b) 19-beam PAT plan; (c) Distributions of target conformality index CI_(95%) and (d) homogeneity index HI under nominal, range errors and setup errors. The mean values (higher for CI_(95%) lower for HI) indicate PAT's higher robustness. DVH is given in figure 2-5(a); metrics of the ependymoma case are summarized in Appendix C table 2-4.

The distributions of $CI_{95\%}$ and *HI* under nominal, range and setup errors are shown in figures 2-2(c) and 2-2(d). In the nominal scenario, PAT has higher mean conformality and homogeneity (Appendix C). Under both range and setup errors, $CI_{95\%}$ has higher mean values and smaller standard deviations. In the PAT plan, the differences between the nominal $CI_{95\%}$ and mean values of $CI_{95\%}$ are always smaller than IMPT under range errors and similar to IMPT under setup errors. This suggests PAT is less sensitive to range errors and similar in robustness to setup errors. The mean HI under both range and setup errors are smaller in the PAT plan with almost half the standard deviation under setup errors, suggesting PAT improves the robustness, more so under setup errors.

2.5.2 Unilateral head and neck

Figure 2-3(a) and 2-3(b) show the nominal dose distributions of the IMPT and PAT plans for the unilateral H&N case. The PTV receives the prescription dose in both plans. The isodose lines 20 to 40 Gy are more conformed to the target in the PAT plan. The left parotid receives significantly less dose for the non-overlapping part with the target. This can be seen as the lower DVH line for the PAT plan in figure 2-6(b). The normal tissue and skin are relatively spared from dose levels above 13 Gy.

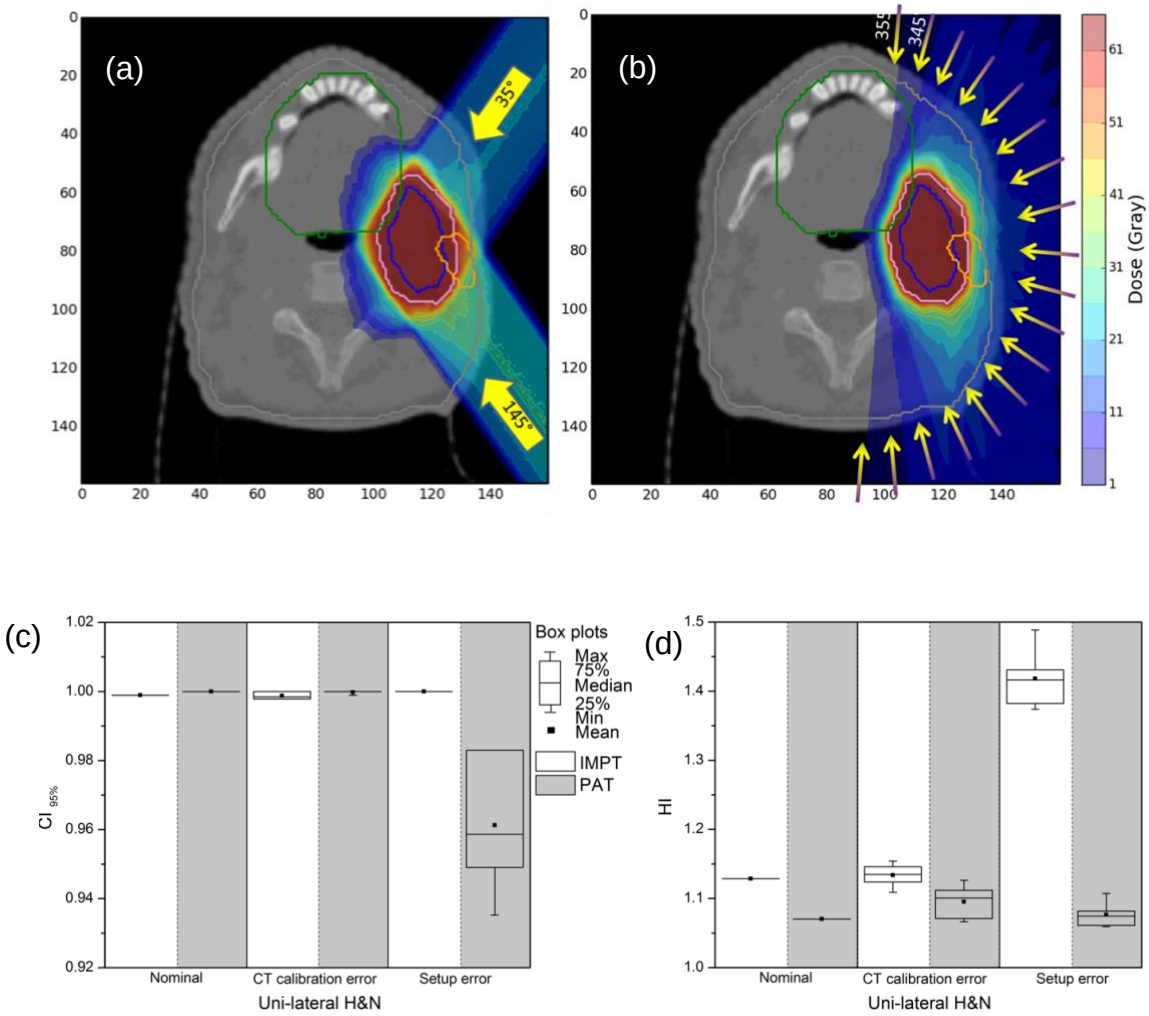

Figure 2-3: Unilateral head and neck case. (a) 2-beam IMPT plan; (b) 19-beam PAT plan; (c) Conformality index CI (95%); (d) homogeneity index HI. The mean CI(95%) indicate that PAT has higher robustness to range errors and worse robustness to setup errors compared to IMPT. PAT plans have lower homogeneity under range and setup errors than IMPT. DVH is given in figure 2-5(b); metrics of the unilateral H&N case are summarized in Appendix C table 2-5.

The distributions of $CI_{95\%}$ and *HI* under nominal, range and setup errors are shown in figure 2-8(b) to 2-8(c). In the nominal scenario and under range errors, PAT and IMPT have similar conformality (Appendix C table 2-5). PAT has worse robustness in terms of CI under setup errors. Under all types of scenarios, PAT has smaller *HI*. This suggests that PAT is more robust than IMPT under range errors but less robust under setup errors.

2.5.3 Bilateral head and neck

Figure 2-4(a) and 2-4(b) show the nominal dose distributions of the bilateral H&N case. PTV1 and PTV2 both receive the prescription doses in IMPT and PAT plans.

The metrics under nominal, range and setup errors are shown in figure 2-4(b) to 4(e). In the nominal scenario for PTV2 (lower dose level), target conformality and homogeneity are similar in PAT and IMPT plans (Appendix C table 2-6); under range errors, PAT has higher CI and similar *HI* to IMPT; under setup errors, PAT has lower *CI* and *HI* than IMPT. For PTV1 (higher dose level), *CI* and *HI* are similar in PAT and IMPT plans; under range errors, PAT has higher *CI* with a smaller standard deviation and larger *HI* with a larger standard deviation; under setup errors, PAT has lower *CI* and *HI*. This suggests that PAT can be more robust to range errors but less robust to setup errors.

(the rest of this page intentionally left blank)

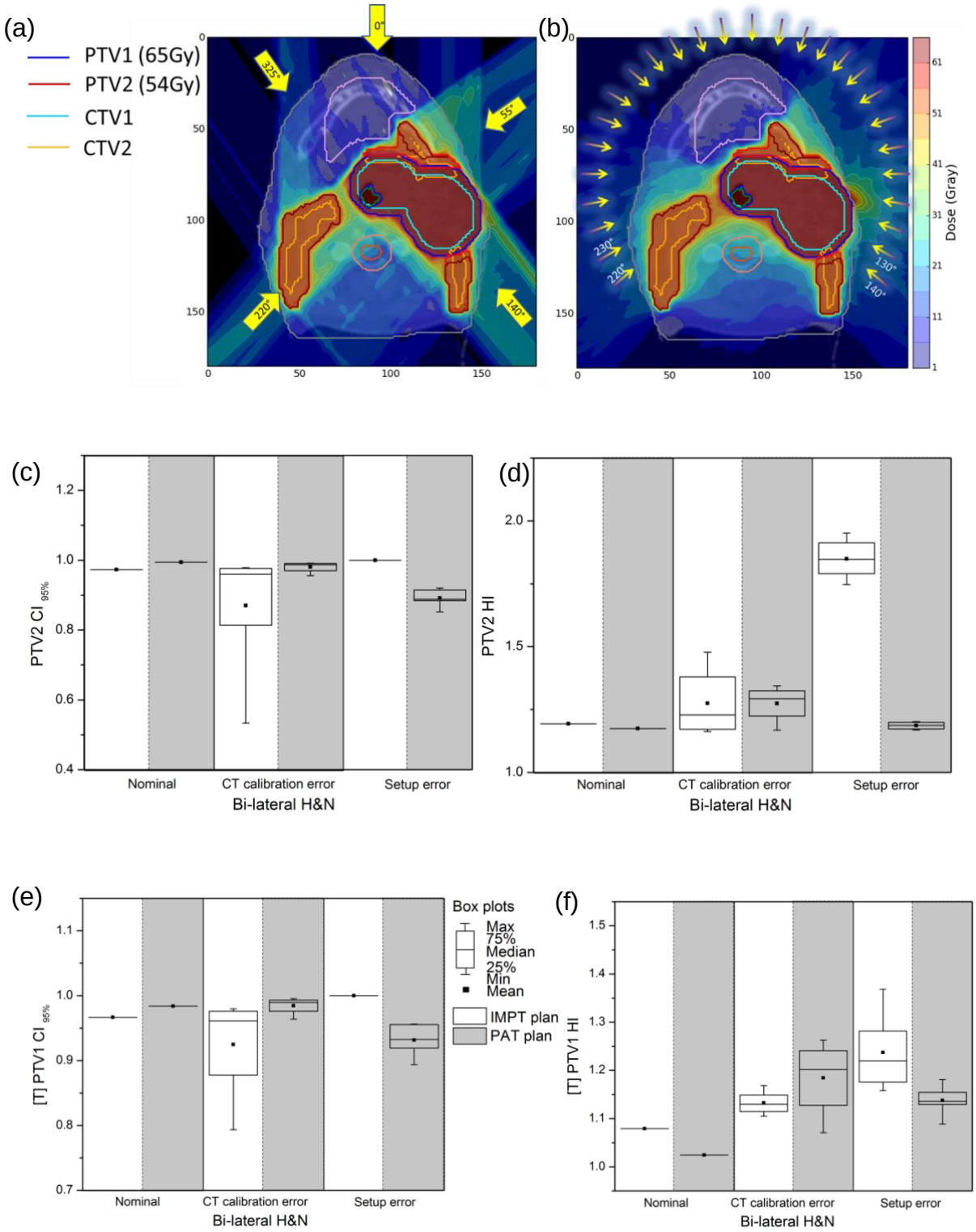

Figure 2-4: Bilateral H&N case. (a) 5-beam IMPT plan; (b) 29-beam PAT plan;

(c) PTV2 (low dose level) conformality index CI_(95%), (d) PTV2 homogeneity index HI, (e) PTV1 CI_(95%) and (f) PTV1 HI. DVH is given in figure 2-5 (c); metrics of the bilateral H&N case are summarized in Appendix C table 2-6.

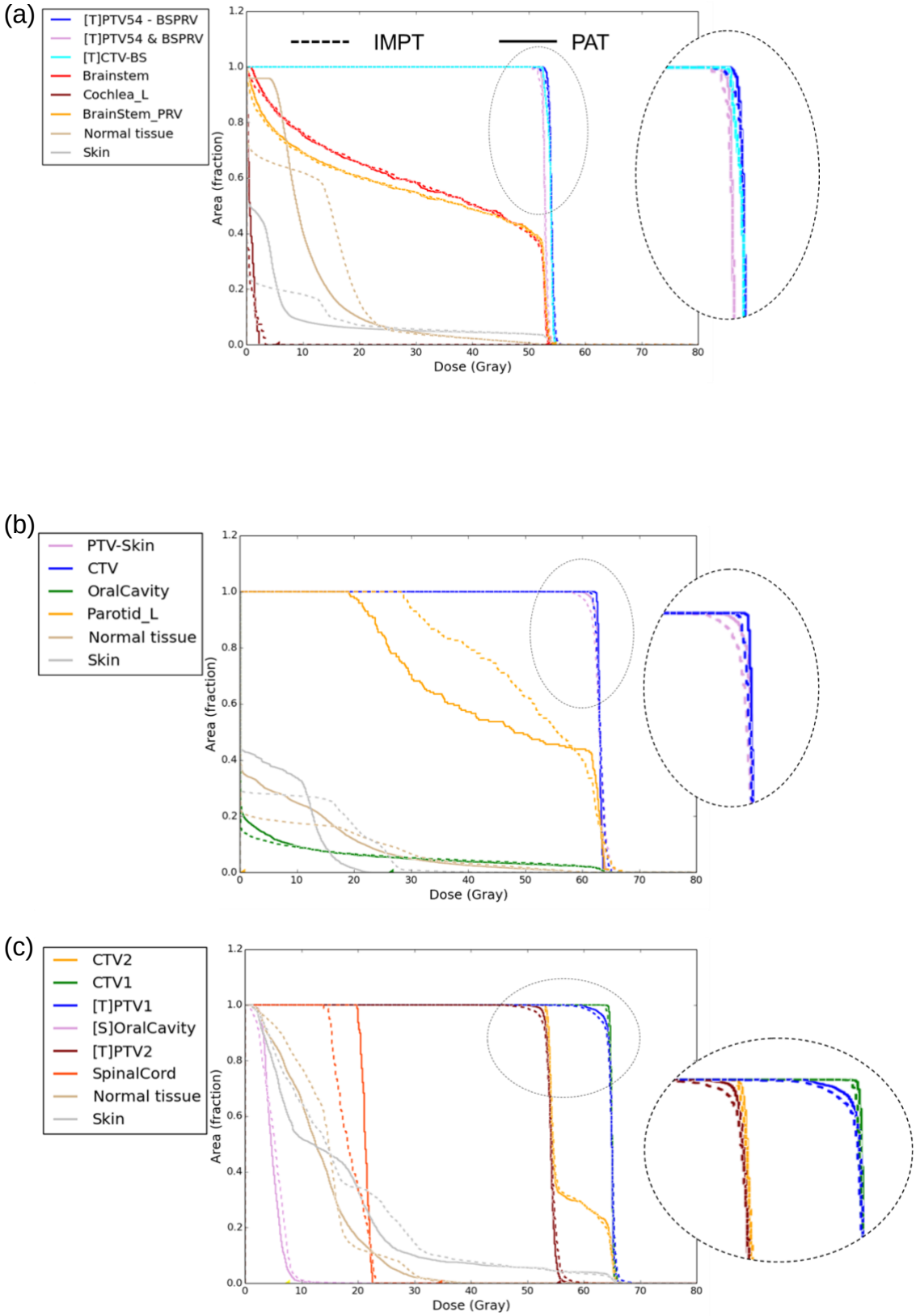

Figure 2-5: DVHs of (a) the ependymoma case, (b) unilateral H&N, and (c) bilateral H&N planned with IMPT (dashed) and PAT (solid). PAT gives similar target doses and spares normal tissue structures.

2.5.4 Integral dose

The difference in the integral dose in the nominal cases received by the main structures in the three clinical cases between IMPT and PAT plans are shown in figure 2-6. In the ependymoma and unilateral H&N case, the difference in integral doses comes mainly from the difference in the normal tissue doses, where normal tissue was defined as tissue excluding the tumour and excluding the OAR with objectives to allow a direct comparison of tissue which was not considered during dose optimisation. The integral dose in the normal tissue is less in the PAT plan for ependymoma (4.8 J less), unilateral H&N (10.9 J less), and the bilateral H&N case (4.9 J less). For the ependymoma and uni-lateral H&N cases, the larger integral dose difference in normal tissue than in the total patient volume indicates that the OARs received more integral dose in the IMPT plans, as the target integral doses were almost identical (figure 2-5). The higher total integral dose difference for the bi-lateral H&N case and the lower normal tissue integral dose difference suggest that the OARs receive higher integral dose in the PAT plan. This was due to the limitation of PAT optimiser planned with full energies, i.e., the beams from the left-hand side were given spots to cover the tumour on the right-hand side of the patient, which raised the dose levels in the central OARs.

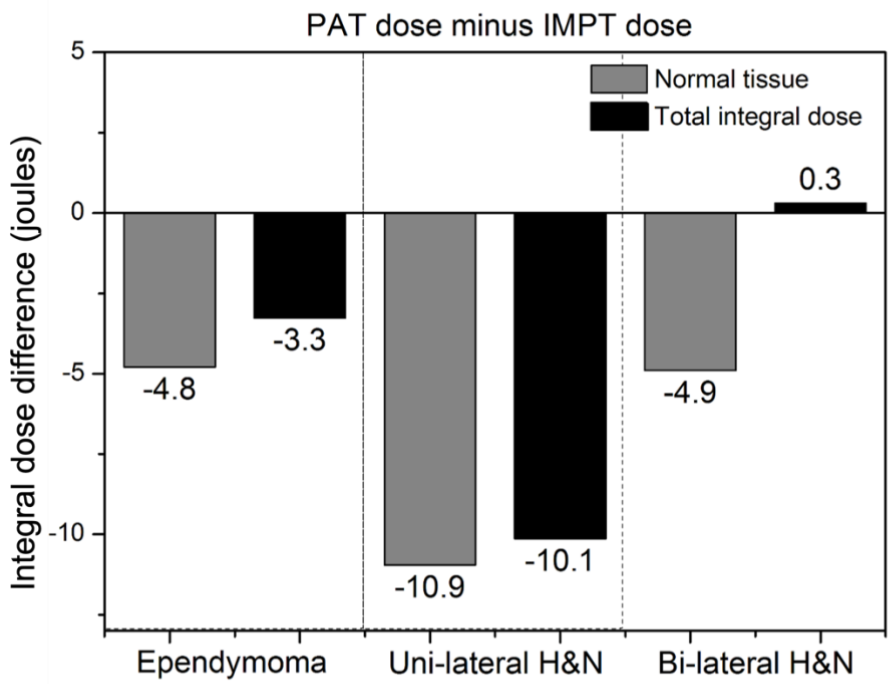

Figure 2-6: Integral dose differences of PAT and IMPT plans for (a) ependymoma; (b) unilateral H&N; (c) bilateral H&N.

2.6 Discussion

This study assessed the intrinsic properties and robustness of unconstrained PAT plans by evaluating the plans under simulated range and setup uncertainties and comparing these to IMPT plans for one brain and two head and neck (H&N) cases. We found that for all cases, PAT plans gave similar or improved target conformality and homogeneity in the nominal scenarios. Although worse robustness in terms of the target conformality was seen in the H&N cases under setup errors, improvement in target robustness can be clearly seen in the ependymoma case and under range error scenarios for the H&N cases. Among the three cases studied, ependymoma benefited consistently from improved robustness to both types of uncertainties from PAT. These findings suggest that PAT improves plan quality under nominal scenarios, improves the robustness on a case-dependent basis under uncertainty scenarios, and perhaps is less sensitive to range errors than setup errors for H&N cases. The worse CIs of PAT plans under setup errors for the relatively shallower H&N cases could be due to the lack of a range shifter, as higher energies were required from more oblique beam angles to ensure dose coverage to the shallower regions of the targets. However, gantry rotation with a range shifter while the beam is active was considered impractical because the range shifter must be placed at short proximity to patient surface which is an irregular topology. This could potentially cause safety issues due to possible patient collisions. Therefore, unless a collision prediction algorithm could foresee this, the impact of the lack of range shifters in PAT plans should be examined for individual cases. In order to draw a statistical conclusion, a systematic study involving a larger range of sites with multiple cases for the same site is recommended.

Some limitations exist for the study. Firstly, plans were planned and evaluated in 2 dimensions, so setup errors were not modelled in the superior-inferior anatomical directions. While this is simpler than the 3D tools used for clinical planning, a 2D evaluation is sufficient to evaluate the behaviour of plans under range and setup uncertainty scenarios when all fields lie within the same plane. Secondly, the system uses a semi-analytical dose calculation rather than a Monte Carlo method. However, calculated doses in water were in good agreement with measured data (within 2%), and analytical dose calculations are still in use for clinical planning at

many centres. Thirdly, the DICOM data were anonymised before they were sent for research purposes, so clinical information was unavailable. However, dose optimisations were carried out based on the clinically contoured structures, original prescribed doses, and original planning objectives used in the clinic, so any relevant clinical factors had already been considered within these entities. Finally, as our aim was to investigate the intrinsic robustness of PAT, we optimized plans without robust optimization. If robust optimization were used, we believe a systematic improvement would be seen for both PAT and IMPT.

2.6.1 Unconstrained vs. constrained PAT

Unconstrained PAT represents the best possible behaviour amongst the possible constrained PAT. However unconstrained PAT may be impractical to deliver as the time to switch the beam energy is one of the limiting factors for the delivery efficiency [32] [34]. The energy layer switch time ranges from 0.5 seconds to several seconds depending on the type of accelerator. Assuming an energy layer switch time of 1 second for a modern cyclotron, a hypothetical tumour of 3 centimetres in diameter, and a 180-degree arc at 10-degree spacing, there would need 190 energy layers in total, assuming 3-millimetre energy layer spacing. This would amount to > 3 minutes for PAT beam-on time during which the patient must stay still. Although this time scale seems acceptable, it would be preferable to reduce the beam-on time as much as possible without losing the advantages of PAT, because the longer the patient stays on the treatment couch, the more likely there will be shifts with respect to the planning CT images.

In PAT optimization it may no longer be necessary to utilise all energy layers inside the PTV from all control points in order to achieve a good dose conformality of the target [16] [37]. However, minimizing the energy layers per control point is expected to degrade the robustness compared to unconstrained PAT. Several strategies for reducing energy layers have been proposed [16] [32 - 36] and many more are still unexplored. The robustness of unconstrained PAT is important to study as it sets a standard which strategically constrained PAT should be compared to.

2.6.2 Wider considerations

For completeness, the results for H&N IMPT plans with a range shifter are included in Appendix D - Appendix E. With a range shifter, the IMPT plans robustness is similar to or worse than without a range shifter under both range and setup uncertainties, which suggests higher robustness when using PAT without a range shifter than with one. The worse robustness, although negligible in magnitude, could be due to spots with larger lateral spreads when a range shifter is used. Not needing a range shifter might add to the advantages of PAT.

In [42 – 44], normal tissue complication probability (NTCP) of organ functions [39, 40, 41] has been used for comparing IMRT, VMAT and TomoTherapy and was shown to be similar or reduced in arc plans (i.e., the latter two) on a case-dependent basis. NTCP has also been used to compare photon and proton plans, the latter showing lower NTCP [45, 46]. We obtained similar results showing that PAT reduced the normal tissue integral dose in all three cases studied. Therefore, in some circumstances, PAT plans might be beneficial in terms of reducing the NTCP. However, when applying longitudinal models of dose-cognitive effects to paediatric brain tumours, the reduction of low dose volumes in proton therapy compared to IMRT is predicted to have long term benefits in preserving the cognitive functions [47]. This might indicate the potential patient groups that could benefit from PAT. Although evaluating the NTCP can be another approach of studying PAT's potential of becoming a next-generation treatment modality, we have not evaluated PAT in terms of NTCP or secondary malignancies yet due to greater uncertainty compared to using a physical evaluation approach.

Risks of developing secondary cancers are a crucial concern with radiation therapy, especially in paediatrics and young adults. Possible contributing factors to secondary malignancies including the type of radiation and the dose and volume of the irradiated area have been reviewed in [48], which described the concern that IMRT is associated with higher risk of secondary cancers than protons due to more normal tissue exposed to low level radiation. In the case of paediatric cancers, there has been higher risks of developing secondary cancers compared to the general population [48]. However, the exact mechanism of secondary

cancers is unknown. Proton therapy is predicted to reduce the integral dose to normal tissues, compared to X-ray radiation therapy, and therefore the overall risk of second malignancies compared to IMRT should be lower [49, 50]. As PAT reduces the integral dose, as shown in the ependymoma and unilateral H&N cases, this advantage should apply to PAT, just as it does to IMPT. The further question is how much difference there might be in estimated second malignancy risk comparing PAT to IMPT, and this is an important area for further study.

2.7 Conclusion

In all three cases studied (ependymoma, unilateral H&N, bilateral H&N), PAT plans improved target conformality, homogeneity, and high-dose sparing of OARs, normal tissue and skin in the nominal scenarios.

Under error scenarios, PAT demonstrated similar or better target robustness for all three cases. However, the robustness was worse under setup errors for the H&N cases due to their shallower target geometries, so robustness is not always improved with PAT and must be evaluated on individual basis. Amongst the three cases, the ependymoma case benefited consistently from PAT in terms of target robustness, which suggests potential in PAT application on similar geometries.

As a characteristic of arc therapy, a larger volume irradiation of normal tissue at low dose levels (under about 10 Gy) was seen in all PAT plans. Combining current knowledge about the benefit of reducing low-dose volumes in preserving cognitive functions, PAT might not be the optimal treatment for paediatric patients but rather for the more elderly patients. However, the low dose bath was modest, and in all three plans the normal tissue (non-tumour and non-OAR tissue) integral dose was reduced with PAT. The OAR integral dose was derived to be higher in the PAT plan for the bilateral H&N case due to limitations of full-energy PAT.

These findings encourage further investigation and development of PAT, including a larger patient sample and the need to strategically select energies especially in the case of bilateral H&N and for better deliverability.

Funding

This research was supported by Cancer Research UK (CRUK) via the funding to Cancer Research UK Manchester Centre: [C147/A18083] and [C147/A25254] and by the NIHR (National Institute of Health Research) Manchester Biomedical Research Centre.

Acknowledgements

We thank Dr Carla Winterhalter for assistance with Monte Carlo simulations, and Dr Christopher Rose for advice that greatly helped improving the program execution efficiency.

2.8 References

[1] S. Takahashi, Conformation radiotherapy-rotation techniques as applied to radiography and radiotherapy of cancer, Acta Radiol 242 (1965) 1–142.

[2] A. Brahme, Optimization of stationary and moving beam radiation therapy techniques, Radiotherapy and Oncology 12 (2) (1988) 129–140.

[3] D. Convery, M. Rosenbloom, The generation of intensity-modulated fields for conformal radiotherapy by dynamic collimation, Physics in medicine & biology 37 (6) (1992) 1359.

[4] T. Bortfeld, A. L. Boyer, W. Schlegel, D. L. Kahler, T. J. Waldron, Realization and verification of three-dimensional conformal radiotherapy with modulated fields, International Journal of Radiation Oncology Biology Physics 30 (4) (1994) 899–908.

[5] T. R. Bortfeld, D. L. Kahler, T. J. Waldron, A. L. Boyer, X-ray field compensation with multileaf collimators, International Journal of Radiation Oncology Biology Physics 28 (3) (1994) 723–730.

[6] J.Stein,T.Bortfeld,B.D¨orschel,W.Schlegel,Dynamicx-raycompensationforconformalradiotherapy by means of multi-leaf collimation, Radiotherapy and Oncology 32 (2) (1994) 163–173.

[7] S. V. Spirou, C. S. Chui, Generation of arbitrary intensity profiles by dynamic jaws or multileaf colli- mators, Medical physics 21 (7) (1994) 1031–1041.

[8] T. R. Mackie, T. Holmes, S. Swerdloff, P. Reckwerdt, J. O. Deasy, J. Yang, B. Paliwal, T. Kinsella, Tomotherapy: a new concept for the delivery of dynamic conformal radiotherapy, Medical physics 20 (6) (1993) 1709–1719.

[9] C. X. Yu, Intensity-modulated arc therapy with dynamic multileaf collimation: an alternative to to- motherapy, Physics in Medicine & Biology 40 (9) (1995) 1435.

[10] M. A. MacKenzie, D. M. Robinson, Intensity modulated arc deliveries approximated by a large number of fixed gantry position sliding window dynamic multileaf collimator fields, Medical physics 29 (10) (2002) 2359–2365.

[11] S. M. Crooks, X. Wu, C. Takita, M. Watzich, L. Xing, Aperture modulated arc therapy, Physics in Medicine & Biology 48 (10) (2003) 1333.

[12] C. Cameron, Sweeping-window arc therapy: an implementation of rotational imrt with automatic beam-weight calculation, Physics in Medicine & Biology 50 (18) (2005) 4317.

[13] G. Tang, M. A. Earl, S. Luan, S. A. Naqvi, C. X. Yu, Converting multiple-arc intensity modulated arc therapy into a single arc for efficient delivery, International Journal of Radiation Oncology Biology Physics 69 (3) (2007) S673.

[14] K. Otto, Volumetric modulated arc therapy: Imrt in a single gantry arc, Medical physics 35 (1) (2008) 310–317.

[15] J. Seco, G. Gu, T. Marcelos, H. Kooy, H. Willers, Proton arc reduces range uncertainty effects and improves conformality compared with photon volumetric modulated arc therapy in stereotactic body radiation therapy for non-small cell lung cancer, International Journal of Radiation Oncology Biology Physics 87 (1) (2013) 188–194.

[16] X. Ding, X. Li, J. M. Zhang, P. Kabolizadeh, C. Stevens, D. Yan, Spot-Scanning Proton Arc (SPArc) Therapy: The First Robust and Delivery-Efficient Spot-Scanning Proton Arc Therapy, International Journal of Radiation Oncology Biology Physics 96 (5) (2016) 1107–1116. doi:10.1016/j.ijrobp.2016.08.049.

[17] J.-E. Rah, G.-Y. Kim, D. H. Oh, T. H. Kim, J. W. Kim, D. Y. Kim, S. Y. Park, D. Shin, A treatment planning study of proton arc therapy for para-aortic lymph node tumors: dosimetric evaluation of conventional proton therapy, proton arc therapy, and intensity modulated radiotherapy, Radiation Oncology 11 (140). doi:10.1186/s13014-016-0717-4.

[18] H. Paganetti, Range uncertainties in proton therapy and the role of monte carlo simulations, Physics in Medicine & Biology 57 (11) (2012) R99.

[19] M. Lowe, A. Aitkenhead, F. Albertini, A. J. Lomax, R. I. MacKay, A robust optimisation approach accounting for the effect of fractionation on setup uncertainties, Physics in Medicine & Biology 62 (20) (2017) 8178.

[20] T. Bortfeld, An analytical approximation of the bragg curve for therapeutic proton beams, Medical physics 24 (12) (1997) 2024–2033.

[21] B. M. Clasie, J. B. Flanz, H. M. Kooy, Interpolation of tabulated proton bragg peaks, Physics in Medicine & Biology 57 (21) (2012) N405.

[22] Van De Water, Steven, et al. "Shortening delivery times of intensity modulated proton therapy by reducing proton energy layers during treatment plan

optimization." International Journal of Radiation Oncology* Biology* Physics 92.2 (2015): 460-468.

[23] D. Pflugfelder, J. Wilkens, U. Oelfke, Worst case optimization: a method to account for uncertainties in the optimization of intensity modulated proton therapy, Physics in Medicine & Biology 53 (6) (2008) 1689.

[24] W. Liu, Y. Li, X. Li, W. Cao, X. Zhang, Influence of robust optimization in intensity-modulated proton therapy with different dose delivery techniques, Medical physics 39 (6Part1) (2012) 3089–3101.

[25] J. J. Wilkens, U. Oelfke, Fast multifield optimization of the biological effect in ion therapy, Physics in Medicine & Biology 51 (12) (2006) 3127.

[26] T. Bortfeld, Optimized planning using physical objectives and constraints, in: Seminars in Radiation Oncology, Vol. 9, Elsevier, 1999, pp. 20–34.

[27] H. Miura, M. Fujiwara, M. Tanooka, H. Doi, H. Inoue, Y. Takada, N. Kamikonya, S. Hirota, Dosimetric and delivery characterizations of full-arc and half-arc volumetric-modulated arc therapy for maxillary cancer, Journal of radiation research 53 (5) (2012) 785–790.

[28] M. Teoh, C. Clark, K. Wood, S. Whitaker, A. Nisbet, Volumetric modulated arc therapy: a review of current literature and clinical use in practice, The British journal of radiology 84 (1007) (2011) 967–996.

[29] M. D’Arienzo, S. Masciullo, V. Sanctis, M. Osti, L. Chiacchiararelli, R. Enrici, Integral dose and radiation-induced secondary malignancies: comparison between stereotactic body radiation therapy and three-dimensional conformal radiotherapy, International journal of environmental research and public health 9 (11) (2012) 4223–4240.

[30] A. Lomax, Intensity modulated proton therapy and its sensitivity to treatment uncertainties 2: the potential effects of inter-fraction and inter-field motions, Physics in medicine and biology 53 (4) (2008) 1043.

[31] A. C. Kraan, S. van de Water, D. N. Teguh, A. Al-Mamgani, T. Madden, H. M. Kooy, B. J. Heijmen, M. S. Hoogeman, Dose uncertainties in impt for oropharyngeal cancer in the presence of anatomical, range, and setup errors, International Journal of Radiation Oncology* Biology* Physics 87 (5) (2013) 888–896.

[32] S. Van de Water, H. M. Kooy, B. J. Heijmen, M. S. Hoogeman, Shortening delivery times of intensity modulated proton therapy by reducing proton energy layers during treatment plan optimization, International Journal of Radiation Oncology* Biology* Physics 92 (2) (2015) 460–468.

[33] S. Van de Water, A. Kraan, S. Breedveld, W. Schillemans, D. Teguh, H. Kooy, T. Madden, B. Heijmen, M. Hoogeman, Improved efficiency of multi-criteria impt treatment planning using iterative resampling of randomly placed pencil beams, Physics in Medicine & Biology 58 (19) (2013) 6969.

[34] W. Cao, G. Lim, L. Liao, Y. Li, S. Jiang, X. Li, H. Li, K. Suzuki, X. R. Zhu, D. Gomez, et al., Proton energy optimization and reduction for intensity-modulated proton therapy, Physics in Medicine & Biology 59 (21) (2014) 6341.

[35] X. Li, G. Liu, G. Janssens, O. De Wilde, V. Bossier, X. Lerot, A. Pouppez, D. Yan, C. Stevens, P. Kabolizadeh, et al., The first prototype of spot-scanning proton arc treatment delivery, Radiotherapy and Oncology 137 (2019) 130–136.

[36] G. Liu, X. Li, A. Qin, W. Zheng, D. Yan, S. Zhang, C. Stevens, P. Kabolizadeh, X. Ding, Improve the dosimetric outcome in bilateral head and neck cancer (hnc) treatment using spot-scanning proton arc (sparc) therapy: a feasibility study, Radiation Oncology 15 (1) (2020) 1–11.

[37] D. Sanchez-Parcerisa, M. Kirk, M. Fager, B. Burgdorf, M. Stowe, T. Solberg, A. Carabe, Range optimization for mono- and bi-energetic proton modulated arc therapy with pencil beam scanning, Physics in Medicine and Biology 61 (21) (2016) N565–N574. doi:10.1088/0031-9155/61/21/N565.

[38] W. Liu, X. Zhang, Y. Li, R. Mohan, Robust optimization of intensity modulated proton therapy, Medical physics 39 (2) (2012) 1079–1091.

[39] J. T. Lyman, Complication probability as assessed from dose-volume histograms, Radiation Research 104 (2s) (1985) S13–S19.

[40] G. J. Kutcher, C. Burman, L. Brewster, M. Goitein, R. Mohan, Histogram reduction method for calculating complication probabilities for three-dimensional treatment planning evaluations, International Journal of Radiation Oncology, Biology, Physics 21 (1) (1991) 137–146. doi:10.1016/0360- 3016(91)90173-2.

[41] C. Burman, G. Kutcher, B. Emami, M. Goitein, Fitting of normal tissue tolerance data to an analytic function, International Journal of Radiation Oncology* Biology* Physics 21 (1) (1991) 123–135.

[42] Alongi F, Giaj-Levra N, Fiorentino A, Mazzola R, Fersino S, Ricchetti F, Ruggieri R. Low-dose bath with volumetric modulated arc therapy in breast cancer:“Much ado about nothing?”. Tumori Journal. 2016 Jul;102(4):335-6.

[43] F. Foroudi, L. Wilson, M. Bressel, A. Haworth, C. Hornby, D. Pham, J. Cramb, S. Gill, K. H. Tai, T. Kron, A dosimetric comparison of 3d conformal vs intensity modulated vs volumetric arc radiation therapy for muscle invasive bladder cancer, Radiation Oncology 7 (1) (2012) 111.

[44] P. A. Myers, P. Mavroidis, N. Papanikolaou, S. Stathakis, Comparing conformal, arc radiotherapy and helical tomotherapy in craniospinal irradiation planning, Journal of applied clinical medical physics 15 (5) (2014) 12–28.

[45]L.Widesott,A.Pierelli,C.Fiorino,A.J.Lomax,M.Amichetti,C.Cozzarini,M.Soukup, R.Schneider, E. Hug, N. Di Muzio, et al., Helical tomotherapy vs. intensity-modulated proton therapy for whole pelvis irradiation in high-risk prostate cancer patients: dosimetric, normal tissue complication probability, and generalized equivalent uniform dose analysis, International Journal of Radiation Oncology* Biology* Physics 80 (5) (2011) 1589–1600.

[46] B. Kaser-Hotz, A. Sumova, A. Lomax, U. Schneider, B. Klink, J. Fidel, H. Blattmann, A comparison of normal tissue complication probability of brain for proton and photon therapy of canine nasal tumors, Veterinary Radiology & Ultrasound 43 (5) (2002) 480–486.

[47] T. E. Merchant, C.-h. Hua, H. Shukla, X. Ying, S. Nill, U. Oelfke, Proton versus photon radiotherapy for common pediatric brain tumors: comparison of models of dose characteristics and their relationship to cognitive function, Pediatric blood & cancer 51 (1) (2008) 110–117.

[48] C. B. Dracham, et al. Radiation induced secondary malignancies: a review article. Radiation oncology journal vol. 36,2 (2018): 85-94. doi:10.3857/roj.2018.00290

[49] B. R. Eaton, S. M. MacDonald, T. I. Yock, N. J. Tarbell, Secondary malignancy risk following proton radiation therapy, Frontiers in oncology 5 (2015) 261.

[50] J.Vogel,L.Lin,L.Litzky,A.Berman,C.SimoneII, Predicted rate of secondary malignancies following adjuvant proton versus photon radiation therapy for

thymoma, International Journal of Radiation Oncology* Biology* Physics 99 (2) (2017) 427–433.

2.9 Supplementary materials

2.9.1 Appendix A. Longitudinal beam profile compared to Monte Carlo simulations

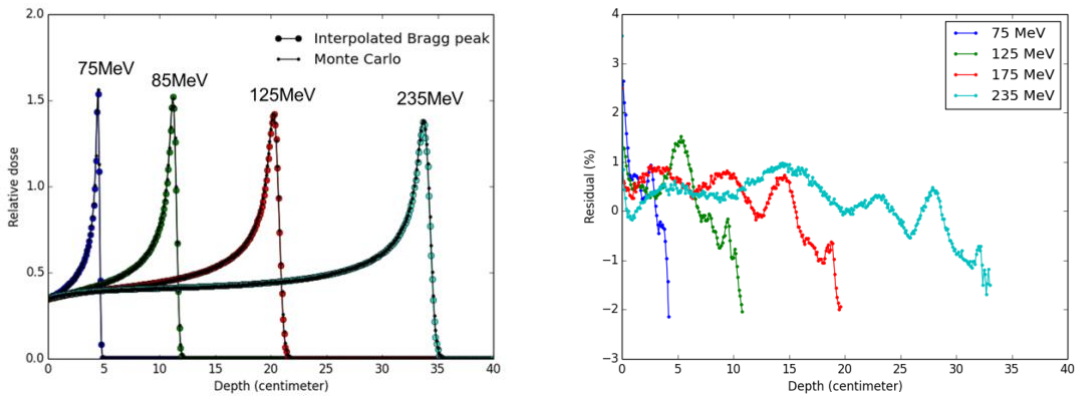

Figure 2-A (a) Bragg peaks interpolated [21] from commissioning measurements in water of a Varian ProBeam system are compared to Monte Carlo simulations carried out in GATE (version 8.1) for 75, 85, 125 and 235 MeV as examples to represent the full therapeutic energy spectrum for proton therapy. (b) The residual between the interpolated Bragg peaks and Monte Carlo simulations, defined as the percentage difference relative to Monte Carlo simulations, are plotted against the depth in water. The interpolation agrees with Monte Carlo to within 2% error.

2.9.2 Appendix B. Planning objectives

The planning objectives for the three clinical cases, ependymoma, unilateral H&N and bilateral H&N, are summarized in table 2-1 to 2-3.

Table 2-1: Optimisation objectives for the ependymoma case. BS: brainstem; PRV: planning OAR volume; SC: spinal cord; PRV & BS PRV: common volume of PTV and BS PRV; PTV – BS PRV: PTV excluding BS PRV.

Structure	Lower dose (Gy), fractional volume	Upper dose (Gy), fractional volume	Lower priority	Upper priority
PTV & BS PRV	52.8, 1.0	52.8, 1.0	120	100
PTV – BS PRV	54.0, 1.0	54.0, 1.0	100	100
BS	-, -	52.8, 1.0	-	70
BS PRV	-, -	54.0, 1.0	-	1
SC PRV	-, -	54.0, 1.0	-	60

Table 2-2: Optimisation objectives for the unilateral H&N case. CTV: clinical target volume; PTV – skin: PTV excluding skin; High dose rind: a 10mm margin was added to the PTV to suppress dose levels outside the PTV.

Structure	Lower dose (Gy), fractional volume	Upper dose (Gy), fractional volume	Lower priority	Upper priority
CTV	57, 1.0	66, 1.0	200	100
PTV – skin	60, 1.0	60, 1.0	100	100
High dose rind	-, -	60, 1.0	-	300
Left parotid	-, -	26, 1.0	-	100

Table 2-3: Optimisation objectives for the bilateral H&N case.

Structure	Lower dose (Gy), fractional volume	Upper dose (Gy), fractional volume	Lower priority	Upper priority
PTV1	64.5, 1.0	65.0, 1.0	100	100
PTV2	54.0, 0.99	54.0, 0.91	100	100
Spinal cord	-, -	46, 1.0	100	100

2.9.3 Appendix C. Metrics.

The full evaluation metrics for the three clinical cases under nominal, range and patient setup errors are summarized in table 2-4 to table 2-6.

Table 2-4: Metric values for the ependymoma case under nominal, CT calibration and setup error scenarios. IMPT was planned without range shifters.

	Nominal		CT calibration error							
	IMPT (without range shifter)	PAT	IMPT (without range shifter)				PAT			
			Mean	Max	Min	Std dev	Mean	Max	Min	Std dev
$CI_{95\%}$	0.996	1.000	0.943	0.996	0.841	0.059	0.987	1.000	0.918	0.033
HI	1.028	1.018	1.056	1.093	1.031	0.023	1.049	1.081	1.026	0.020
Brainstem PRV										
$V_{30\%}$	0.93	0.95	0.93	0.96	0.90	0.02	0.97	1.00	0.93	0.03
$V_{60\%}$	0.91	0.98	0.90	0.93	0.87	0.03	0.95	0.99	0.89	0.04
$V_{90\%}$	0.88	0.93	0.89	0.92	0.85	0.03	0.93	0.98	0.86	0.05
Normal tissue										
V_{10Gy}	0.62	0.40	0.62	0.62	0.62	0.00	0.40	0.41	0.39	0.00
V_{20Gy}	0.15	0.10	0.15	0.16	0.14	0.01	0.10	0.10	0.10	0.00
V_{30Gy}	0.04	0.04	0.04	0.04	0.04	0.00	0.04	0.04	0.04	0.00
Skin										
V_{10Gy}	0.18	0.09	0.18	0.19	0.18	0.00	0.09	0.09	0.08	0.00
V_{20Gy}	0.07	0.06	0.07	0.07	0.07	0.00	0.06	0.06	0.06	0.00
V_{30Gy}	0.06	0.05	0.89	0.92	0.85	0.00	0.05	0.05	0.05	0.00
			Setup error							
			IMPT (without range shifter)				PAT			
			Mean	Max	Min	Std dev	Mean	Max	Min	Std dev
$CI_{95\%}$			0.97	1.00	0.93	0.03	0.98	1.00	0.95	0.02

HI			1.03	1.04	1.02	0.01	1.03	1.03	1.02	0.01
Brainstem PRV										
$V_{30\%}$			0.93	0.95	0.92	0.01	0.98	0.98	0.98	0.00
$V_{60\%}$			0.91	0.93	0.89	0.02	0.96	0.96	0.96	0.00
$V_{90\%}$			0.89	0.91	0.86	0.02	0.94	0.95	0.93	0.00
Normal tissue										
V_{10Gy}			0.62	0.63	0.61	0.01	0.40	0.41	0.39	0.01
V_{20Gy}			0.15	0.16	0.14	0.01	0.10	0.10	0.09	0.01
V_{30Gy}			0.04	0.05	0.03	0.01	0.04	0.05	0.04	0.01
Skin										
V_{10Gy}			0.18	0.07	0.06	0.00	0.14	0.41	0.08	0.00
V_{20Gy}			0.18	0.07	0.06	0.00	0.07	0.10	0.06	0.00
V_{30Gy}			0.18	0.07	0.05	0.00	0.05	0.05	0.05	0.00

Table 2-5: Metric values for the unilateral H&N case under nominal, CT calibration and setup error scenarios. IMPT was planned with range shifters.

	Nominal		CT calibration error							
	IMPT (with range shifter)	PAT	IMPT (with range shifter)				PAT			
			Mean	Max	Min	Std dev	Mean	Max	Min	Std dev
$CI_{95\%}$	0.999	1.000	0.999	1.000	0.998	0.000	1.000	1.000	0.999	0
HI	1.13	1.08	1.13	1.15	1.11	0.02	1.10	1.13	1.07	0.03
Oral cavity										
$V_{30\%}$, $V_{60\%}$, $V_{90\%}$	0.87	0.88	0.69	0.85	0.63	0.08	0.64	0.74	0.59	0.06
Normal tissue										
V_{10Gy}	0.20	0.25	0.20	0.21	0.19	0.01	0.25	0.25	0.25	0.06

V_{20Gy}	0.15	0.12	0.15	0..16	0.15	0.00	0.12	0.12	0.11	0.00
V_{30Gy}	0.07	0.05	0.07	0.07	0.07	0.00	0.05	0.05	0.05	0.00
Skin										
V_{10Gy}	0.27	0.34	0.27	0.27	0.27	0.00	0.34	0.34	0.34	0.00
V_{20Gy}	0.18	0.01	0.18	0.18	0.18	0.00	0.01	0.01	0.01	0.00
V_{30Gy}	0.01	0.00	0.01	0.01	0.01	0.00	0.00	0.00	0.00	0.00
			Setup error							
			IMPT (with range shifter)				PAT			
			Mean	Max	Min	Std dev	Mean	Max	Min	Std dev
$CI_{95\%}$			1.00	1.00	1.00	0.00	0.96	0.98	0.94	0.02
HI			1.42	1.49	1.37	0.04	1.08	1.11	1.06	0.02
Oral cavity										
$V_{30\%}$, $V_{60\%}$, $V_{90\%}$			1.00	1.00	1.00	0.00	0.99	1.00	0.99	0.00
Normal tissue										
V_{10Gy}			0.25	0.26	0.25	0.00	0.25	0.26	0.24	0.01
V_{20Gy}			0.24	0.24	0.12	0.00	0.12	0.12	0.12	0.00
V_{30Gy}			0.23	0.23	0.22	0.00	0.05	0.05	0.05	0.00
Skin										
V_{10Gy}			0.29	0.30	0.29	0.00	0.34	0.34	0.33	0.00
V_{20Gy}			0.29	0.29	0.28	0.00	0.01	0.02	0.01	0.01
V_{30Gy}			0.28	0.28	0.28	0.00	0.00	0.00	0.00	0.00

Table 2-6: Metric values for the bilateral H&N case under nominal, CT calibration and setup error scenarios. IMPT was planned with range shifters.

	Nominal		CT calibration error	
	IMPT (with	PAT	IMPT (with range shifter)	PAT

	range shifter)									
			Mean	Max	Min	Std dev	Mean	Max	Min	Std dev
PTV1 $CI_{95\%}$	0.967	0.984	0.929	0.980	0.794	0.075	0.985	0.995	0.964	0.014
PTV1 HI	1.079	1.024	1.133	1.169	1.105	0.023	1.184	1.263	1.071	0.082
PTV2 $CI_{95\%}$	0.973	0.994	0.871	0.979	0.533	0.177	0.981	0.992	0.956	0.017
PTV2 HI	1.193	1.175	1.275	1.478	1.163	0.131	1.274	1.344	1.168	0.076
Spinal cord										
$V_{30\%}$, $V_{60\%}$, $V_{90\%}$	1.00	1.00	1.00	1.00	1.00	1.00	1.00	1.00	1.00	1.00
Normal tissue										
V_{10Gy}	0.77	0.65	0.77	0.77	0.77	0.00	0.65	0.65	0.65	0.00
V_{20Gy}	0.13	0.16	0.13	0.13	0.12	0.00	0.16	0.16	0.16	0.00
V_{30Gy}	0.03	0.02	0.03	0.04	0.03	0.00	0.02	0.02	0.02	0.00
Skin										
V_{10Gy}	0.63	0.52	0.63	0.64	0.63	0.00	0.52	0.53	0.52	0.00
V_{20Gy}	0.34	0.33	0.34	0.35	0.32	0.01	0.36	0.38	0.32	0.03
V_{30Gy}	0.13	0.10	0.13	0.14	0.11	0.01	0.11	0.13	0.09	0.01
			Setup error							
			IMPT (with range shifter)				PAT			
			Mean	Max	Min	Std dev	Mean	Max	Min	Std dev
PTV1 $CI_{95\%}$			1.00	1.00	1.00	0.00	0.932	0.956	0.894	0.024
PTV1 HI			1.24	1.37	1.16	0.08	1.138	1.181	1.088	0.031
PTV2 $CI_{95\%}$			1.00	1.00	1.00	0.00	0.891	0.920	0.852	0.024
PTV2 HI			1.85	1.95	1.75	0.08	1.186	1.202	1.169	0.014
Spinal cord										

$V_{30\%}$, $V_{60\%}$, $V_{90\%}$			1.00	1.00	1.00	1.00	1.00	1.00	1.00	1.00
Normal tissue										
V_{10Gy}			0.99	0.99	0.99	0.00	0.66	0.66	0.65	0.00
V_{20Gy}			0.95	0.95	0.95	0.00	0.16	0.16	0.16	0.00
V_{30Gy}			0.90	0.91	0.89	0.01	0.02	0.03	0.02	0.00
Skin										
V_{10Gy}			0.99	0.99	0.99	0.00	0.52	0.52	0.52	0.00
V_{20Gy}			0.90	0.91	0.90	0.00	0.35	0.36	0.34	0.01
V_{30Gy}			0.81	0.82	0.80	0.01	0.10	0.12	0.10	0.01

2.9.4 Appendix D. Metrics for the unilateral H&N cases without a range shifter

Table 2-7: Metric values for the unilateral H&N case under nominal, CT calibration and setup error scenarios. IMPT was planned without a range shifter.

	Nominal		CT calibration error							
	IMPT (without range shifter)	PAT	IMPT (without range shifter)				PAT			
			Mean	Max	Min	Std dev	Mean	Max	Min	Std dev
$CI_{95\%}$	0.998	1.000	0.998	1.000	0.994	0.002	1.000	1.000	0.999	0.00
HI	1.13	1.08	1.14	1.15	1.12	0.01	1.10	1.13	1.07	0.03
Oral cavity										
$V_{30\%}$, $V_{60\%}$, $V_{90\%}$	0.75	0.88	0.48	0.51	0.44	0.03	0.64	0.74	0.59	0.06
Normal tissue										
V_{10Gy}	0.17	0.25	0.18	0.18	0.17	0.00	0.25	0.25	0.25	0.00
V_{20Gy}	0.14	0.12	0.14	0.14	0.14	0.00	0.12	0.12	0.11	0.00
V_{30Gy}	0.06	0.05	0.07	0.07	0.06	0.00	0.05	0.05	0.05	0.00
Skin										
V_{10Gy}	0.27	0.34	0.27	0.27	0.27	0.00	0.34	0.34	0.34	0.00
V_{20Gy}	0.17	0.01	0.16	0.16	0.16	0.00	0.01	0.01	0.01	0.00
V_{30Gy}	0.01	0.00	0.01	0.01	0.00	0.00	0.00	0.00	0.00	0.00
			Setup error							
			IMPT (without range shifter)				PAT			
			Mean	Max	Min	Std dev	Mean	Max	Min	Std dev
$CI_{95\%}$			0.97	0.99	0.95	0.02	0.96	0.98	0.94	0.02
HI			1.10	1.13	1.08	0.02	1.08	1.11	1.06	0.02
Oral cavity										

$V_{30\%}$, $V_{60\%}$, $V_{90\%}$			0.91	0.92	0.89	0.01	0.99	1.00	0.99	0.00
Normal tissue										
V_{10Gy}			0.098	0.105	0.098	0.097	0.25	0.26	0.24	0.01
V_{20Gy}			0.036	0.045	0.032	0.044	0.12	0.12	0.12	0.00
V_{30Gy}			0.007	0.016	0.001	0.006	0.05	0.05	0.05	0.00
Skin										
V_{10Gy}			0.28	0.29	0.28	0.00	0.34	0.34	0.33	0.00
V_{20Gy}			0.14	0.14	0.13	0.00	0.01	0.02	0.01	0.01
V_{30Gy}			0.01	0.01	0.00	0.00	0.00	0.00	0.00	0.00

2.9.5 Appendix E. Metrics for the bilateral H&N cases without a range shifter

Table 2-8: Metric values for the bilateral H&N case under nominal, CT calibration and setup error scenarios. IMPT was planned without a range shifter.

	Nominal		CT calibration error							
	IMPT (without range shifter)	PAT	IMPT (without range shifter)				PAT			
			Mean	Max	Min	Std dev	Mean	Max	Min	Std dev
PTV1 $CI_{95\%}$	0.969	0.984	0.970	0.978	0.945	0.016	0.985	0.995	0.964	0.014
PTV1 HI	1.082	1.024	1.137	1.180	1.082	0.043	1.184	1.263	1.071	0.082
PTV2 $CI_{95\%}$	0.975	0.994	0.972	0.984	0.942	0.020	0.981	0.992	0.956	0.017
PTV2 HI	1.190	1.175	1.344	1.505	1.160	0.147	1.274	1.344	1.168	0.076
Spinal cord										
$V_{30\%}$, $V_{60\%}$, $V_{90\%}$	1.00	1.00	1.00	1.00	1.00	1.00	1.00	1.00	1.00	1.00
Normal tissue										
V_{10Gy}	0.77	0.65	0.77	0.77	0.77	0.00	0.65	0.65	0.65	0.00
V_{20Gy}	0.12	0.16	0.12	0.12	0.12	0.00	0.16	0.16	0.16	0.00
V_{30Gy}	0.03	0.02	0.03	0.03	0.03	0.00	0.02	0.02	0.02	0.00
Skin										
V_{10Gy}	0.64	0.52	0.63	0.64	0.63	0.00	0.52	0.53	0.52	0.00
V_{20Gy}	0.34	0.33	0.34	0.35	0.34	0.01	0.36	0.38	0.32	0.03
V_{30Gy}	0.15	0.10	0.14	0.15	0.12	0.01	0.11	0.13	0.09	0.01
			Setup error							
			IMPT (without range shifter)				PAT			
			Mean	Max	Min	Std dev	Mean	Max	Min	Std dev

PTV1 $CI_{95\%}$			0.911	0.850	0.869	0.031	0.932	0.956	0.894	0.024
PTV1 HI			1.706	1.135	1.035	0.033	1.138	1.181	1.088	0.031
PTV2 $CI_{95\%}$			0.873	0.902	0.852	0.021	0.891	0.920	0.852	0.024
PTV2 HI			1.203	1.286	1.170	0.043	1.186	1.202	1.169	0.014
Spinal cord										
$V_{30\%}$, $V_{60\%}$, $V_{90\%}$			1.00	1.00	1.00	1.00	1.00	1.00	1.00	1.00
Normal tissue										
V_{10Gy}			0.77	0.79	0.75	0.01	0.66	0.66	0.65	0.00
V_{20Gy}			0.12	0.13	0.12	0.01	0.16	0.16	0.16	0.00
V_{30Gy}			0.03	0.03	0.03	0.00	0.02	0.03	0.02	0.00
Skin										
V_{10Gy}			0.64	0.65	0.62	0.01	0.52	0.52	0.52	0.00
V_{20Gy}			0.34	0.35	0.34	0.01	0.35	0.36	0.34	0.01
V_{30Gy}			0.14	0.16	0.13	0.01	0.10	0.12	0.10	0.01

Chapter 3. ELEANOR-PAT, An Energy Layer Selection Strategy for Proton Arc Therapy Based on Energy Layer Coverage Abilities

Authors

[*,†]Yunzhou Xia

[*,†]Adam H Aitkenhead

[†,‡]Robert Appleby

[*,†,‡]Michael J Merchant

[*,†,‡]Karen J Kirkby

[*,†]Ranald I MacKay

Affiliations

[*]Division of Cancer Sciences, Faculty of Biology, Medicine and Health, University of Manchester, United Kingdom

[†]Christie Medical Physics and Engineering, The Christie NHS Foundation Trust, Manchester, United Kingdom

[‡]Cockcroft Institute, United Kingdom

3.1 Rationale and strategy

Proton arc therapy (PAT) has the potential to further improve plan quality compared to intensity-modulated proton therapy (IMPT). However, PAT optimised with full energies per beam angle (FPAT) is impractical to deliver due to the energy layer switching time being magnitudes longer than the time spent on delivering the proton spots and on the scanning path. Currently only two energy reduction strategies exist which are spot scanning proton arc therapy (SPArc [1] – [5]) and proton mono-energetic arc therapy (PMAT [6]). Both strategies have their advantages and shortcomings as described in Chapter 1. Here I proposed a novel energy pre-selection strategy, ELEANOR-PAT (Energy Layer sElection bAsed oN cOveRage for Proton Arc Therapy) and showed that it successfully reduced the total number of energy layers delivered in PAT while maintaining the dosimetric advantages that FPAT possesses and that it is generalisable to eight ependymoma cases with differing geometries. Other potential energy reduction strategies had been explored before choosing ELEANOR-PAT as the main strategy to investigate. Section 3.2 describes this work not as part of the journal-format thesis starting in section 3.3, but as a separate thesis section to describe the preparatory work that led to the evolution of ELEANOR-PAT.

Individual author contributions are as follows. I modified the MATLAB code of matRad to support dose calculations based on beam commissioning data, single-field optimisation, energy layer reduction, plan analysis, robustness analysis and comparison to clinical dose evaluation sheets used at the Christie proton therapy centre. Adam H. Aitkenhead provided the commissioning data, anonymised DICOM CT and DICOM structure data for the eight ependymoma cases and their original planning dose objectives. I proposed ELEANOR-PAT, coded the energy layer reduction strategies and carried out the related analysis. Michael J. Merchant, Adam H. Aitkenhead, Robert Appleby, Ranald I. MacKay proposed alternative strategies, provided daily supervision as well as advice on the physical and clinical aspects of the strategies which included the deliverability. Karen J. Kirkby provided the opportunity for project funding. All authors have reviewed and commented on the manuscript.

3.2 Journey to the ELEANOR-PAT energy selection strategy

Energy reduction is important for deliverable PAT plans due to the scale of time spent on energy modulation in IMPT delivery. The time spent on energy modulation could be investigated in terms of accelerator designs, but this is outside the scope of this thesis. The aim of energy reduction strategies is to reduce the total number of energy layers to be delivered. However, with a reduced number of energy layers, the PAT plan quality degrades compared to FPAT as there are fewer proton spots available for dose optimisation, i.e., less degrees of freedom. Therefore, while reducing the total number of energy layers in a PAT plan, the proposed energy reduction strategy should not cause any plan degradation compared to the IMPT plan planned for the same case.

For a cyclotron (the type of accelerator installed at the Christie Proton Therapy Centre), due to hysteresis constraint of the magnet, the energy is always decreased from the maximum available energy (250 MeV at the Christie Proton Therapy Centre). This means that the time spent on energy modulation depends on whether it is an energy increase or decrease. According to the commissioning data obtained at the Christie proton therapy centre, an energy decrease (about 0.6 seconds) is faster than an energy increase (about 0.9 seconds). For a synchrotron, this difference also exists because of hysteresis of the magnet components along the synchrotron ring. Therefore, the proposed energy reduction strategy should also aim to reduce the number of energy increases [3].

In terms of the algorithm implementation, if energy reduction is incorporated into dose optimisation, i.e., SPArc, the dose optimisation process becomes time-consuming because the optimiser must calculate extra loss function components and remove low-weighted energy layers as additional processes. Therefore, I took an approach which is similar to PMAT, where the energy layers are selected prior to dose optimisation according to some designed energy selection strategy. This way, the number of proton spots fed into dose optimisation is less than FPAT, so the dose optimisation process is faster than FPAT dose optimisation.

From the above, a ‘sawtooth’ strategy was investigated. Within the ‘sawtooth’ strategy, the envelope enclosed by the maximum and minimum water equivalent depths of the target is equally divided into sections, e.g., 4 sections in figure 3-1. Within each section, a group of energies decreases from the maximum water equivalent depth to the minimum water equivalent depth, so the energies only decrease to fill the water equivalent thickness of the target. The red crosses indicate the maximum and minimum water equivalent depths of the target seen from beam’s eye view at the planned beam angles from 0 to 350 degrees at 10-degree interval. The blue circles are the energies selected by the ‘sawtooth’ strategy with a user-defined number of four groups of three energy increase actions, resulting in four groups of selected energies in descending order. It was found that the higher the number of groups, the better the CI and HI (figure 3-2).

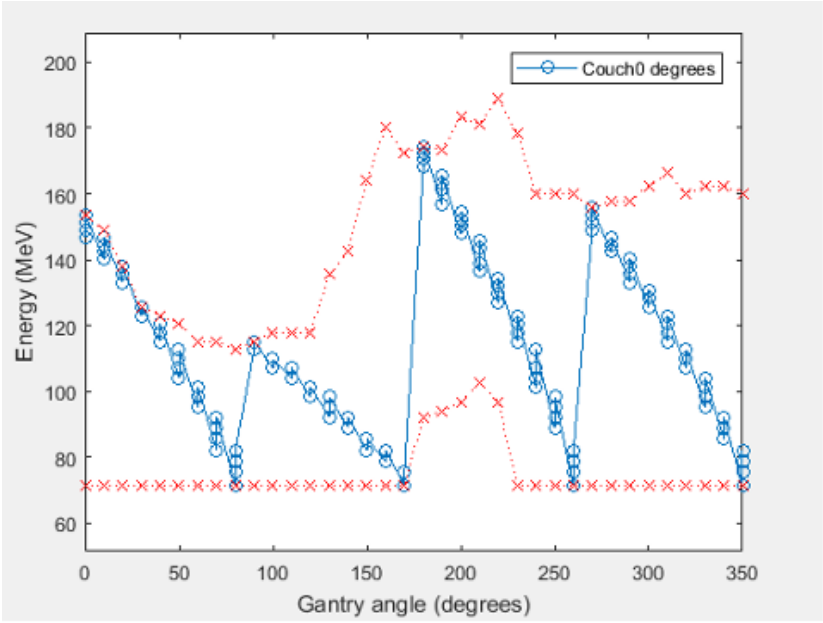

Figure 3-1: Illustration of the ‘sawtooth’ energy reduction strategy, where the energy (blue circles) only decreases between the maximum and minimum water equivalent thicknesses of the target (red crosses), and repeats for a number of times (number of groups) as defined by the user, e.g. 4 groups in this example.

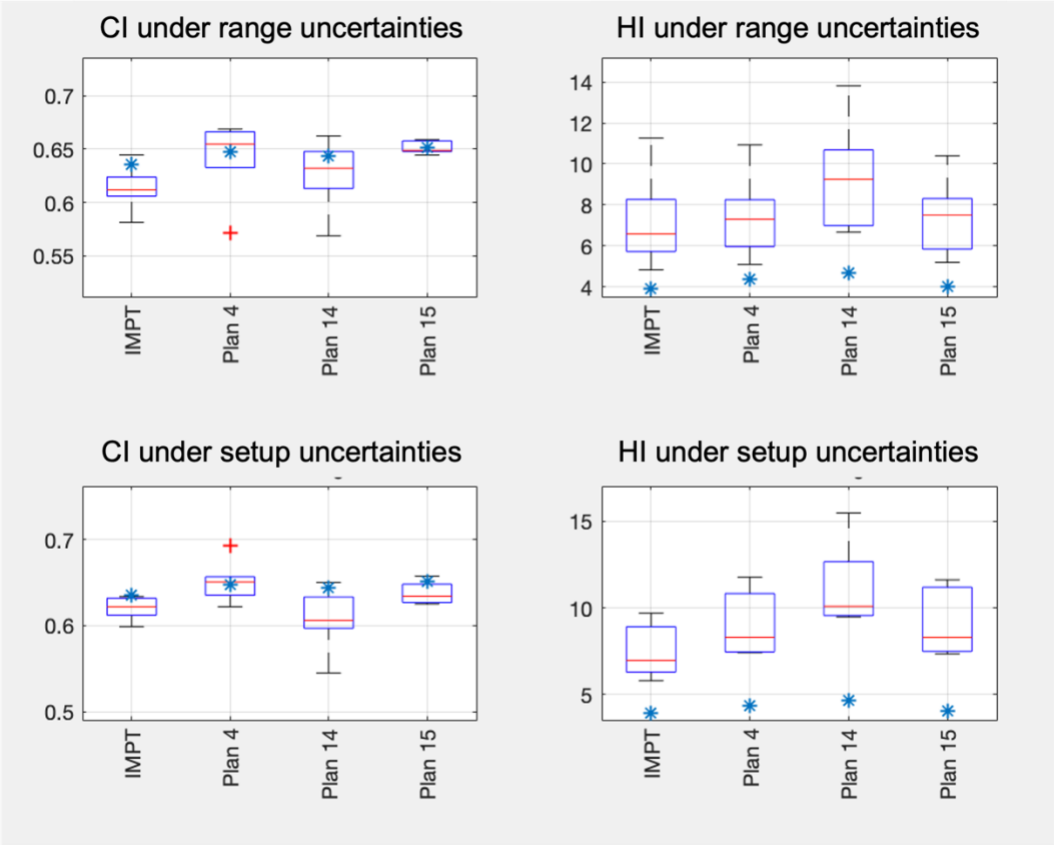

Figure 3-2: Comparison of CI and HI evaluated under the nominal scenario (blue star) and uncertainty scenarios (boxes) of the 'sawtooth' energy reduction strategy with 12 groups of energy decreases (Plan 4), 4 groups (plan 14) and 36 groups (plan 15) for an example ependymoma case P1, compared to the IMPT plan. More envelopes give better CI and HI.

The second strategy investigated was called the 'coverage' strategy, which was the initial form of ELEANOR-PAT (Energy Layer sElection bAsed oN cOveRage for PAT) strategy as described in detail in section 3.5. ELEANOR-PAT pre-selects energy layers based on the volume of the target each energy layer is able to cover and adds energy layers iteratively until robustness objectives are met. The 'coverage' strategy is the first part of ELEANOR-PAT, i.e., it does not consider the iterative addition of energy layers for the purpose of robustness as the last stage of ELEANOR-PAT. The 'coverage' strategy was motivated by finding the minimum number of proton spots required to provide adequate radiation coverage to the target. Compared to the 'sawtooth' strategy, the 'coverage' strategy and the ELEANOR-PAT strategy do not need to specify the number of groups (of energy decreases) which is a parameter that directly affects the plan quality with the 'sawtooth' strategy. Although the 'coverage' and ELEANOR-PAT strategies do not aim to reduce the number of energy increases, this was mitigated in Chapter 4 where the energies selected by the ELEANOR-PAT strategy are interpolated

across finer angles between the planned beam angles such that the number of energy increases equals the number of planned beam angles.

The third strategy investigated was called the ‘influence’ strategy which was inspired by the ‘coverage’ strategy. The ‘influence’ strategy was similar to ‘coverage’ strategy except that it sorts the spots in the order of the total amount of dose influence delivered to the target, so the energy layers with spots that deposit more dose in the target are selected. Because the energy selection process happens before dose optimisation, the dose influence of each spot is calculated based on the spot profile defined within the beam model. This becomes contradictory because a spot with a lower dose influence before dose optimisation can be given a higher weight after dose optimisation. Therefore, the ‘coverage’ strategy was developed further into ELEANOR-PAT as described in Chapter 3. The ELEANOR-PAT strategy then incorporated the ‘sawtooth’ strategy for deliverability in Chapter 4. The ‘coverage’ strategy was compared to the randomly selected energies to assess whether they are useful.

3.3 Abstract

Proton arc therapy (PAT) has shown the potential of improving plan quality compared to intensity-modulated proton therapy (IMPT). However, PAT delivered with full energies (FPAT), may be impractical due to the long energy layer switching times. I present a novel energy layer selection strategy, ELEANOR-PAT, to select the energy layers that are the most efficient at covering the target with dose prior to dose optimisation. The ELEANOR-PAT algorithm was validated with eight ependymoma cases with differing geometries under nominal and uncertainty scenarios.

ELEANOR-PAT offered 25% - 84% reduction of energy layers compared to FPAT and satisfied clinical dose and robustness requirements as specified by The Christie Proton Therapy Centre. The delivery time calculation suggested beam-on times of within 3 minutes per treatment, a significant time saving compared to IMPT considering beam switching times at multi-room proton therapy centres. ELEANOR-PAT plans indicated superior brainstem and skin sparing, and lower integral doses than IMPT on geometry-dependent basis. ELEANOR-PAT has the flexibility to select energy layers that deliver dose to smaller volumes of critical organs-at-risk, as a result of which the brainstem doses were 2% - 4% lower under nominal scenarios, and 13% - 18% lower under uncertainty scenarios. The ELEANOR-PAT can be easily implemented within the planning workflow, requiring no other changes to the existing algorithm, showing the potential of compatibility with IMPT treatment planning software.

ELEANOR-PAT is an effective energy layer selection strategy and a promising candidate for the practical PAT delivery of ependymoma cases.

Keywords: proton arc therapy, energy layer, robustness

3.4 Introduction

Arc therapy is a common technique used in photon radiation therapy for its ability to improve dose conformality and to greatly reduce the delivery time of treatments [7]. For these reasons, arc therapy for protons has been given great interest in recent years in the hope of combining the dosimetric benefits of protons and the delivery efficiency of arc therapy. Early plan comparison studies showed that proton arc therapy (PAT) planned with full energies for each beam angle improves target dose conformality and organs-at-risk sparing compared to intensity-modulated (scanned) proton therapy (IMPT) [8] - [10]. These dosimetric advantages were mainly due to the lack of exit dose of protons compared to photons and the more degrees of freedom, i.e., higher number of proton beamlets or proton spots in PAT dose optimisation compared to IMPT.

The delivery efficiency of PAT, however, is not as straightforward as photon arc therapy. This is due to the additional modulation of energies per beam angle in IMPT compared to intensity-modulated radiotherapy. The speed of energy modulation in IMPT is limited by the control of accelerator parts, e.g., the movement of energy degraders in and out of the beam path for cyclotrons or the cycle time in synchrotron rings, which makes the time spent on energy modulation on the scale of seconds, about three orders of magnitude longer than the time spent on intensity modulation (delivering dose to proton spots). The total time spent on energy modulation per treatment is then the product of the total number of energy modulations and the time spent on modulating the energy when required. This means that PAT with full energies would be incredibly time-consuming to deliver due to the large number of modulations of energy layers as the result of many beam angles.

Several studies report PAT strategies to reduce the number of energy layers. Ding *et al.* proposed a SPArc algorithm where dose optimisation starts with the full energies from all beam angles and then iteratively distributes energy layers into finer beam angles, removes low-weighted energy layers, and re-optimises the plan until a desired plan and angular spacing are reached [1] - [3]. SPArc was shown to achieve clinically relevant plans for a range of sites [4][5], but the additional

iterative process adds to the dose optimisation time [1], and the dose optimisation algorithm must be amended to account for these changes. On the other hand, Sanchez-Parcerisa et al. proposed to use only one or two pre-selected energy layers at the centre of the target [6]. This mono-energetic or bi-energetic energy pre-selection strategy is easily compatible with existing treatment planning software (TPS) as it only requires a separate module before dose optimisation. However, selecting one or two energy layers at the centre of the target compromised the plans with a large low dose bath due to limitations to tumour geometries [11] and their robustness were not assessed. The added dimensionality of rotational delivery for protons with the constraints on energy modulation and delivery-time form a complex problem where it is not easily understood how to achieve clinically relevant plans for generalised tumour geometries with an energy selection/reduction strategy that is time-efficient and easily compatible with existing TPS.

We propose an approach of pre-selecting energy layers prior to dose optimisation. The approach, named as ELEANOR-PAT (**E**nergy **L**ayer s**E**lection b**A**sed o**N** c**O**ve**R**age for **P**roton **A**rc **T**herapy), is based on a pre-assessment of the dose coverage abilities of candidate energy layers. The ELEANOR-PAT algorithm selects the energy layers which deliver dose to larger volumes of the target, i.e., higher energy layer coverage, preferentially over others (or smaller volumes of prioritised OARs for overlapping structures) with the constraint of meeting target dose constraints. As a result, the most efficient energy layers are selected while the target meets dose objectives. ELEANOR-PAT will be easily compatible with existing TPS as it is carried out separately before dose optimisation, which will be more time efficient compared to the full-energy PAT due to the reduced number of proton beamlets. We show that ELEANOR-PAT leads to clinically acceptable, robust, and delivery-efficient PAT plans for a group of brain tumours with varying geometries.

3.5 Method

This section consists of three parts: in section 3.5.1, we describe the clinically used dose optimisation process for IMPT which forms the PAT dose optimisation

process after energy layer selection using ELEANOR-PAT; in section 3.5.2, we describe the implementation of ELEANOR-PAT; in section 3.5.3, we describe the validation of ELEANOR-PAT via a group of eight ependymoma cases with varying geometries.

3.5.1 Dose optimisation

IMPT planning requires the planner to define beam angles and planning objectives at the start of the planning process. From each beam angle chosen, a number of beamlets from the energy layers will be delivered, where a beamlet represents the irradiation path of a single spot. The dose delivered to each voxel by each proton beamlet is calculated and constructed as a 2-dimensional dose-influence matrix. The matrix product of the dose-influence matrix and a vector of beamlet weights forms a dose vector, and the beamlet weights are optimised such that the dose vector meets the planning objectives. The speed of dose optimisation will be governed by the size of the dose influence matrix. ELEANOR-PAT pre-selects a set of energies, so a reduced dose-influence matrix with less energy layers and so less beamlets makes dose optimisation faster than full-energy PAT and produces a deliverable PAT plan.

3.5.2 Implementation of ELEANOR-PAT

The ELEANOR-PAT algorithm was implemented in MatRad (version Alan v2.1.0), a widely used open-source treatment planning software for radiotherapy planning for educational and research purposes [12][13]. The ELEANOR-PAT algorithm was implemented after the construction of the dose-influence matrix prior to the optimisation of beamlet weights. For each target voxel, the energy layer with the highest target coverage ability, which can be found from the dose influence matrix, is selected. This selection process is performed for all target voxels starting with those covered by the least number of energy layers. As the result, the solution where the minimum number of energy layers required to maximise target coverage, or alternatively with the option of achieving target coverage and minimising OAR coverage (described in section 3.5.2.3), is found. From this, a second dose-influence matrix with a reduced size is used for dose optimisation. A

flowchart summarising ELEANOR-PAT's implementation is provided in Appendix A. A conceptual illustration of ELEANOR-PAT is given in Appendix B.

3.5.2.1 Energy layer's coverage ability

In ELEANOR-PAT, an energy layer's coverage ability is related to the number of voxels the proton beamlets deliver dose to. If an energy layer covers many target voxels, it is said to have a high target coverage ability. High target coverage abilities tend to happen in the three situations described below or a mixture of them. The target coverage abilities, i.e., the exact number of target voxels receiving dose from an energy layer, can be quantified from the dose-influence matrix.

Situation 1: the energy layer passes through more tissue. This typically occurs where the energy layer stops in the distal part of the target.

Situation 2: the energy layer contains more beamlets than others. This typically occurs in the middle of the target where the number of spots delivered tends to be greater.

Situation 3: the energy layer contains bigger proton spots that cover more voxels. This typically occurs in shallower regions of the target for lower energies.

3.5.2.2 The XIA (energy layer's coverage) factor

Of the three situations described in 3.5.2.1, situation 1 easily dominates as the entrance dose of proton beamlets cover a large number of target voxels, and so ELEANOR-PAT would select a single highest energy from every beam angle. The resulting plan is similar to the concept of distal-edge tracking [14], where the distal target edge is tracked with the Bragg peak to maximise the dose fraction delivered to the target and minimises the dose delivered to healthy tissue. Such a plan indeed offers a solution with very few energy layers (only one per beam angle) but

could suffer robustness issues as the Bragg peaks are positioned closely to the distal boundary between target and healthy tissue.

We therefore introduced a dose threshold factor when constructing the first dose-influence matrix, which was used for ELEANOR-PAT only, i.e., no threshold for dose optimisation. We called this factor the **X**-percentage **I**sodose cover**A**ge (XIA) factor. The XIA factor determines the coverage ability of an energy layer and is defined as the percentage threshold of dose relative to 100% at the Bragg peak of a beamlet. For example, if the XIA factor is 80%, then for each beamlet, only > 80% Bragg peak isodose region contributes to the coverage ability of the energy layer (figure 3-3). This reduces the dominance of situation 1 and consequently selects more energy layers than a 0% XIA factor (no dose threshold) as a larger XIA factor means "worse" coverage ability of energy layers. A XIA factor of 0% leads back to the single-energy 'distal-edge tracked' PAT plans. A value of 80% was used as the default XIA factor based on evaluations of ELEANOR-PAT plans optimised with XIA factors ranging from 40% to 80% at 10% intervals. The effect of varying the XIA factor on the plan quality is provided in the Results section 3.6.

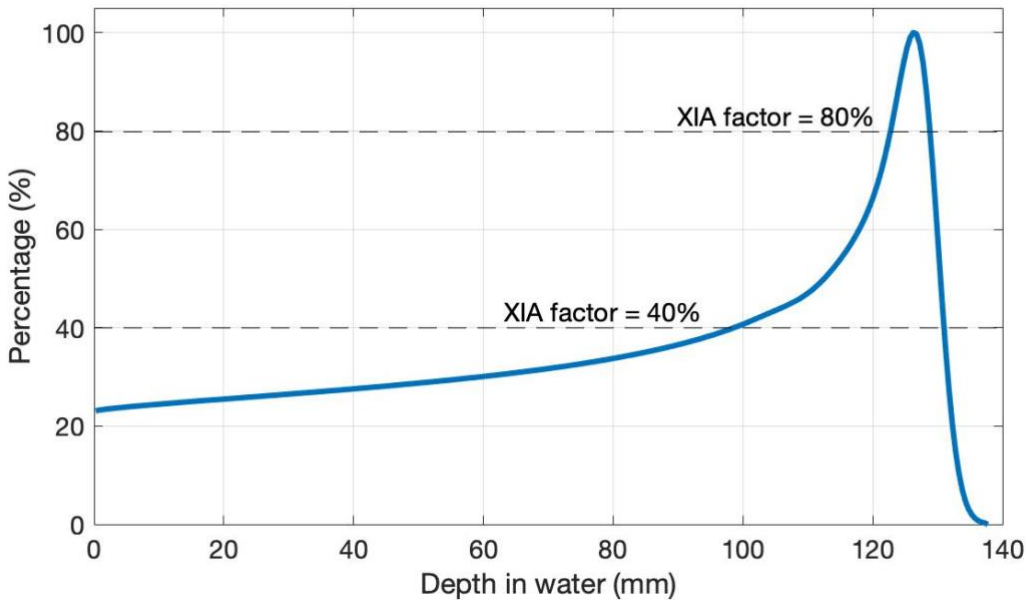

Figure 3-3: Percentage depth-dose curve of a 130 MeV proton beam explains the XIA factor. A value of 80% means only the peak region greater than 80% contributes to the coverage of this energy layer. When using a XIA factor of 80%, individual energy layers cover a smaller volume than 40% and leads to more energy layers selected, and consequently better plans due to more degrees of freedom for dose optimisation.

3.5.2.3 Finding the minimum number of energy layers with ELEANOR-PAT

From the dose-influence matrix with 80% XIA factor, a table was formed with the dimension of the number of target voxels. The table stores 1) for each target voxel, which energy layers (defined by the 80% XIA factor) cover it, and 2) for each energy layer that covers the target voxel, the exact numbers of target and OAR voxels it covers in total. This table is then sorted so that it starts with the target voxel covered by the least number of energy layers. Starting with the first target voxel, the energy layer with the highest target coverage ability is selected. If a later target voxel can be covered by any of the previously selected energy layers, no additional energy layer will be selected for the later target voxel. Done in this order, the selection guarantees full target coverage with the least number of energy layers (defined by the 80% XIA factor). A conceptual step-by-step illustration of finding the minimum energy layers is provided in Appendix B.

For cases where there is a critical OAR overlapping with the target, the number of beamlets falling inside the OAR must be minimised to spare it. Instead of selecting the energy layer with the highest target coverage ability for each target voxel in the table, the energy layer with the lowest OAR coverage ability can be selected. This still guarantees target coverage but preferentially selects energy layers that cover less OAR voxels. A comparison between selecting energy layers with the highest target coverage abilities and with the lowest OAR coverage abilities is provided in the results (section 3.6.1.2).

For ease of delivery, we considered the case where the gantry rotates at a constant speed to deliver an arc. This was simulated by selecting energy layers evenly across equally spaced beam angles.

3.5.3 Validation of ELEANOR-PAT

3.5.3.1 Treatment planning

8 ependymoma cases, P1 – P8, with differing geometries, locations and volumes were used retrospectively to validate the generalisation of ELEANOR-PAT. Table 3-1 provides a description of the cases, prescription doses, primary OARs, the planned beam angles, and the use of range shifters. Single-field optimisation was used in IMPT as it met clinical dose and robustness requirements under eight uncertainty scenarios, which included 2 range uncertainties (-3.5%, +3.5%) and 6 setup uncertainties (3 mm shift in left-right, superior-inferior, anterior-posterior). PAT plans adopted multi-field optimisation as each beam angle was not required to deliver the full energies. PAT plans were also evaluated under the uncertainty scenarios and met robustness requirements. PAT were planned with 10-degree spacing between control points (following [9]) and with the same dose objectives as IMPT. Partial arcs were chosen by the planner based on the beam angles that would reduce the amount of normal tissue irradiated in the beam path. The option of selecting energy layers with the lowest OAR coverage abilities was applied in four cases (P1, P6, P7, P8) as they contained critical OARs overlapping the target.

ELEANOR-PAT plans were optimised for the 8 ependymoma cases and compared to the respective IMPT plans and full-energy PAT (FPAT) plans, in terms of dose, robustness, and estimated beam-on time. All plans were optimised within MatRad.

Table 3-1: Eight ependymoma cases, P1 – P8, were used to validate the ELEANOR-PAT algorithm. The below table describes their geometries, prescriptions, beam angles and the uses of range shifters for IMPT and PAT (including ELEANOR-PAT, FPAT and PAT-random) plans. PAT plans were delivered at couch angle zero degree.

				IMPT		PAT	
Case identifier	CTV volume (cc) and approximate location	Prescription to CTV and number of fractions (fx)	Primary OAR	Gantry (G) and couch (T) angles (°)	Range shifter (cm)	Gantry (G) and couch (T) angles (°)	Range shifter (cm)
P1	18 cc Posterior to and	54 Gy 30 fx	Brainstem	G120 T0 G180 T0	None	G90 – G270	None

	overlapping brainstem.			G240 T0			
P2	45 cc Posterior to and enclosing brainstem.	54 Gy 30 fx	Brainstem	G135 T0 G225 T0 G180 T0	2 2 2	G90 – G270	None
P3	43 cc Forehead right hand side.	59.4 Gy 33 fx	Skin	G10 T0 G320 T0	3 3	G230 – G50	None
P4	67 cc Forehead left hand side.	59.4 Gy 33 fx	Left eye	G45 T0 G320 T0	5 5	G320 – G90	None
P5	118 cc Off-centre to the left-hand side.	59.4 Gy 33 fx	Brainstem	G70 T0 G175 T0 G105 T305	5 5 5	G40 – G220	None
P6	64cc Off-centre to the left-hand side and encloses brainstem.	59.4 Gy 33 fx	Brainstem	G115 T0 G150 T0 G190 T0	2 2 2	G115 – G245	None
P7	99 cc Central and enclosing brainstem.	59.4 Gy 33 fx	Brainstem	G180 T0 G110 G330 G250 T30	None	G90 – G270	None
P8	9 cc Superior to and overlapping brainstem.	59.4 Gy 33 fx	Brainstem	G80 T0 G280 T0 G300 T90	None	G90 – G270	None

3.5.3.2 Plan and robustness evaluation

Plans were assessed against the clinical brain and head and neck assessment criteria used at the Christie Proton Therapy Centre. CTV D98%, D95% and D2% were required to be >90%, >95%, and <110% prescription respectively under the nominal and the eight uncertainty scenarios. Brainstem D0.1cc, D50% and D10% must be < 58 Gy, < 54 Gy and < 56 Gy respectively. Spinal cord maximum dose must be < 54 Gy. Eye D90%, D50%, D10% must be < 10 Gy, < 30 Gy and < 54 Gy respectively. Maximum dose for skin with 2mm thickness must be < 66 Gy. Integral dose was calculated according to equation 3-1 to represent the total energy imparted to the patient [15]:

Equation 3-1: Definition of the integral dose used in Chapter 3.

$$Integral\ dose = \sum_i D_i * \rho_i * V_i$$

where D_i, ρ_i, and V_i are the dose, density, and voxel volume of the ith voxel in the body.

If an ELEANOR-PAT plan did not meet robustness requirements initially, the number of energy layers per beam angle was increased iteratively by selecting the energy layer that has the next highest target coverage. If the new plan satisfied the robustness requirements, it became the final ELEANOR-PAT plan.

3.5.3.3 Estimation of beam-on time

Beam-on times were calculated based on an energy layer switch time of 900 milliseconds for an energy increase and 600 milliseconds for an energy decrease (based on commissioning data from The Christie), and a conservative estimate of the average delay between adjacent spots of 2.5 milliseconds based on typical scanning slew rates and beam switching delays. The dose rate for individual energy layers was calculated based on the assumption that a dose rate of 2 Gy/litre/minute [16][17] could be delivered to any target volume at any depth. It was assumed that the PAT plans were delivered in one continuous arc in the order

of increasing beam angles and decreasing energies, without beam breaks or patient re-positioning, so the beam-on time is the time from delivering the first spot to the last spot.

3.5.3.4 Comparison to randomly selected energy layers

To evaluate the effectiveness of ELEANOR-PAT, we compared ELEANOR-PAT to an alternative energy layer selection strategy, which should be unbiased and give deliverable plans. These were satisfied by a random energy selection strategy that chooses from the set of energies that cover the target (PAT-random). The number of energy layers per beam angle in PAT-random was kept the same as that in the ELEANOR-PAT plans.

3.6 Results

3.6.1 Plan and robustness evaluation

3.6.1.1 Target coverage

ELEANOR-PAT plans met all clinical dose requirements under nominal (error-free) scenarios. CTV D98%, D95% and D2% ranged from 94% to 99%, 97% to 100% and 100% to 103% for ELEANOR-PAT plans (Appendix C), which suggests that ELEANOR-PAT plans had excellent target dose coverages. The FPAT plan metrics for CTV coverages were generally better than IMPT and ELEANOR-PAT, suggesting the advantages of using more energy layers, although the differences were within 1%.

3.6.1.2 OAR sparing, skin dose, and integral dose

Brainstem was spared better in ELEANOR-PAT plans for P1, P2 and P5 than IMPT plans as shown in figure 3-4. These cases had the target situated between

OARs and the beam entrance points. For cases where the target enclosed the brainstem or spinal cord (P6, P7), or where the target was superior to the brainstem (P8), the brainstem or spinal cord doses were very similar (P7, P8) or higher (P6) for PAT than IMPT plans (Appendix C). The higher brainstem dose for P6 was due to the specific target geometry, i.e., target situates superior to the brainstem, and perhaps due to the arc in the transversal plane rather than the coronal plane (matRad does not support couch rotations). Eye doses were similar for P4.

The maximum skin doses were 4% - 18% lower in four ELEANOR-PAT plans than IMPT (figure 3-5 and Appendix C) and similar for two cases out of the seven cases with available skin contours. The lower skin dose was due to the target prescription dose spread over a larger angular range, covering a larger area of skin.

Integral doses for the CTVs were very similar across the three types of plans. A comparison of the brain integral doses (figure 3-6) shows reductions in PAT plans, ranging from 3% to 21% for three cases which are deeper-seated targets. Higher integral doses, between 23% and 52% increases were seen for shallower targets.

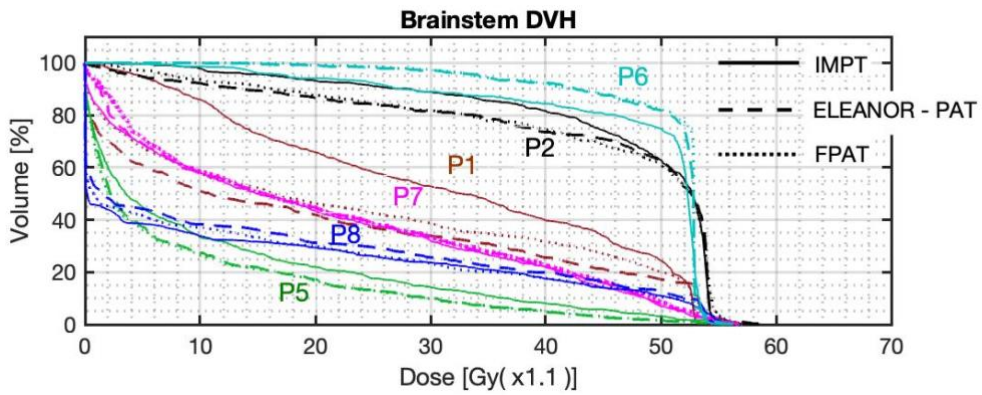

Figure 3-4: Brainstem DVHs for three cases (P1, P2, P5) show reductions in brainstem doses in ELEANOR-PAT (dashed) and FPAT (dotted) plans compared to IMPT (solid line). The other three cases (P6, P7, P8) show similar or higher brainstem dose levels due to their individual geometries and planning priorities.

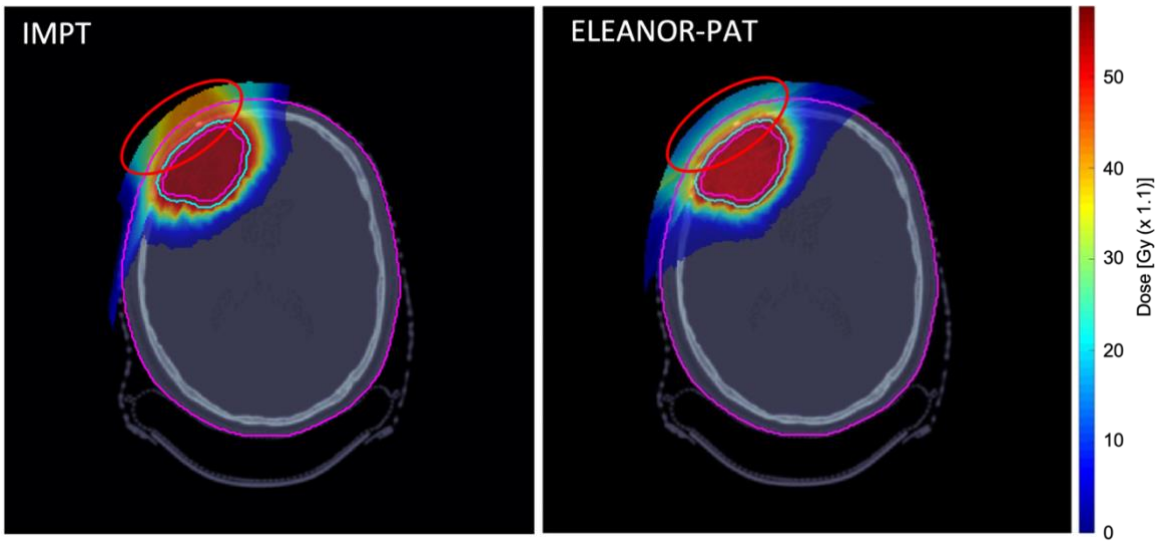

Figure 3-5: An example of the maximum skin dose for P3 shows that skin dose is lower in the ELEANOR-PAT plan than IMPT, but dose covers a larger area of skin. Magenta: CTV; Cyan: PTV; Pink: patient contour.

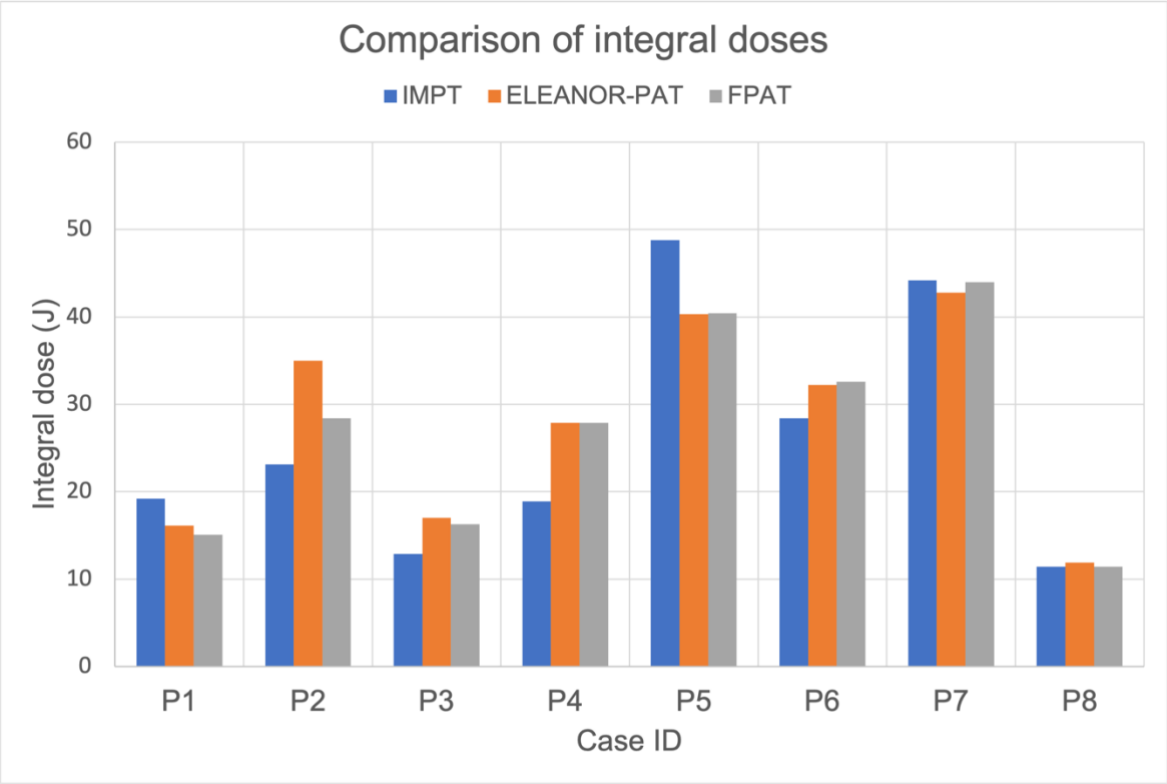

Figure 3-6: A comparison of the integral doses for the eight ependymoma cases amongst IMPT, ELEANOR-PAT and FPAT plans.

3.6.1.3 Robustness evaluation

ELEANOR-PAT plans met clinical robustness requirements for two cases with shallow targets. The other cases met robustness requirements after the numbers of energy layers were increased from the initial ELEANOR-PAT solutions, going from 2 to 12 layers per beam angle to values from 5 to 17 per beam angle for the robust solutions. DVHs with uncertainty bands in figure 3-7 show higher robustness with more energy layers selected per beam angle.

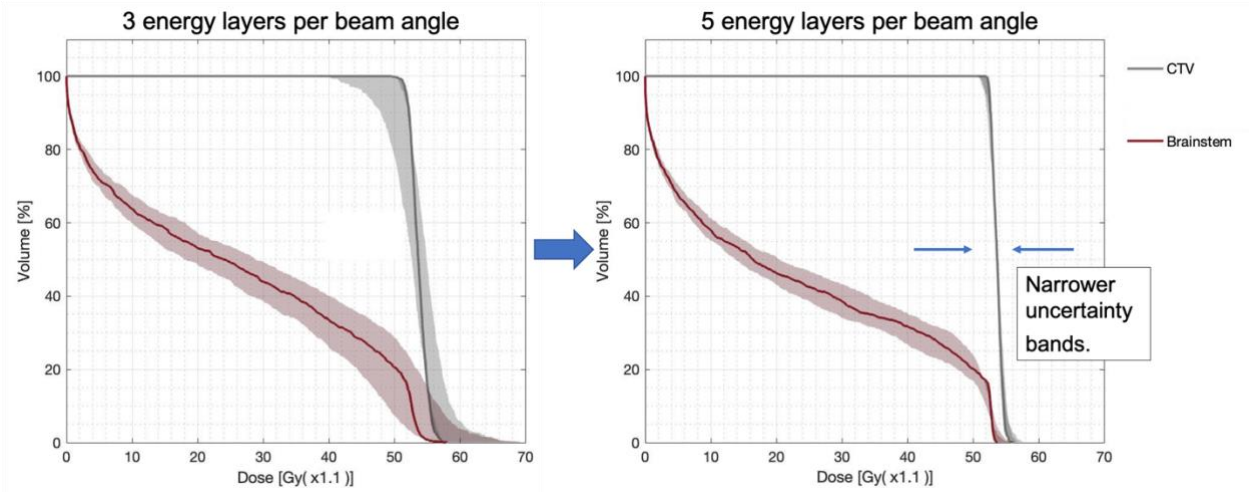

Figure 3-7: Left: CTV and brainstem DVHs for an example case's (P1) ELEANOR-PAT plan, optimised with 3 energy layers per beam angle, shows larger uncertainty bands (under the six setup and two range error scenarios) than ELEANOR-PAT plan with 5 energy layers per beam angle. This shows higher robustness for plans with more energy layers per beam angle.

3.6.1.4 The option of avoiding OARs

For the four cases where brainstem overlaps with the target, the maximum brainstem doses were 2% - 4% lower using the option of avoiding the OARs during ELEANOR-PAT (method section 3.5.2.3) under nominal scenarios, and 13% - 18% lower under uncertainty scenarios.

3.6.2 Beam-on times

ELEANOR-PAT reduced the number of energy layers by between 25% and 84% compared to FPAT, leading to reduced beam-on times of between 27 and 153 seconds for ELEANOR-PAT plans (figure 3-8). The additional energy layers for improving robustness increased the beam-on times to between 60 and 185 seconds, making robust ELEANOR-PAT plans deliverable under about 3 minutes.

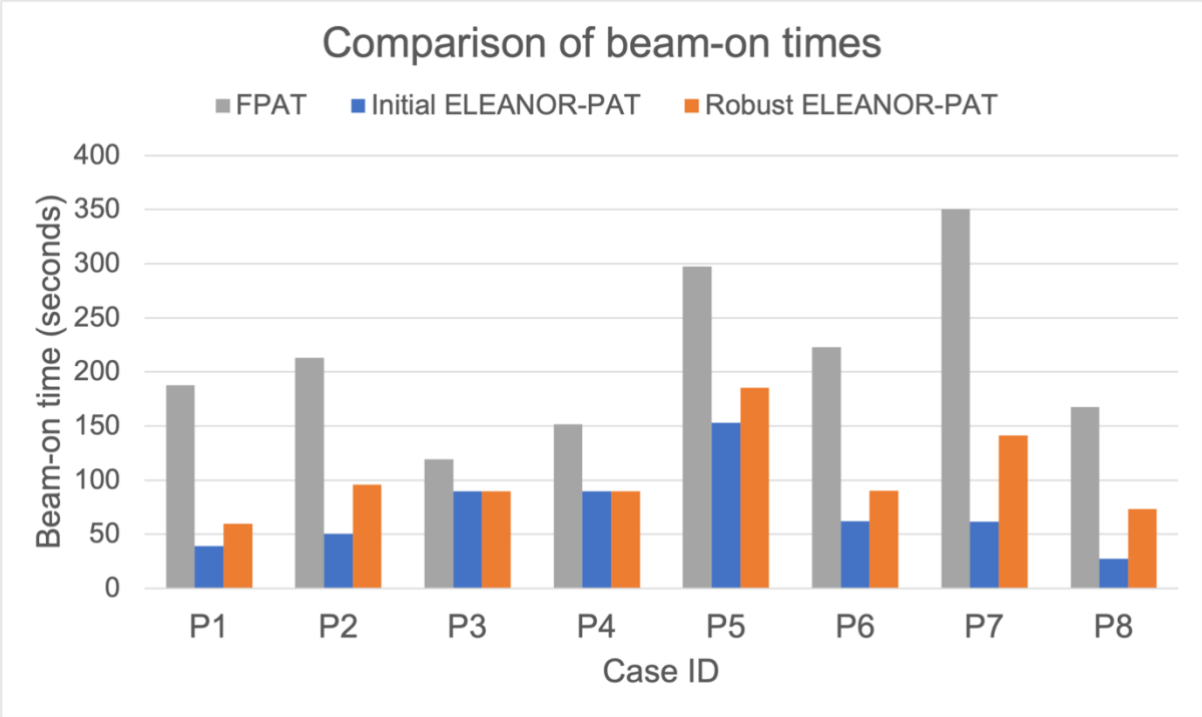

Figure 3-8: Estimated beam-on times of ELEANOR-PAT plans compared to FPAT plans show reductions between 25% to 84%. It was assumed that FPAT was interpolated and delivered in one continuous arc. First-pass ELEANOR-PAT always met the nominal (error-free) dose requirements, but not always the robustness requirements, so the number of energy layers was increased until robustness requirements were met.

3.6.3 Comparison to PAT-random

Five PAT-random plans passed the clinical dose criteria under nominal scenarios but showed higher brainstem and skin doses than the ELEANOR-PAT plans (Appendix C). The other three PAT-random plans failed to meet the dose requirements on CTV coverages. The brain maximum doses were 1.3 % - 13.9 % higher in PAT-random plans than ELEANOR-PAT plans, suggesting ‘hot spots’, i.e., worse homogeneity. Under uncertainty scenarios, none of the PAT-random plan met the dose requirements in terms of CTV coverages. OAR doses exceeding the clinical limits were seen in five cases. These suggest that

ELEANOR-PAT is a reliable strategy for achieving clinically acceptable and robust plans.

3.6.4 The effect of varying the XIA factor

A XIA factor of 40% yielded the least energy layers and 80% yielded the most energy layers. All ELEANOR-PAT plans optimised with 40%-80% XIA factors passed the assessment criteria under nominal scenarios. However, plans with 40% XIA factor failed to meet robustness requirements. Figure 3-9 shows the target homogeneity, defined as (D95% - D5% / prescription dose), of IMPT and ELEANOR-PAT planned with varying XIA factors. Trends of decreasing HI values can be seen for increasing XIA factors, suggesting better target homogeneity for higher XIA factor values.

Figure 3-9 shows longer estimated beam-on times for higher XIA factor values. The choice of the XIA factor is about the balance between plan quality and delivery time. As the difference in beam-on times is relatively short (about 30 seconds) compared to the reduction in the overall beam-on times, a higher XIA factor value of 80% is recommended, which gives better plan qualities. On the other hand, at centres where the difference in beam-on times might be a considerable improvement to patient throughput, lower values could be advantageous.

(the rest of this page intentionally left blank)

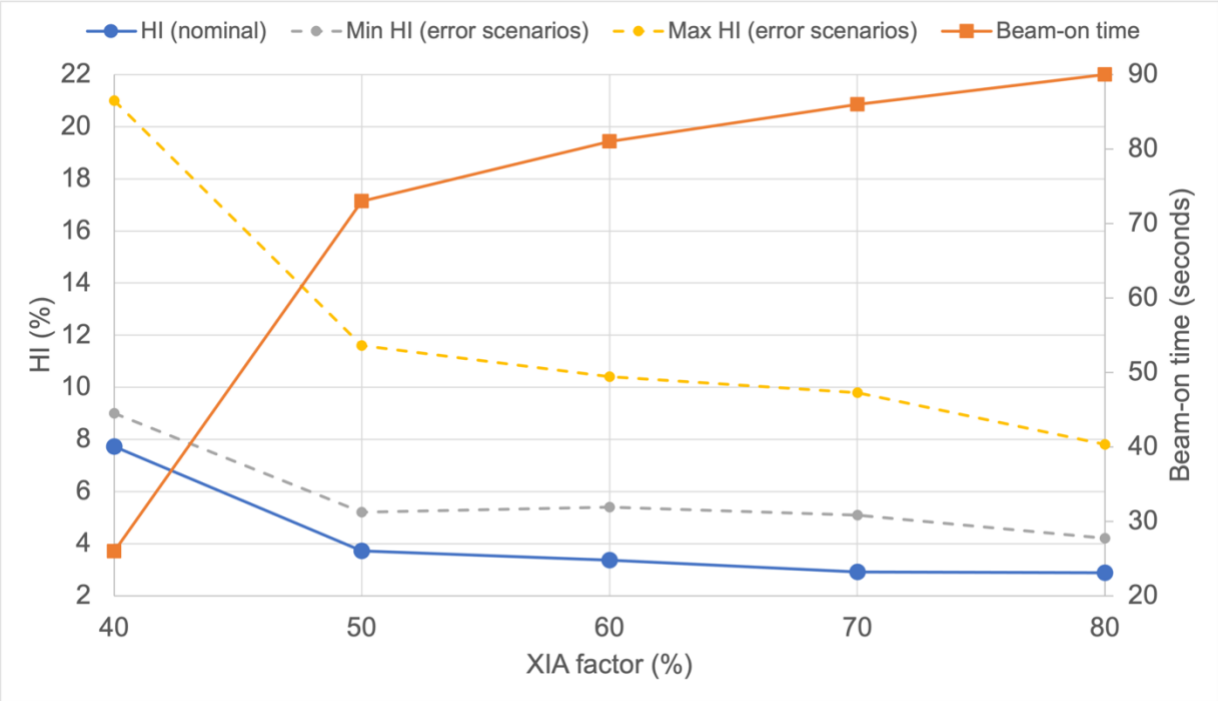

Figure 3-9: The XIA factor, a metric for energy layer coverage ability, plotted against the homogeneity index and estimated-on time for a representative case (P3). Homogeneity index, defined as (D95% - D5% / prescription dose), improves with increasing XIA factor. Robustness of the ELEANOR-PAT plans, represented with the maximum and minimum HI under error scenarios, improves with increasing XIA factors. However, a higher XIA factor value leads to longer beam-on times.

3.7 Discussion

ELEANOR-PAT successfully reduced the number of energy layers and satisfied the clinical and robustness requirements for a general group of ependymoma cases. Using ELEANOR-PAT, the estimated beam-on times were reduced from a range of 2 - 6 minutes for FPAT to 1 - 3 minutes. The estimated beam-on times suggest a constant gantry rotation speed ranging between 1 - 3 degrees per second for a single arc, which is a practical regime as it is lower than the upper speed limit of proton gantries (usually 6 degrees per second) and would not require gantry acceleration when delivering the arc. From the algorithmic perspective, ELEANOR-PAT would be easily compatible with existing TPS as it is a separate module inserted before the dose optimisation module. In addition, dose optimisation for ELEANOR-PAT is much faster than the full energy layers due to the reduced dose-influence matrix, assuming the same optimiser and hardware are used.

Brainstem and spinal cord were the primary OARs in this study. They are vital organs for controlling both voluntary and involuntary activities of the body and are also known to be serial organs in which damages to any sub-unit would cause entire organ failure. When normal tissue overlaps a tumour, it is challenging to spare the normal tissue while maintaining the prescription dose to the target wrapping around the OAR. The doses delivered to the brainstem outside of the target were notably lower when planned with ELEANOR-PAT than IMPT. This suggests that ELEANOR-PAT provides better sparing of the brainstem in these cases.

Skin dose is a concern in proton therapy due to the lack of a skin-sparing effect for proton beams [18][19]. High skin dose has the risk of causing severe skin toxicity [20]. We showed that the maximum skin doses were systematically lower in six out of seven ELEANOR-PAT plans compared to IMPT (Appendix C), which suggests the potential application of ELEANOR-PAT to reduce the skin dose on a case-dependent basis.

Compared to IMRT, the lack of exit dose in IMPT usually means lower integral dose, which typically means fewer normal tissue complications than IMRT [21]. Using comparable experience from photons, where a bigger volume of normal tissue is exposed to lower doses in VMAT, there are concerns that this may increase the incidence of second cancers in long-term survivors compare to IMRT [22].

Reductions of the integral dose were seen in three ELEANOR-PAT plans where the targets were deeper-seated. We observe this reduction to be depth- and case-dependent, which suggests that PAT could potentially bring fewer normal tissue complications than IMPT. Therefore, the integral dose and risk of secondary cancers must be examined case-by-case.

Although demographic or clinical information were not available as the DICOM data were anonymised, dose optimisations were carried out based on the clinically contoured structures, original prescriptions, and original planning objectives used

in the clinic, so most relevant clinical factors had already been considered within these entities.

3.7.1 Delivery time

To model the delivery of ELEANOR-PAT plans under continuous gantry rotation, energies for each layer are interpolated from the 10-degree control point spacing. The interpolation has negligible effects on plan quality as the plans are re-optimised on the interpolated energy layers. For the cases in this study, the dose differences after interpolation and re-optimisation were within 1% for targets and OARs. Estimated beam-on times of the interpolated ELEANOR-PAT plans are also unchanged because the number of energy layers, the number of spots and spot monitor units are the same.

Although IMPT delivery has shorter beam-on times than ELEANOR-PAT due to a smaller number of energy layers, it has additional factors to consider. For example, IMPT usually involves the delivery of multiple beams, which requires time to rotate the gantry and couch to the correct positions. At multi-room proton therapy centres, beam is often switched between treatment rooms on completion of a single beam angle delivery to maximise patient throughput, although this increases the fraction time for an individual patient [23]. In addition, range shifters in IMPT take time to move in and out of the beam path, and we showed that range shifters were not necessary for ELEANOR-PAT. We estimate beam-on times for ELEANOR-PAT plans to be within 3 minutes, which are a significant improvement of delivery efficiency compared to IMPT.

3.7.2 Advantages and limitations of ELEANOR-PAT

Selecting energy layers prior to dose optimisation in ELEANOR-PAT brings several algorithmic advantages. Dose optimisation is fast compared to FPAT because of the reduced dose-influence matrix. Although energy layer pre-selection takes additional time, it can generally be completed on the minute scale. The algorithm would be easily incorporated into existing TPS as a separate module before dose optimisation, which enables the choice of planning IMPT and PAT

using the same software without having to amend the established dose optimisation algorithm.

From the planning perspective, ELEANOR-PAT can achieve clinically acceptable plans for a range of target geometries, locations, and sizes, making it applicable for general (brain) cases. The selected energy layers are the minimum number of energy layers required to ensure target dose coverage for a defined XIA factor.

Robust requirements were always met within 5 iterations of energy layer selections with ELEANOR-PAT. First-pass ELEANOR-PAT solutions (using the minimum number of energy layers) failed to meet dose objectives due to insufficient numbers of layers for meeting both nominal and robustness requirements. This was expected as robustness was not an assessment criterion for the first-pass choice of energy layers. Figure 3-7 shows robustness improvement with the increased number of energy layers and this was due to a higher number of proton beamlets. If an ELEANOR-PAT plan failed to meet robustness requirements, the number of energy layers was increased which required a low computational overhead.

3.8 Conclusions

In this study, we present ELEANOR-PAT as a novel energy layer selection algorithm for proton arc therapy which has been demonstrated for eight different brain cases. ELEANOR-PAT can substantially reduce the delivery time of proton arc therapy while improving tissue sparing and ensuring robustness compared to intensity-modulated proton therapy. It has the potential to be easily fitted into existing treatment planning software as a separate module, offering a flexible, economic, and time-efficient solution to reduce the energy layers strategically for proton arc therapy.

3.9 References

[1] Ding, X., Li, X., Zhang, J.M., Kabolizadeh, P., Stevens, C. and Yan, D., 2016. Spot-scanning proton arc (SPArc) therapy: the first robust and delivery-efficient spot-scanning proton arc therapy. *International Journal of Radiation Oncology* Biology* Physics*, *96*(5), pp.1107-1116.

[2] Ding, X., Li, X., Qin, A., Zhou, J., Yan, D., Stevens, C., Krauss, D. and Kabolizadeh, P., 2018. Have we reached proton beam therapy dosimetric limitations? – a novel robust, delivery-efficient and continuous spot-scanning proton arc (SPArc) therapy is to improve the dosimetric outcome in treating prostate cancer. *Acta Oncologica*, *57*(3), pp.435-437.

[3] Liu, G., Li, X., Zhao, L., Zheng, W., Qin, A., Zhang, S., Stevens, C., Yan, D., Kabolizadeh, P. and Ding, X., 2020. A novel energy sequence optimization algorithm for efficient spot-scanning proton arc (SPArc) treatment delivery. *Acta Oncologica*, *59*(10), pp.1178-1185.

[4] Li, X., Kabolizadeh, P., Yan, D., Qin, A., Zhou, J., Hong, Y., Guerrero, T., Grills, I., Stevens, C. and Ding, X., 2018. Improve dosimetric outcome in stage III non-small-cell lung cancer treatment using spot-scanning proton arc (SPArc) therapy. Radiation Oncology, 13(1), pp.1-9.

[5] Ding, X., Zhou, J., Li, X., Blas, K., Liu, G., Wang, Y., Qin, A., Chinnaiyan, P., Yan, D., Stevens, C. and Grills, I., 2019. Improving dosimetric outcome for hippocampus and cochlea sparing whole brain radiotherapy using spot-scanning proton arc therapy. *Acta Oncologica*, *58*(4), pp.483-490.

[6] Sanchez-Parcerisa, D., Kirk, M., Fager, M., Burgdorf, B., Stowe, M., Solberg, T. and Carabe, A., 2016. Range optimization for mono-and bi-energetic proton modulated arc therapy with pencil beam scanning. *Physics in Medicine & Biology*, *61*(21), p.N565.

[7] Palma, D.A., Verbakel, W.F., Otto, K. and Senan, S., 2010. New developments in arc radiation therapy: a review. Cancer treatment reviews, 36(5), pp.393-399.

[8] Rah, J.E., Kim, G.Y., Oh, D.H., Kim, T.H., Kim, J.W., Kim, D.Y., Park, S.Y. and Shin, D., 2016. A treatment planning study of proton arc therapy for para-aortic lymph node tumors: dosimetric evaluation of conventional proton therapy, proton

arc therapy, and intensity modulated radiotherapy. *Radiation Oncology*, *11*(1), pp.1-10.

[9] Seco, J., Gu, G., Marcelos, T., Kooy, H. and Willers, H., 2013. Proton arc reduces range uncertainty effects and improves conformality compared with photon volumetric modulated arc therapy in stereotactic body radiation therapy for non-small cell lung cancer. *International Journal of Radiation Oncology* Biology* Physics*, *87*(1), pp.188-194.

[10] Blanco Kiely, J.P. and White, B.M., 2016. Dosimetric feasibility of single-energy proton modulated arc therapy for treatment of chordoma at the skull base. *Acta Oncologica*, *55*(9-10), pp.1243-1245.

[11] Bertolet, A, and A Carabe. “Proton monoenergetic arc therapy (PMAT) to enhance LETd within the target.” Physics in medicine and biology vol. 65,16 165006. 19 Aug. 2020, doi:10.1088/1361-6560/ab9455

[12] Cisternas, E. , et al. "matRad - a multi-modality open source 3D treatment planning toolkit." Springer International Publishing (2015).

[13] Wieser, H. , et al. "Development of the open-source dose calculation and optimization toolkit matRad." Medical Physics 44.6(2017).

[14] J. O. Deasy, D. M. Shepard, and T. R. Mackie, ‘‘Distal edge tracking: A proposed delivery method for conformal proton therapy using intensity modulation,’’ in XIIth International Conference on the Use of Computers in Radiation Therapy, edited by D. D. Leavitt and C. Starkschall Medical.

[15] Murshed H, et al. Dose and volume reduction for normal lung using intensity-modulated radiotherapy for advanced-stage non-small-cell lung cancer. Int J Radiat Oncol Biol Phys. 2004;58(4):1258–67.

[16] Mellenberg D.E. Varian Particle Therapy. AAPM Varian Proton Symposium, 2013. URL: https://www.aapm.org/meetings/2013AM/documents/VarianProtonSymposiumAAPM.pdf [Accessed: 5th August 2021]

[17] Göbel H. Dose delivery system of the Varian ProBeam system with continuous beam. Workshop on innovative delivery systems in particle therapy, 2017. URL: https://agenda.infn.it/event/12108/contributions/12217/attachments/9000/10188/Holger.pdf [Accessed: 5th August 2021]

[18] Gaito, S et al. “Skin Toxicity Profile of Photon Radiotherapy versus Proton Beam Therapy in Paediatric and Young Adult Patients with Sarcomas.” Clinical oncology (Royal College of Radiologists (Great Britain)) vol. 33,8 (2021): 507-516. doi:10.1016/j.clon.2021.03.009

[19] Kern, A., Bäumer, C., Kröninger, K., Wulff, J. and Timmermann, B., 2021. Impact of air gap, range shifter, and delivery technique on skin dose in proton therapy. *Medical Physics*, *48*(2), pp.831-840.

[20] Moskvin, V., Lasley, F.D., Ray, G.L., Gautam, A.S., Cheng, C.W., Das, I.J. and Buchsbaum, J.C., 2014. Acute skin toxicity associated with proton beam therapy in spine and brain patients. *Journal of Radiation Oncology*, *3*(2), pp.195-203.

[21] Patyal, B., 2007. Dosimetry aspects of proton therapy. Technology in cancer research & treatment, 6(4_suppl), pp.17-23.

[22] Hall, E.J., 2006. Intensity-modulated radiation therapy, protons, and the risk of second cancers. *International Journal of Radiation Oncology* Biology* Physics*, *65*(1), pp.1-7.

[23] Aitkenhead, A H et al. “Modelling the throughput capacity of a single-accelerator multi treatment room proton therapy centre.” The British journal of radiology vol. 85,1020 (2012): e1263-72. doi:10.1259/bjr/27428078

3.10 Appendix

3.10.1 Appendix A: Flowchart for ELEANOR-PAT

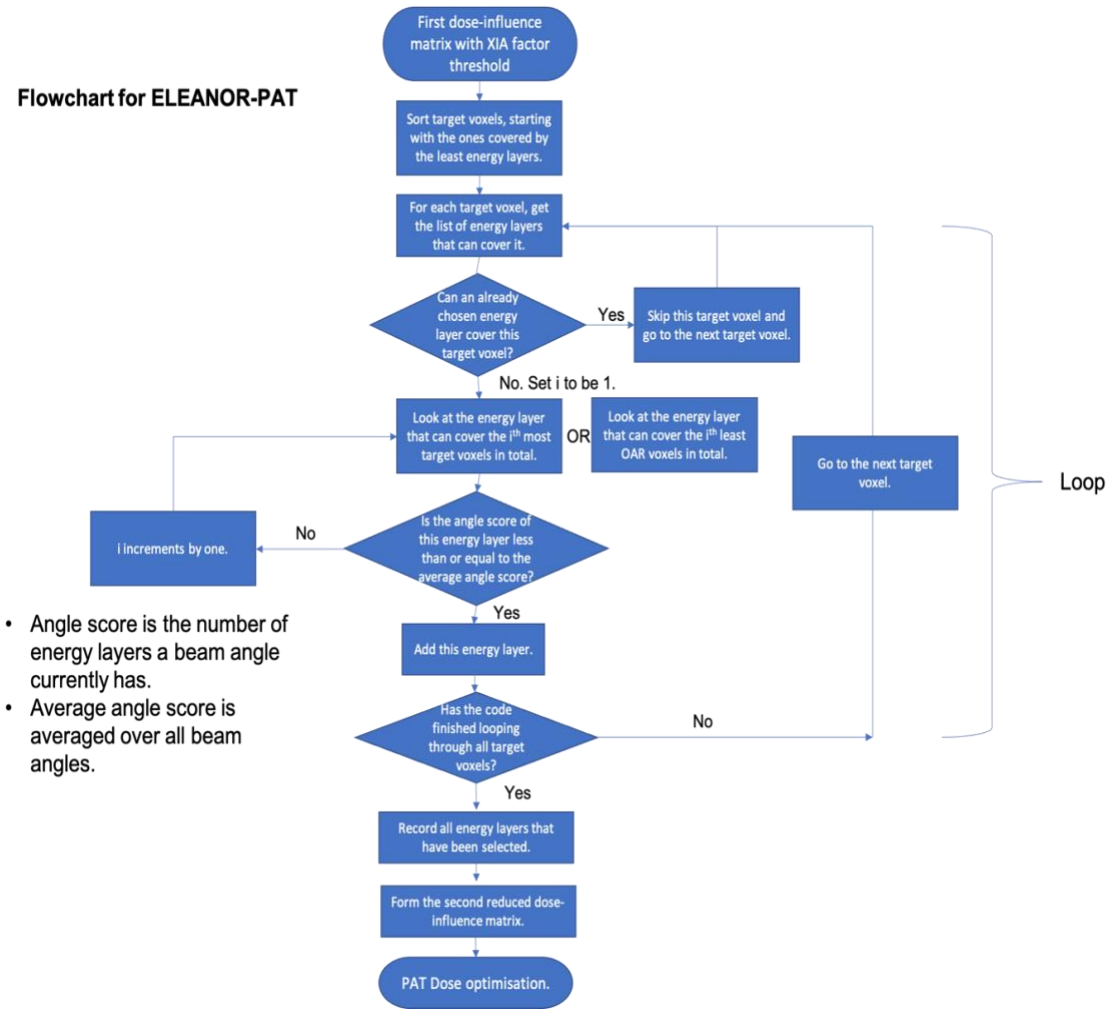

Figure A1: Flowchart for ELEANOR-PAT.

3.10.2 Appendix B: A conceptual illustration of finding the minimum energy layers

A conceptual illustration of finding the minimum energy layers with the goal of covering seven example target voxels is shown in figure B1, with 3 different XIA factors: 80% in figure B1(a), 60% in figure B1(b) and 0% in figure B1(c). There is a rectangular target (dark grey) inside the external contour (outer light grey rectangle). Two example beams, coming in from 90 degrees (Beam 1) and from 180 degrees (Beam 2), leave 5 energies and 3 energies respectively inside the target. The energies belonging to Beam 1 are labelled from 1a to 1e, with energy 1a being the highest energy (longest range). Beam 2's energies are numbered 2a to 2c, with 2a being the highest energy. According to the definition of the XIA factor, only the > 80% Bragg peak isodose regions (orange bands) contribute to target coverage abilities during the energy layer selection process. The goal is to find the minimum energy layers to cover the seven example target voxels (blue and black squares). The steps are as follows:

1) Create a full dose-influence matrix with 80% XIA factor for the seven target voxels.
2) From the dose-influence matrix, find how many and which energy layers cover each target voxel (figure B1(d)).
3) Sort the table according to column 2, the number of energy layers covering the target voxel (figure B1(d)).
4) Energy layers {1c, 2b, 2c} are selected because voxel 2, 5, 7 can only be covered by one energy layer.
5) Voxel 1 cannot be covered by any of the previously selected energy layer, so {1b} or {2a} is required. {1b} is selected because it also covers voxel 4 and 6, but {2a} does not cover any other target voxels (i.e. {1b} has higher target coverage ability than {2a}).
6) No additional energy layers are selected for voxel 3, 4, and 6, because they can be covered by at least one previously selected energy layers.
7) The minimum number of required energy layers is 4. These are {1b, 1c, 2b, 2c}. The order of voxels 2,5,7 and of voxels 1,3,4,6 do not matter – the same energy selections will always be reached.

The same algorithm is applied to 60% and 0% XIA factor (larger orange bands to indicate higher target coverage abilities with smaller XIA factors). The minimum number of energy layers is 3 for 60% XIA factor and they are {1b, 1c, 2b}. The minimum number of energy layers is 1 for 0% XIA factor and it is {1a} or {2a}.

Smaller XIA factors mean larger energy layer coverage, so lead to less energy layers required.

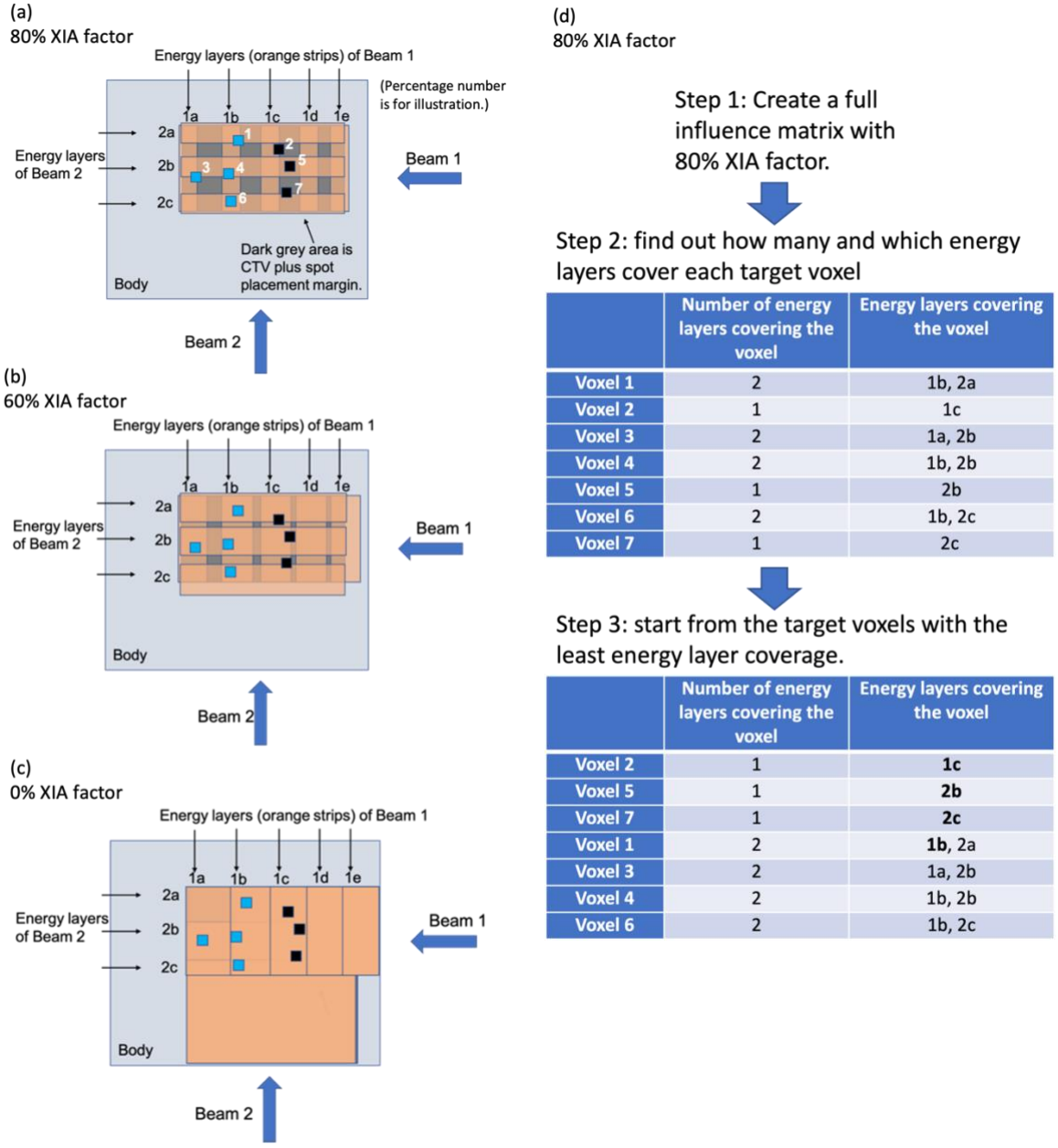

	Number of energy layers covering the voxel	Energy layers covering the voxel
Voxel 1	2	1b, 2a
Voxel 2	1	1c
Voxel 3	2	1a, 2b
Voxel 4	2	1b, 2b
Voxel 5	1	2b
Voxel 6	2	1b, 2c
Voxel 7	1	2c

	Number of energy layers covering the voxel	Energy layers covering the voxel
Voxel 2	1	**1c**
Voxel 5	1	**2b**
Voxel 7	1	**2c**
Voxel 1	2	**1b**, 2a
Voxel 3	2	1a, 2b
Voxel 4	2	1b, 2b
Voxel 6	2	1b, 2c

Figure B1: Illustration for ELEANOR-PAT (Energy Layer Reduction based on Coverage for Proton Arc Therapy). The goal is to find the minimum number of energy layers required to cover a target with dose. This figure illustrates the concept of the ELEANOR-PAT for seven example target voxels. (a)-(c) illustrate ELEANOR-PAT with different XIA factors. A high XIA factor, e.g., 80%, requires more energy layers than a low XIA factor, e.g. 0%, because energy layers defined with 0% XIA factor covers more target than defined with a higher XIA factor value. (d) Illustration for the process of finding the minimum required energy layers with 80% XIA factor. The minimum solution in this example is 4 energy layers and these are indicated in bold.

3.10.3 Appendix C: Metrics comparison for IMPT, ELEANOR-PAT, PAT-random and FPAT plans.

Table C1: Target and OAR metrics for IMPT, robust ELEANOR-PAT, PAT-random, and FPAT plans, under nominal and error scenarios. No. Layers is the number of energy layers per beam angle. Green highlight indicates a plan has passed clinical dose requirements. Red highlight indicates a plan has failed to meet the clinical requirements. All robust ELEANOR-PAT plans met nominal and robustness requirements. PAT-random plans which have the same number of energy layers as the robust ELEANOR-PAT plans failed to meet clinical requirements, suggesting the effectiveness of ELEANOR-PAT.

		Nominal scenario						Error scenarios							
								Minimum dose			Maximum dose				
		CTV			BS	Skin	Brain	CTV			CTV			BS	Skin
		D98%	D95%	D2%	D0.1cc	Max	Max	D98%	D95%	D2%	D98%	D95%	D2%	D0.1cc	Max
Criteria		> 90%	> 95%	< 110%	< 5800 cGy	< 6600 cGy		> 90% ± 2%	> 95% ± 2%	< 110% ± 2%	> 90% ± 2%	> 95% ± 2%	< 110% ± 2%	< 5800 cGy	< 6600 cGy
ID	Plan (No. layers)														
P1	IMPT	97	98	101	5344	/	5529	97	98	101	97	98	102	5344	/
	ELEANOR-PAT (5)	97	97	102	5373	/	5617	91	95	104	95	97	107	5545	/
	PAT random (5)	96	97	104	5469	/	5719	86	89	105	95	96	116	6223	/
	FPAT	98	98	103	5442	/	5711	90	92	102	98	99	113	6167	/
P2	IMPT	99	99	103	5612	3672	5821	96	99	103	99	99	103	5674	3842
	ELEANOR-PAT (8)	99	100	101	5723	3306	5928	94	95	102	99	99	105	5723	3413
	PAT random (8)	98	99	102	5583	2319	6510	93	96	104	97	98	108	5865	2387
	FPAT	99	100	101	5571	1906	5972	93	96	101	99	99	106	5770	1964
P3	IMPT	99	99	102	0	4956	6138	96	96	102	99	99	104	0	5447
	ELEANOR-PAT (9)	96	97	100	0	4755	6128	95	95	100	96	97	105	0	5093
	PAT random (9)	97	98	103	0	4314	6488	96	97	103	100	102	111	0	4646
	FPAT	98	98	103	0	3976	6481	96	97	103	99	100	109	0	4632
P4	IMPT	98	98	102	0	5559	6169	96	97	102	98	98	105	0	6174
	ELEANOR-PAT (11)	97	97	103	0	5884	6358	95	96	103	99	100	109	0	6108
	PAT-random (11)	92	93	109	0	5075	6912	89	92	109	92	94	116	0	5349

	FPAT	98	98	103	0	5813	6354	96	97	103	100	101	109	0	6057
P5	IMPT	99	99	101	5686	5528	6042	93	95	101	99	99	101	5776	5872
	ELEANOR-PAT (17)	98	99	102	5592	4722	6133	90	95	102	96	98	105	5668	5134
	PAT-random (17)	97	98	102	5203	4869	6211	83	90	103	97	98	107	5416	5397
	FPAT	98	99	101	5552	4688	6128	91	95	101	97	98	106	5636	5096
P6	IMPT	97	98	101	5396	4912	6060	96	97	101	97	98	102	5538	5175
	ELEANOR-PAT (11)	98	99	101	5405	4938	6007	95	97	102	98	98	106	5531	5108
	PAT-random (11)	88	89	102	5440	4432	6367	85	87	103	87	89	105	5771	4646
	FPAT	98	98	100	5405	4749	6007	95	97	101	98	98	104	5481	4946
P7	IMPT	94	98	102	5644	1956	6296	81	87	102	98	97	102	5737	1993
	ELEANOR-PAT (12)	94	98	102	5694	1980	6279	90	95	102	98	100	107	5727	2016
	PAT-random (12)	62	85	111	4268	2087	7149	58	81	111	86	79	113	4701	2125
	FPAT	95	98	102	5706	1902	6128	95	98	102	97	101	106	5891	1941
P8	IMPT	98	98	102	5598	1121	6107	96	96	102	98	98	102	5594	1154
	ELEANOR-PAT (6)	99	99	101	5478	961	6037	93	96	102	98	98	105	5705	985
	PAT-random (6)	90	91	102	5504	1146	6123	89	90	102	92	97	109	5761	1187
	FPAT	99	99	101	5491	810	6053	95	99	101	98	99	111	5783	831

Chapter 4. Assessment of proton arc therapy plans under continuous delivery emulation

Authors

[*,†]Yunzhou Xia

[*,†]Adam H Aitkenhead

[†,‡]Robert Appleby

[*,†,‡]Michael J Merchant

[*,†,‡]Karen J Kirkby

[*,†]Ranald I MacKay

Affiliations

[*]Division of Cancer Sciences, Faculty of Biology, Medicine and Health, University of Manchester, United Kingdom

[†]Christie Medical Physics and Engineering, The Christie NHS Foundation Trust, Manchester, United Kingdom

[‡]Cockcroft Institute, United Kingdom

4.1 Rationale and strategy

Proton arc therapy (PAT) has the potential to further improve plan quality compared to intensity-modulated proton therapy (IMPT). PAT is planned with fixed control points but delivered with a continuously rotating gantry. This can cause undesired dose disagreements between the plan and delivery. I assessed whether the dose distributions under emulated continuous gantry motion are clinically acceptable for the eight ependymoma cases optimised with the ELEANOR-PAT energy selection strategy described in Chapter 3. The process of producing clinically acceptable ELEANOR-PAT plans was reported when continuous gantry motion is considered.

Individual author contributions are as follows. I coded the emulator algorithm in MATLAB and performed the analysis. Adam H. Aitkenhead provided the log files which recorded the number of monitor units and time stamps delivered at each spot for commissioning at the Christie proton therapy centre. Michael J. Merchant, Adam H. Aitkenhead, Robert Appleby, and Ranald I. MacKay gave daily supervision and advice on the parameter settings for the emulator to account for deliverability. Karen J. Kirkby provided the opportunity for project funding. All authors have reviewed and commented on the manuscript.

4.2 Abstract

Proton arc therapy (PAT) is planned with fixed control points but delivered with a continuously rotating gantry. This can cause undesired dose disagreements between the plan and delivery. I assessed whether the dose distributions under emulated continuous gantry motion are clinically acceptable for the eight ependymoma cases. I also report the process of producing clinically acceptable ELEANOR-PAT plans when continuous gantry motion is considered.

The plan under continuous gantry rotation was modelled with a proof-of-concept emulator, which predicts the dose distribution by recalculating the plan based on predicted time stamps of the proton spots. The emulated dose distributions were assessed against clinical dose requirements and compared to the plans using local gamma analysis with [3mm, 3%] criteria. Four plans for each case, which include the static control point plan (original ELEANOR-PAT plan) and interpolations to n = 1, 2, 3 energy layers per finer control point, were re-optimised and emulated.

Four out of eight static control point plans passed the clinical requirements, but none met the gamma analysis requirement of 95%. All n = 1 interpolated plans passed the clinical dose and gamma analysis requirements.

PAT plans optimised with fixed control points are different to the plans under continuous delivery at clinically unacceptable levels. Evaluation of the dose differences must be carried out during the planning stage and accompanied with both clinical dose assessment and gamma analysis. Interpolation to one energy layer per control point should always be applied for the ELEANOR-PAT strategy.

4.3 Introduction

Proton arc therapy (PAT) is a promising candidate for the next generation proton therapy technology because of the ability to further improve target conformality and organ-at-risk (OAR) sparing, as well as the potential to greatly reduce the treatment time compared to intensity modulated proton therapy (IMPT) [1] - [9]. PAT is planned with fixed control points at small angular spacings, usually 1 to 10 degrees, to approximate an arc [1] – [4][8]. In early plan comparison studies, PAT was optimised with full energy layers from the control points [1] – [3]. Although these full-energy PAT plans showed dosimetric improvements compared to IMPT, they were in-principle impractical (time-consuming) to deliver as the energy layer switching time dominated the treatment [4][6][9]. Therefore, to fully exploit the deliverability of PAT, several groups have published energy layer reduction strategies which aimed to reduce the number of energy layers per control point to a practical level without losing the dosimetric advantages of PAT [4][6][9]. The angular spacings of the reduced PAT plans ranged between 1 and 10 degrees, and each control point had either one or multiple energies. However, when the fixed control points as planned are delivered with a continuously rotating gantry, the delivered dose could differ to the planned dose which is undesired.

Knowledge can be translated from the experience of the development of photon arc therapy, i.e., volumetric modulated arc therapy (VMAT), where the angular spacing between control points was an important parameter as it determined how well the delivered dose matched the planned dose [10]. Between control points, the multi-leaf collimators are in motion, so a smaller angular spacing means closer agreement to the planned dose distribution. A similar concern exists for PAT because smaller angular spacings mean smaller geometry variations from the proton beam's eye view, but it also leads to heavier calculation load and slower delivery due to more proton spots involved.

For protons, another factor affecting the dose agreement is the number of spots a control point delivers. This is because the spots are delivered sequentially (unlike VMAT which is a shaped-field technique), which means that with continuous gantry rotation they would be delivered from different beam angles to their planned

control points. This delay could cause a large dose difference as protons are sensitive to tissue density variations. In addition, if a control point contains multiple energies [1][4][9], the time delay in delivering the spots will be longer than if there were just one energy as the energy layer switching time dominates over the time spent on delivering the spots, and so it will cause larger dose differences. If these dose differences are beyond clinical tolerances, the PAT plan will not meet clinical approval standards. This necessitates the need to predict these dose differences prior to delivery and this should be evaluated as part of the planning process.

In Chapter 3, we introduced a concept for energy layer selection based on energy layer coverage abilities (ELEANOR-PAT) and described the ELEANOR-PAT algorithm. PAT plans from our previous study were planned with 10-degree spacing, a value chosen as a balance between computational load and plan quality. These ELEANOR-PAT plans had multiple energies per control point and satisfied clinical dose and robustness requirements, but the deliverability was outside the scope of that conceptual study. Compared to 1-degree control-point spacing, ELEANOR-PAT plans can cause a larger dose difference due to the relatively coarser spacing and multiple energies per control point. Fortunately, an advantage of the ELEANOR-PAT algorithm is that the energies selected can be easily interpolated across finer control points within the 10-degree control-point spacing, which means that the number of energy layers per control point and the control-point spacing can be varied by the planner with little computational cost.

This paper evaluates the method of assuring that ELEANOR-PAT plans optimised with fixed control points meet clinical standards when continuous gantry rotation is considered. We also extend our investigation to explore the effects of varying the control-point spacing and the number of energy layers per control point on the planned dose distribution which can be translated as a general theme to other PAT strategies as the two variables are independent of the strategies. To simulate the dose under continuous gantry rotation, a proof-of-concept emulator was proposed which calculated a separate time stamp for each proton spot according to the delivery sequence. The ELEANOR-PAT plans were then recalculated based on these predicted time stamps to give the dose distributions under continuous gantry rotation, which were compared to the planned dose distributions. Variations of the control-point spacing and the number of energy layers per control point were

achieved by interpolation of the selected energy layers into finer control points and re-optimised. We show that the ELEANOR-PAT strategy must always be followed by a full interpolation of energy layers to one per control point.

4.4 Method

4.4.1 Plans

Three types of ELEANOR-PAT plans were investigated:

1) Static control point plans, from our previous study, where $n = N$ energies were selected for each control point at 10-degree spacing. The values of N ranged between 5 and 17 for the eight ependymoma cases, P1 – P8, described in the previous study (Chapter 3).

2) Fully interpolated plans, with one energy layer per control point ($n = 1$). These were then re-optimised for the original planning objectives.

3) Partially interpolated plans, with n ($n > 1$) energy layers per control point. The rationale for partial interpolation was to investigate the influence of the number of energy layers per control point as a general theme for other existing PAT energy reduction strategies which use multiple energies per control point. These partially interpolated plans were also re-optimised for the original planning objectives.

This resulted in four plans for each of the eight cases which were optimised within matRad (version Alan v2.1.0 [11][12]). An example is presented in figure 4-1(a)-(b) which show the energies against control points for the static and fully interpolated plans of an example case, P1. Five energies were selected for each control point in the static plan (figure 4-1(a)) and were interpolated to one energy per finer control point in the fully interpolated plan (figure 4-1(b)).

(a)

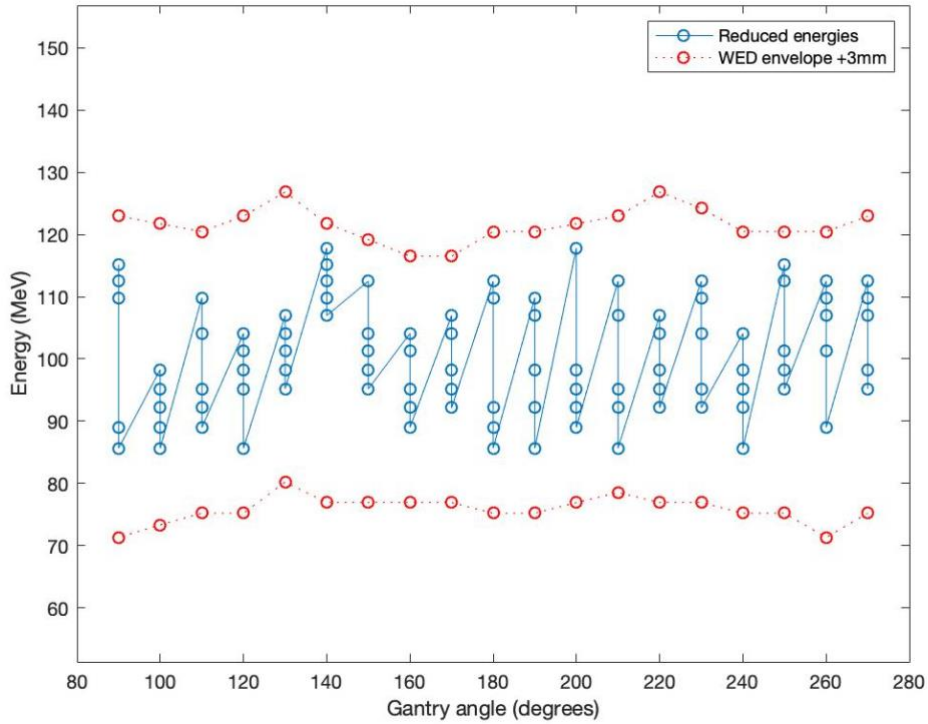

(b)

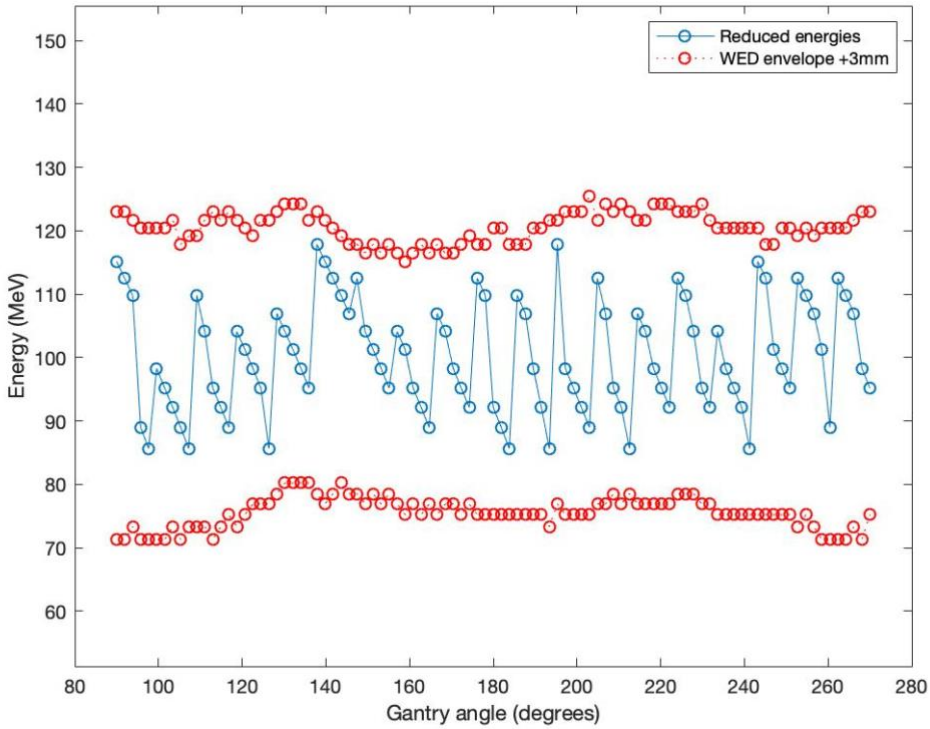

Figure 4-1: Energies versus the gantry angles for the planned control points for (a) the static control-point plan, (b) fully interpolated plan, where the energies (blue circles) from (a) were interpolated evenly across the control-point spacing, resulting in one energy for every finer control point (blue circles) in (b). The blue circles indicate the selected energies. The red circles trace out the beam energies which correspond to the minimum and maximum water equivalent depths (WED) of the target seem from every gantry angle.

4.4.2 A proof-of-concept emulator

To emulate the dose under continuous gantry rotation, each proton spot was given a time stamp which specified its predicted delivery time. This was achieved by sorting the proton spots in their delivery order: control points were sorted by gantry angle; energies of the same control point were sorted from the highest to the lowest as an energy decrease is faster than an energy increase [1][4]; the proton spots belonging to an energy layer were sorted to follow a zig-zag scanning sequence. The predicted time stamp of each spot was then calculated based on the following parameters:

1) energy layer switch time (ELST), assumed to be 0.6 seconds for an energy decrease and 0.9 seconds for an energy increase (based on commissioning data from The Christie Proton Therapy Centre),

2) spot scanning speed, assumed to be 5 metres per second (a conservative estimate) in both horizontal and vertical scanning directions,

3) energy-dependent rates of monitor units (MU), derived from the commissioning data at the Christie Proton Therapy Centre.

4) constant gantry rotation speed, ω degrees per second, calculated based on the control point that took the longest time to deliver the spots. The value of ω was calculated using equation 4-1:

Equation 4-1: Calculation of the maximum gantry rotation speed assuming constant gantry rotation speed.

$$\omega = \frac{\Delta\,\theta}{\max\{\,T_{cp}\}}$$

where $\Delta\,\theta$ is the planned angular spacing, $\{\,T_{cp}\,\}$ is the set of times spent on the planned control points, and T_{cp} is defined as the sum of the time spent on ELST, spot scanning and MU delivery at a control point.

Equation 4-1 calculates the maximum gantry rotation speed given the above parameters and the assumption of constant rotation speed. The mode of delivery

modelled by the emulator was that the spots could be delivered before the gantry reaches the planned control point to evenly distribute the time delay amongst the spots. The time stamp for delivering the first spot of a control point, $t_{\{spot\ 1\}}$, is given by equation 4-2:

Equation 4-2: The time stamp for starting delivering the spots belonging to a beam angle (or control point).

$$t\{spot\ 1\} = \ t - \frac{1}{2} \times T_{cp}$$

where t is the time stamp for when the gantry reaches the control point and T_{cp} is the total time spent on the control point. The delivered beam angle of the first spot, $\theta\ \{spot\ 1\}$, is therefore given by equation 4-3:

Equation 4-3: The predicted actual beam angle at which a proton spot is delivered assuming constant and continuous gantry rotation.

$$\theta\ \{spot\ 1\} = \ \theta - \omega \ \times \frac{1}{2} \times \ T_{cp}$$

where θ is the gantry angle of the control point $spot\ 1$ belongs to.

4.4.2.1 Implementation of the emulator

After a PAT plan was optimised, a steering file containing the gantry angles of the control points, energies, spot positions and MUs was saved in Matlab file format (version R2018a). The emulator, written as a Matlab function, processed the steering file according to the sorting sequence described in section 4.4.2 to produce a new steering file containing the predicted delivery angle, energy, spot position and MU for each spot. This new steering file was then fed back into matRad to calculate the emulated dose distribution for the plans.

4.4.2.2 Assessment of emulated plans

Emulated dose distributions were assessed in two ways: 1) evaluated against the current clinical brain and head and neck assessment criteria used at the Christie Proton Therapy Centre, and 2) quantitative comparison to the planned dose distributions using gamma analysis [13]. Clinical target volume (CTV) D98%, D95% and D2% were required to be > 90%, > 95%, and < 110% prescription, respectively. Brainstem D0.1cc, D50% and D10% were required to be < 58 Gy, < 54 Gy and < 56 Gy, respectively. Spinal cord maximum dose must be < 54 Gy, and eye D90%, D50%, D10% must be < 10 Gy, < 30 Gy and < 54 Gy, respectively. Maximum dose for skin with 2mm thickness must be < 66 Gy. Conformality index (CI) defined as (V95% / target volume) and homogeneity index (HI) defined as ((D95% - D5%) / prescription) were evaluated for the CTV. Values of 1.0 for CI and HI mean ideal conformality and homogeneity. Local gamma analysis was used with assessment criteria of [3%, 3mm] and lower threshold of 10% following the criteria for patient specific quality assurance in use at the Christie Proton Therapy Centre. A pass rate > 95% is an acceptable agreement between the plan and its emulated dose distribution.

4.5 Results

4.5.1 Assessment of emulator performance

Figure 4-2(a) shows the planned beam angle (blue) for each spot in the order they would be delivered in the static control-point plan for an example case, P1. The 19 horizontal steps correspond to the 19 fixed control points at 10-degree angular spacing within a 180-degree partial arc. The red line in figure 4-2(a) shows the emulated gantry positions for the spots under continuous gantry rotation. The inclination of the red data points shows that the spots are ‘delivered’ from increasing gantry angles. The vertical gap in the red data points between the point of delivering the final spot of a control point and the next gantry angle corresponds to a period where no spots are delivered – a result of equation 4-1. Figure 4-2(b) shows the planned and emulated gantry angles for the fully interpolated plan. The differences between the emulated gantry angles and the planned static control points are considerably less in figure 4-2(b). This suggests that the emulated dose

distribution of the fully interpolated plan matches better to the planned dose than the static control-point plan.

(a) Static control-point plan

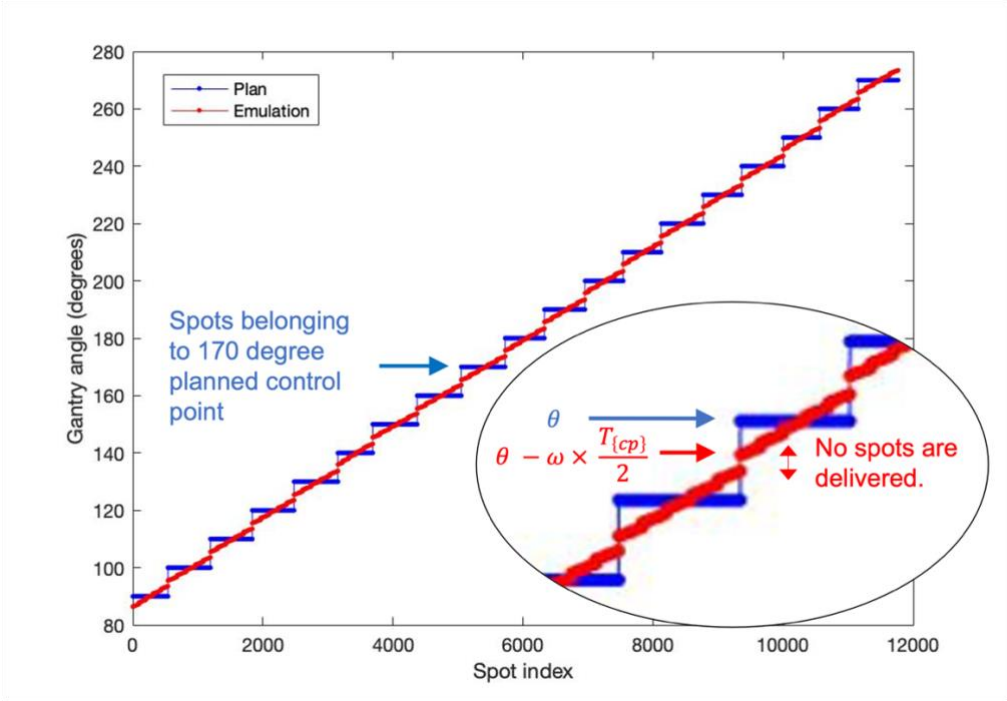

(b) Fully interpolated plan

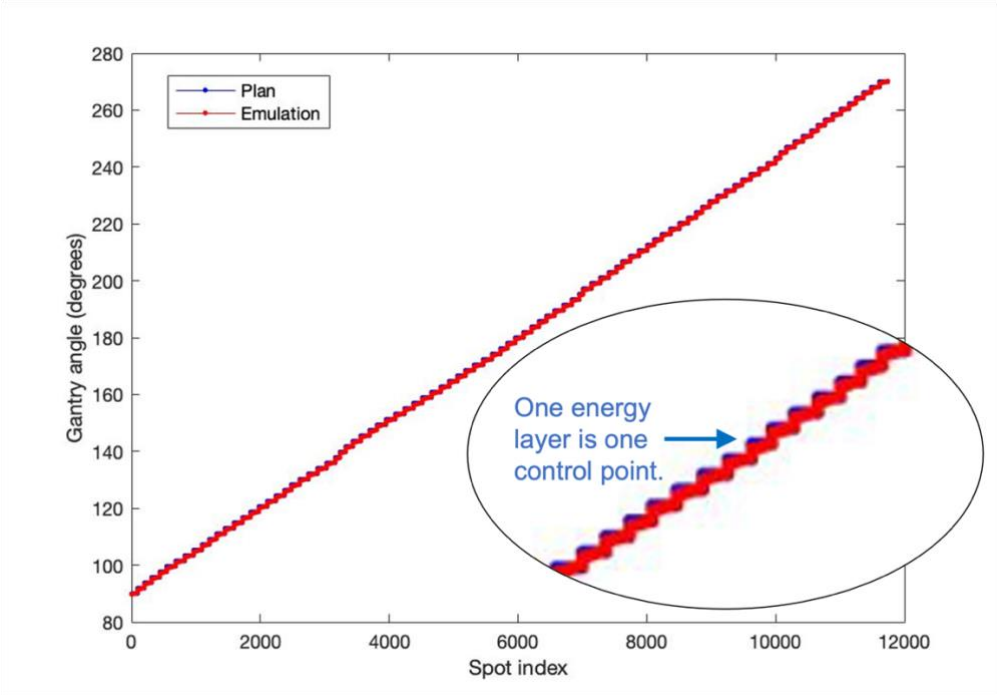

Figure 4-2: (a) Emulated gantry angle for each spot in the static control-point plan for an example case, P1. Blue data points represent the planned control points for the spots with 10-degree angular spacing and arc angular range of 90 to 270 degrees; Red data points show the emulated gantry positions for the spots under continuous gantry rotation. (b) Emulated gantry angle for each spot in the fully interpolated plan (one energy layer per control point) for the same example case. The offset of the emulated gantry positions to the planned gantry positions are smaller than that in (a).

4.5.2 Clinical assessment of the interpolated plans

Only four out of eight emulated dose distributions for the static control-point plans *(n = N)* met the clinical dose requirements (figure 4-3), which shows that ELEANOR-PAT plans with 10-degree spacing do not consistently meet the clinical requirements. The metrics that tended to fail the clinical dose requirements were CTV D95% and D5%, which were parameters relevant to the target conformality and homogeneity. An example assessment sheet is provided in Appendix A. In contrast, all fully interpolated plans (*n* = 1) satisfied the clinical requirements. The number of emulated plans that met the clinical dose requirements improved with decreasing *n*. Figure 4-4 shows the CTV's CIs and HIs of the emulated dose and planned dose, which become worse with increasing *n*. This shows that PAT energy reduction strategies should always aim for *n* = 1. For ELEANOR-PAT, there was no advantage for using n > 1 as energies are pre-selected, but this investigation of *n* is independent of energy layer reduction algorithm and translatable to other energy reduction strategies which do not report the use of interpolation.

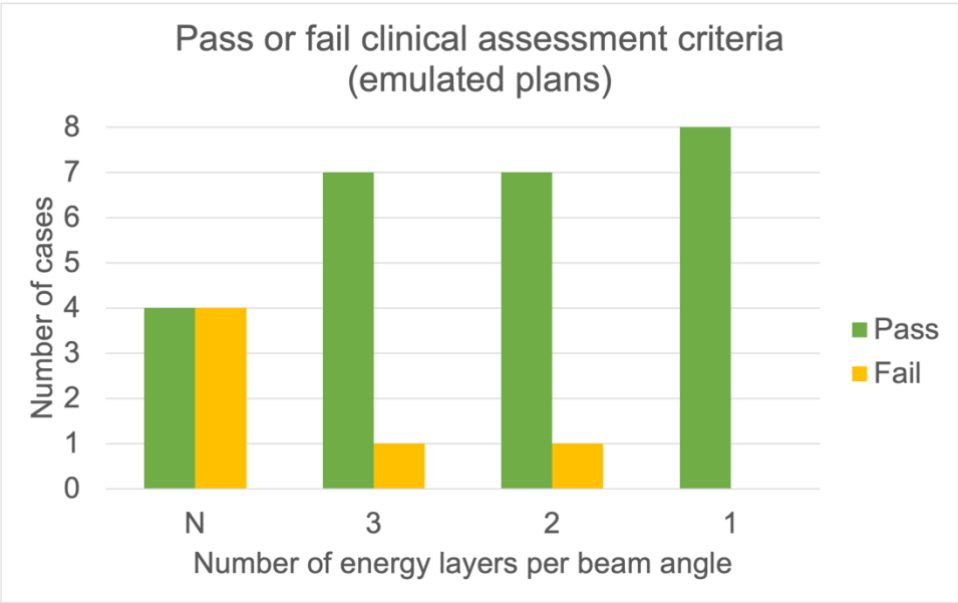

Figure 4-3: The number of emulated plans that passed the clinical requirements (Christie head and neck assessment sheet, example in Appendix A) increases with decreasing number of energy layers per beam angle. All fully interpolated plans with n = 1 satisfied the clinical requirements. N represents the static control point plans.

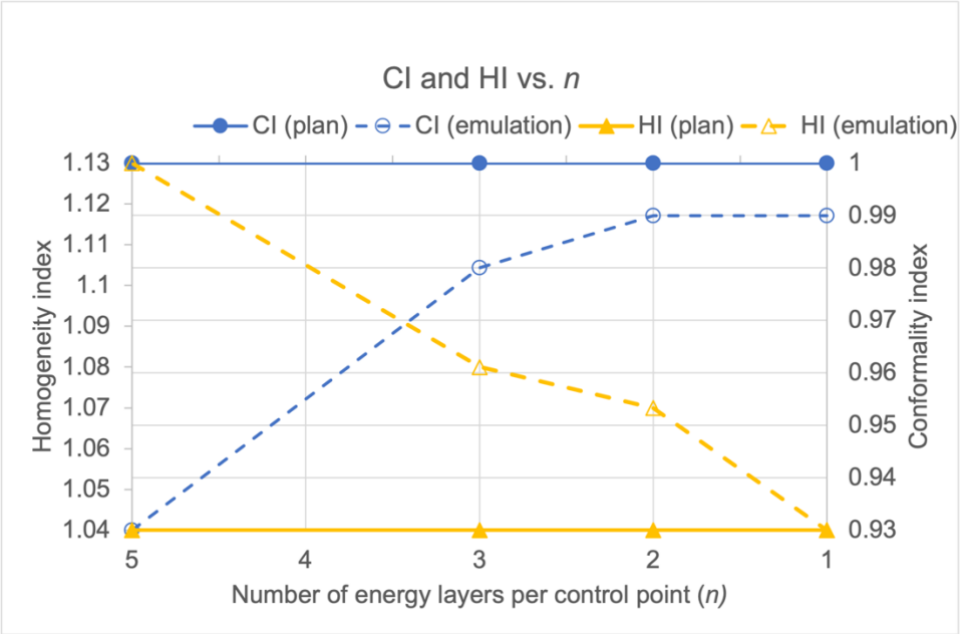

Figure 4-4: Conformality index (CI) and homogeneity index (HI) of the plans and their emulated dose distributions improve with decreasing n, the number of energy layers per control point, for an example case P1.

4.5.3 Gamma pass rates of the plans

Figure 4-5 shows the gamma pass rate of the emulated dose distributions compared to the plans for all eight cases, plotted against the number of energy layers per control point, *n*. A clear trend of increasing gamma pass rate with decreasing number of energy layers can be seen. All cases had > 95% gamma pass rate with *n* = 1. With *n* = 2 or 3, only 7 and 5 cases had > 95% gamma pass rate respectively. The gamma pass rates were all below 95% for the static control-point plans. This shows that the static control point plans with multiple energies per control point are clinically unacceptable considering continuous gantry rotation. In contrast, fully interpolated plans matched well to their emulated dose distributions, and the reason is the negligible delays in delivering the spots. This means that the energies should always be fully interpolated to achieve clinically acceptable plans.

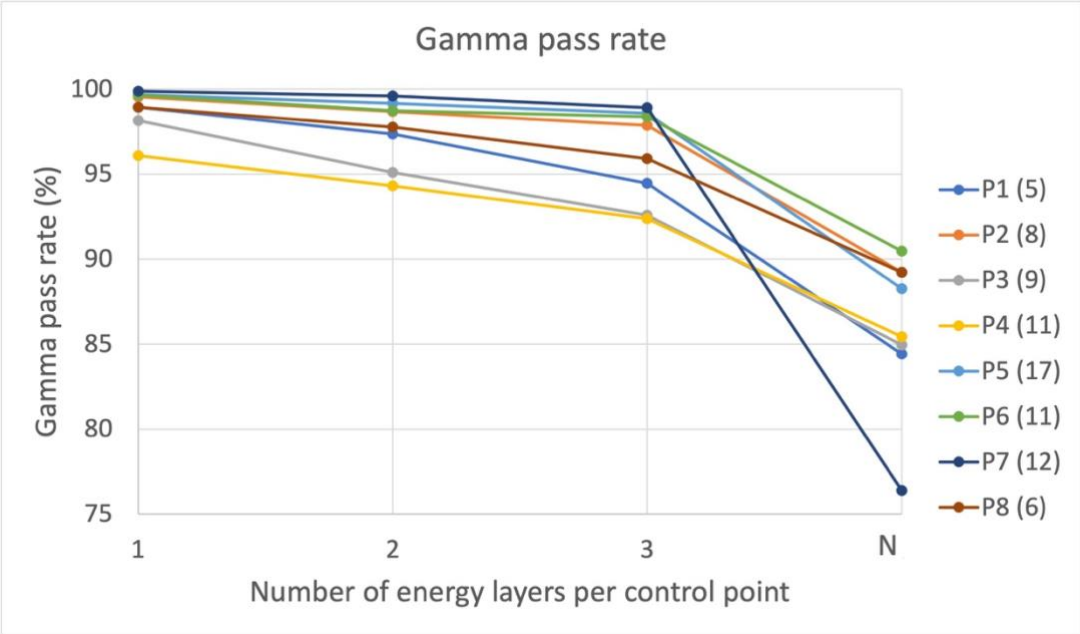

Figure 4-5: Gamma pass rate comparing the emulated dose distributions to the plans shows increasing trends with decreasing number of energy layers per control point. Gamma pass rate ([3%, 3mm] local criteria) is > 95 % for all cases with one energy layer per control point. The numbers in the brackets are the number of energy layers per coarse control point before interpolation of the energy layers into finer control points.

Figure 4-6 shows the gamma pass rate plotted against the control-point spacing. A clear trend of increasing gamma pass rate with decreasing angular spacing can be seen. An angular spacing < 2 degrees guarantees acceptable gamma pass rate for seven cases, and an angular spacing < 1-degree guarantees > 95% gamma pass rates for all cases. This shows that smaller angular spacings lead to better dose agreement between the plan and emulated dose distribution. Therefore, angular spacings < 1 ~ 2 degrees should be the aim when planning PAT with the ELEANOR-PAT strategy, which were always achieved with full interpolation of energy layers. The full interpolation does not introduce additional computational cost, but for other strategies that do not preselect energies, optimising with small angular spacings of 1 ~ 2 degrees leads to heavier computational workload due to more spots involved. For cases that had lower gamma pass rates than others (e.g. P5, P8), their characteristics which include the tumour geometries, sizes, locations and energies selected had been considered, but none showed a direct correlation with the gamma pass rate.

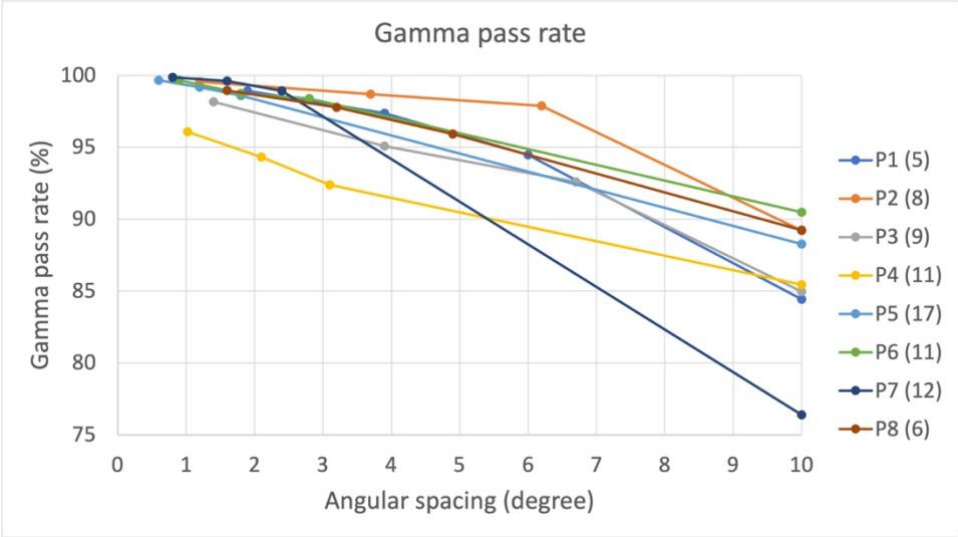

Figure 4-6: Gamma pass rate comparing the emulated dose distributions to the plans increases with decreasing control-point spacing.

Figure 4-7 shows the planned dose distributions, emulated dose distributions, and their gamma value distributions for a static control-point plan and a fully interpolated plan for an example case, P1. The gamma pass rates were 84.4% and 98.9% respectively. Differences in the entrance doses between figure 4-7 (a) and figure 4-7 (c) can be observed as gamma failures in figure 4-7(e). The gamma pass rate tends to fail on the edges and distal ends of the beam, which arise due to the angular offsets between the plan and emulation which in turn cause differences in the beam ranges. These dose differences must be carefully evaluated. Figure 4-7(e) shows a low gamma pass rate region which is outside the patient contour and is therefore excluded from the assessment.

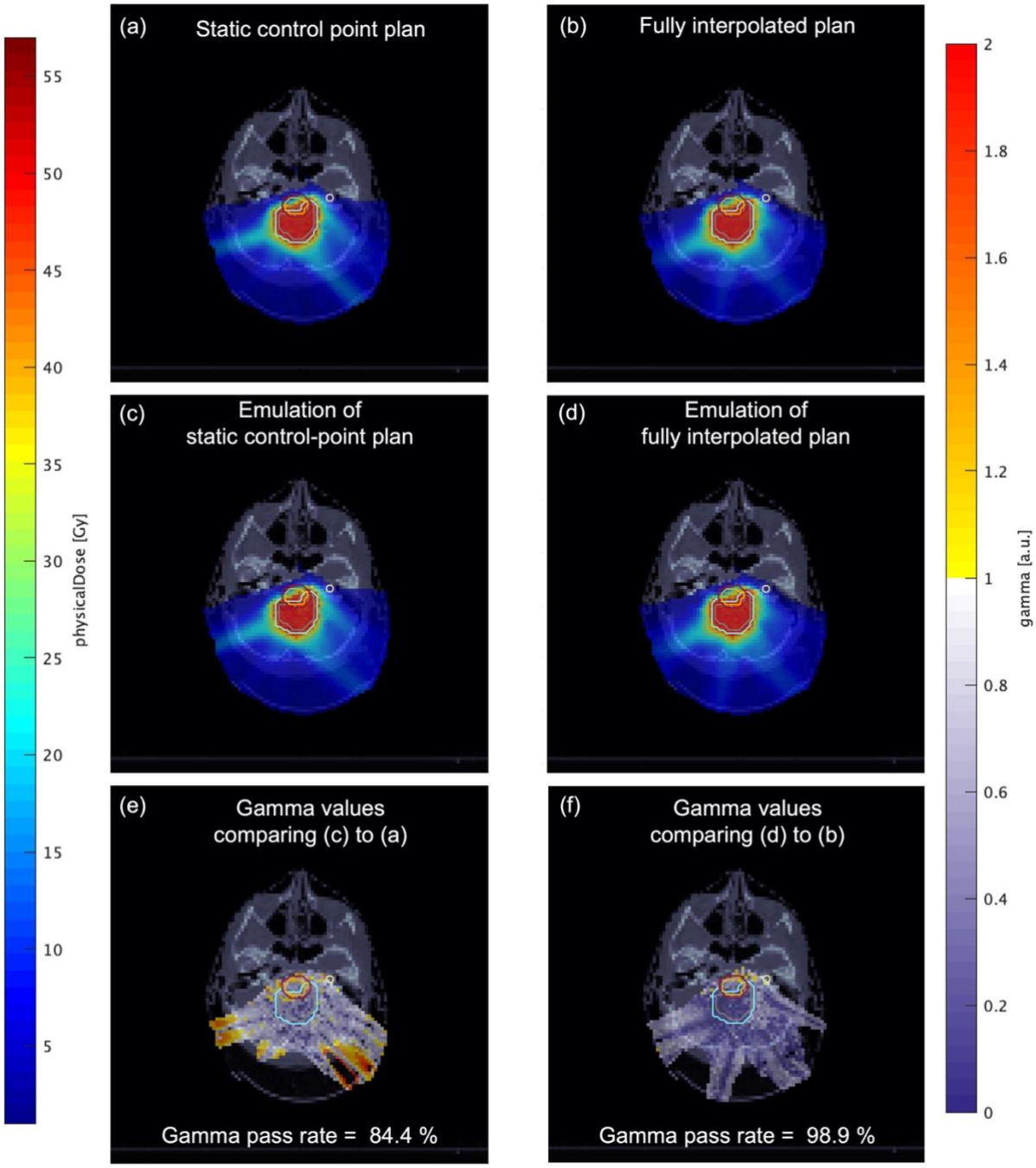

Figure 4-7: Left column containing figures (a) (c) (e) show the dose distributions for the static control-point plan, its emulated dose distribution, and their gamma value distribution in an axial slice at the isocentre. Right column containing figures (b) (d) (f) show the same distributions for the fully interpolated plan. Emulation of the fully interpolated plan has higher gamma pass rate than the static control-point plan. Grey contour: CTV, Cyan: PTV, yellow: brainstem core, red: brainstem.

4.6 Discussion

Common PAT plans do not consider gantry rotation during the planning stage, but the dose distribution under continuous gantry rotation can be different to the plan because of the delays in delivering the spots and protons' sensitivity to tissue

density variations. We evaluated the impact of continuous gantry rotation on the static control point plans generated by the ELEANOR-PAT strategy by using a proof-of-concept emulator to predict the dose distribution considering the time components of delivery. With machine parameters derived from the commissioning data at the Christie proton therapy centre, only half of the static control-point plans passed the clinical assessment criteria. This was because the emulated gantry positions caused a spatial difference in dose delivery of the plan due to the control points containing multiple energy layers and ELST dominated over the other time components. The gamma pass rate was higher for the interpolated plans, and all fully interpolated plans achieved > 95% gamma pass rate. This shows the necessity of full interpolation to one energy per control point for the ELEANOR-PAT strategy which take very little extra computational memory as energies are preselected prior to dose optimisation. Full interpolation should therefore always be applied following energy layer selections with the ELEANOR-PAT algorithm and this rationale extends to other strategies with multiple energy layers per control point.

4.6.1 Assumptions for the emulator

The emulator was used as a tool to predict the dose distribution of a PAT plan considering continuous gantry rotation. The ELST and rate of MU were derived from the commissioning data, but the scanning speed of 5 metres per second was a rather a conservative estimation. However, recalculating the emulated dose distributions with a scanning speed of 20 metres per second only perturb the gamma pass rates by < 1%. This indicates that the scanning speed is not a consequential factor, but ELST is as it is on a longer time scale.

The spot profiles were simulated with fixed beams, but in reality, they are delivered with a rotating gantry which will deform the spot profile and range. Under continuous gantry rotation, the tissue densities the beam traverses through can be different to the plan. However, the angular range traversed by the gantry (gantry speed is on the order of degrees per second with a maximum limit of 6 degrees per second) during the time spent on delivering dose to a spot (milliseconds) is

relatively small for these differences to take effects, so this deformation of spot profile and range is clinically irrelevant.

Although the emulator is a useful tool to assess whether statically optimised PAT plans meet clinical requirements under continuous gantry rotation, it does not model the actual delivery where there are fluctuations in machine parameters. These fluctuations exist primarily in the beam current which can affect PAT plans as gantry is continuously rotating. In contrast, they do not affect IMPT as the beams are delivered with fixed gantry positions. Variations in beam current lead to spatial errors in PAT dose distribution. Therefore, to improve the accuracy of emulation, time must be allowed for the beam to adjust to the potential fluctuations. This will result in a slower rotation speed and longer delivery but is relatively short compared to the ELST. For a future version of the emulator, fluctuations could be considered by modelling them as probability distributions as it was considered for IMPT in the context of total patient throughput for a proton therapy centre [14].

4.6.2 Clinical assessment

Four out of eight emulated dose distributions of the static control-point plans met the clinical dose requirements but none satisfied the 95% gamma pass rate criteria when compared against the fixed control point plans. These failures in the gamma analysis would mean failure of patient-specific QA. Considering the time and effort put into treatment planning and patient-specific QA, the dose agreement between the fixed control point dose distribution and the emulated dose distribution should be evaluated as part of the clinical assessment sheet for PAT plans to increase the efficiency of the treatment planning process, instead of leaving this evaluation until patient-specific QA.

4.6.3 Gamma pass rate analysis

Figures 4-5 and 4-6 indicate dependency of dose agreement between emulation and the plans on the number of energy layers per beam angle and on the angular spacing. A clear convergence to > 95% gamma pass rate with one energy layer

per beam angle, and a clear trend of increasing gamma pass rate with decreasing angular spacing can be seen. This shows the necessity of full interpolation following the ELEANOR-PAT strategy, which gives both one energy layer per control point and the minimum angular spacing. Towards the lower limit of angular spacing (< 1 degree) the gamma pass rates converge to > 95%, but it is unnecessary for all plans to go down to 1 degree spacing because the emulated dose distributions for most of the plans passed the gamma analysis criteria with angular spacing > 1 degree and smaller angular spacings would prolong the delivery time. ELEANOR-PAT strategy is ideal as it preselects energies, but for other strategies where preselection is not the method then optimising with one degree spacing is computationally inefficient.

4.6.4 Future work

The variations in the gamma pass rates indicate their dependency on case-specific characteristics. As this study was limited to eight cases, no definable characteristics were seen to cause a direct correlation, but a future study involving more cases will be required to explore case-specific dependencies. Nevertheless, full interpolation to one energy layer per control point is expected to always give > 95% gamma pass rate as the spatial difference in dose delivery is only caused by delays in the spot delivery time which is negligible compared to the ELST. If in rare circumstances where the gamma pass rate is below the clinical requirement in a plan with one energy layer per control point, the solution is to decrease the gantry rotation speed in order to reduce the spatial differences.

4.7 Conclusions

We describe a complete methodology for producing clinically acceptable proton arc therapy plans when using the ELEANOR-PAT (energy layer reduction strategy based on coverage) strategy with full interpolation of energy layers. Our recommendation for energy layer interpolation based on this analysis is that one energy layer per control point is required for clinically acceptable plans. Clinical dose assessment criteria should be used together with gamma analysis to assess whether an emulated dose distribution agrees with the fixed control point plan.

4.8 References

[1] Rah, J.E., Kim, G.Y., Oh, D.H., Kim, T.H., Kim, J.W., Kim, D.Y., Park, S.Y. and Shin, D., 2016. A treatment planning study of proton arc therapy for para-aortic lymph node tumors: dosimetric evaluation of conventional proton therapy, proton arc therapy, and intensity modulated radiotherapy. Radiation Oncology, 11(1), pp.1-10.

[2] Seco, J., Gu, G., Marcelos, T., Kooy, H. and Willers, H., 2013. Proton arc reduces range uncertainty effects and improves conformality compared with photon volumetric modulated arc therapy in stereotactic body radiation therapy for non-small cell lung cancer. International Journal of Radiation Oncology* Biology* Physics, 87(1), pp.188-194.

[3] Blanco Kiely, J.P. and White, B.M., 2016. Dosimetric feasibility of single-energy proton modulated arc therapy for treatment of chordoma at the skull base. Acta Oncologica, 55(9-10), pp.1243-1245.

[4] Ding, X., Li, X., Zhang, J.M., Kabolizadeh, P., Stevens, C. and Yan, D., 2016. Spot-scanning proton arc (SPArc) therapy: the first robust and delivery-efficient spot-scanning proton arc therapy. International Journal of Radiation Oncology* Biology* Physics, 96(5), pp.1107-1116.

[5] Ding, X., Li, X., Qin, A., Zhou, J., Yan, D., Stevens, C., Krauss, D. and Kabolizadeh, P., 2018. Have we reached proton beam therapy dosimetric limitations? – a novel robust, delivery-efficient and continuous spot-scanning proton arc (SPArc) therapy is to improve the dosimetric outcome in treating prostate cancer. Acta Oncologica, 57(3), pp.435-437.

[6] Liu, G., Li, X., Zhao, L., Zheng, W., Qin, A., Zhang, S., Stevens, C., Yan, D., Kabolizadeh, P. and Ding, X., 2020. A novel energy sequence optimization algorithm for efficient spot-scanning proton arc (SPArc) treatment delivery. Acta Oncologica, 59(10), pp.1178-1185.

[7] Li, X., Kabolizadeh, P., Yan, D., Qin, A., Zhou, J., Hong, Y., Guerrero, T., Grills, I., Stevens, C. and Ding, X., 2018. Improve dosimetric outcome in stage III non-small-cell lung cancer treatment using spot-scanning proton arc (SPArc) therapy. Radiation Oncology, 13(1), pp.1-9.

[8] Ding, X., Zhou, J., Li, X., Blas, K., Liu, G., Wang, Y., Qin, A., Chinnaiyan, P., Yan, D., Stevens, C. and Grills, I., 2019. Improving dosimetric outcome for hippocampus and cochlea sparing whole brain radiotherapy using spot-scanning proton arc therapy. Acta Oncologica, 58(4), pp.483-490.

[9] Sanchez-Parcerisa, D., Kirk, M., Fager, M., Burgdorf, B., Stowe, M., Solberg, T. and Carabe, A., 2016. Range optimization for mono-and bi-energetic proton modulated arc therapy with pencil beam scanning. Physics in Medicine & Biology, 61(21), p.N565.

[10] Boylan, C. J. , C. G. Rowbottom , and R. I. Mackay . "The use of a realistic VMAT delivery emulator to optimize dynamic machine parameters for improved treatment efficiency. " Physics in Medicine & Biology 99.13(2011):4119-4133.

[11] Cisternas, E. , et al. "matRad - a multi-modality open source 3D treatment planning toolkit." Springer International Publishing (2015).

[12] Wieser, H. , et al. "Development of the open-source dose calculation and optimization toolkit matRad." Medical Physics 44.6(2017).

[13] Low, D A et al. “A technique for the quantitative evaluation of dose distributions.” Medical physics vol. 25,5 (1998): 656-61. doi:10.1118/1.598248

[14] Aitkenhead AH, Bugg D, Rowbottom CG, Smith E, Mackay RI. Modelling the throughput capacity of a single-accelerator multitreatment room proton therapy centre. Br J Radiol. 2012 Dec;85(1020):e1263-72. doi: 10.1259/bjr/27428078. PMID: 23175492; PMCID: PMC3611733.

4.9 Appendix

4.9.1 Appendix A: Examples of the Christie brain and head and neck assessment form

Table A1 and A2 show snippets of the clinical assessment forms used for evaluating the static control point plan and its emulation respectively for an example case, P3. All metrics, which include CTV D98%, D95%, D2% and skin maximum dose satisfied clinical requirements in the static control point plan. However, D95% failed to meet the clinical requirement in the emulation. The patient maximum dose, although without mandatory requirement, is also higher in the emulation than the plan. This shows that the static control point plan is insufficient to meet clinical requirements when considering continuous gantry rotation and such an assessment form must be accompanied with gamma analysis.

Table A1: Evaluation form for the static control point plan of an example case, P3:

Structure	Volume	Dose required	Dose received /cGy
CTV_High	98%	>90% (5346)	5718
	95%	>95% (5643)	5733
	mean	Reported	5815
	2%	<110% (6534)	5941

Structure	Volume	Constraint (Mandatory in bold)	Dose received /cGy

		(P)= Primary (S)= Secondary	
Patient	Max	Reported	6128
Skin	Max	<6600 cGy	4755

Table A2: Evaluation form for the emulation of the static control point plan of P3.

Structure	Volume	Dose required	Dose received /cGy
CTV_High	98%	>90% (5346)	5507
	95%	>95% (5643)	5555
	mean	Reported	5786
	2%	<110% (6534)	6146

Structure	Volume	Constraint (Mandatory in bold) (P)= Primary (S)= Secondary	Dose received /cGy
Patient	Max	Reported	6505
Skin	Max	<6600 cGy	4729

Chapter 5. Final discussion

The aim of this thesis was to explore the advantages of PAT and whether these advantages can still be realised when considering practical deliveries. In the course of radiotherapy development, photon arc therapy, i.e., VMAT, is known to provide faster treatments with improved target conformality compared to IMRT [1]. Whether similar advantages exist for PAT in comparison to IMPT was unknown at the start of this work.

With many more proton spots involved in dose optimisation, PAT plans are shown to possess qualities such as higher target conformality and better OAR sparing compared to IMPT. The robustness of PAT plans also improves on a case-dependent basis as on average each proton spot delivers a lower dose. However, PAT suffers from a larger low dose bath which is an intrinsic property of any arc therapy plan. One of the main advantages of proton therapy is the lower integral dose compared to conventional radiotherapy. This advantage may be adversely affected when moving from IMPT to PAT.

Prior to the start of this work, a number of studies examined the dosimetric potential of PAT plans optimised with full energies from every planned beam angle [2][3]. The reason for studying full-energy PAT (FPAT) was that it represented the version of PAT with the highest degrees of freedom (spots) which means that FPAT brings better plan qualities compared to any constrained PAT, i.e., PAT with reduced energies.

The dosimetric studies on FPAT [2][3] involved a range of sites and showed improved dose distributions (higher target conformality and OAR sparing). However, due to limitations on the energy switching time (greater than 1 second for an energy change), it was soon realised that FPAT would be impractical to deliver due to the total number of energy switches involved. In lieu of improvements in beam switching time, the prospect of delivering PAT in current centres relies on reducing the number of energies in PAT from the treatment

planning perspective. The aim of the thesis (section 1.5) revolved around two aspects:

1. further exploration of dosimetric aspects of PAT including the level of robustness, and

2. investigate ways to plan PAT treatments such that it would be practically deliverable.

At the initiation of this work there was no commercial software capable of planning for PAT and so an in-house developed program was needed to ensure the flexibility to support the development of PAT-specific functions. This challenge was initially solved in Chapter 2 of the thesis by amending an in-house developed Python program used originally for IMPT investigations [4] to adapt to PAT planning needs. For example, the original code used for the work as described in [4] had to reconstruct the 2D dose distribution upon every optimisation iteration, which led to memory problems when translated to PAT. The 2D reconstruction was abandoned in Chapter 2 and was replaced with a 1D dose vector which is a matrix product of a 2D fluence map of the patient and a 1D vector of the spot weights. The amended in-house Python program proved to be a flexible platform and was extended for rapid testing of PAT. The in-house Python program was extended to investigate up to 90 beams at 4-degree angular spacing to analysis the FPAT plan quality. It was found that the higher the number of beams, the better the target conformality, but robustness was not always better as shown for the H&N cases. However, the Python program was limited to planning in 2D, so later in Chapter 3, it was necessary to migrate to the 3D open-source treatment planning tool, matRad, which was amended to incorporate PAT-specific functions, e.g., energy reduction strategies and plan comparison functions.

FPAT is considered impractical to deliver due to the total number of energy layers involved. Before the start of this work, two PAT energy reduction strategies existed, which were SPArc [5] - [12] and PMAT [13][14]. The rationale is that PAT plans with carefully chosen energy layers should still be able to optimise to clinically acceptable PAT plans. SPArc and PMAT both have their advantages and limitations. SPArc works for a range of sites but requires a large computational

overhead. PMAT allows manipulation of the LET distribution, but whether it generalises to different tumour geometries has not been reported. This encouraged investigations for a third energy reduction strategy, ELEANOR-PAT, which was carried out in Chapter 3 of the thesis and showed both the generalisability to a variety of brain tumour geometries and the potential computational efficiency owing to energy layer preselection.

The last part of the work (Chapter 4) was a theoretical investigation of the estimated delivery time of ELEANOR-PAT plans, and of whether the continuously 'delivered' PAT plans were different to the statically optimised PAT plans. By predicting the actual beam angles of each proton spot's delivery based on the time components of typical IMPT deliveries, an emulator was created to predict the resultant dose distributions of continuously delivered PAT plans. This study showed that PAT plans with fewer energy layers planned per beam angle have less differences to the static plans under the assumption of continuous gantry rotation, and so are more likely to pass clinical dose requirements. This finding is due to the longer scale of energy layer switching times compared to the spot delivery and scanning times.

5.1 Proton arc therapy: a study of the inherent robustness to treatment uncertainties

Chapter 2 presents a study that compared FPAT to IMPT in terms of the dose under nominal and error scenarios for three cases: one ependymoma, one unilateral H&N and one bilateral H&N. PAT plans under nominal scenario had been investigated for a lung case [2] and para-aortic lymph node cases [3] before the start of this work and showed improved target conformality and OAR sparing. However, for complex geometries such as the brain and H&N, there was no study which reported the potential applications of PAT. Tumour sites in the brain and H&N are sites that would potentially benefit from PAT because the close-by OARs, e.g., brainstem, optical chiasm and lymph nodes must be protected from high dose of radiation. Therefore, three representative geometries of the brain and H&N sites were chosen as the subject of investigation in Chapter 2.

5.1.1 Dose characteristics of PAT

Results from Chapter 2 (figures 2.2 – 2.4) showed that PAT improved target conformality under nominal scenarios compared to IMPT. This was expected due to the increased number of proton spots involved in dose optimisation. The brainstem in the ependymoma case was spared better at dose levels above 10 Gy, and the parotid was spared better at all dose levels in the unilateral H&N case. The bilateral H&N case showed similar target coverage and OAR sparing for IMPT and PAT plans, perhaps because that the PAT plans were planned with full energies from all beam angles.

Interestingly the robustness was not always improved in the PAT plans. The CI and HI computed under range and setup errors separately were improved in the ependymoma case, but either showed larger spreads or worse nominal values for the H&N cases. This is perhaps due to the shallower targets in the H&N cases, but this would require more similar geometries to verify. However, the results suggest that the robustness of PAT plans is not guaranteed to improve and must be assessed on a case-by-case basis.

5.1.2 Low dose baths in PAT

Low dose baths below about 10 Gy are present in all three cases studied in Chapter 2, but these are unavoidable because the target is irradiated from a wider range of beam angles. The reduction of low dose volumes in proton therapy compared to IMRT is predicted to have long term benefits in terms of preserving cognitive functions in paediatric patients [15], so PAT might be a more suitable option for adult patients. However, indications for proton therapy for adult patients are less acknowledged compared to paediatric patients [16], so PAT might add to the treatment options for adult patients while IMPT stays as the recommendation for paediatric patients when PAT is clinically approved.

5.1.3 The value of 2D analysis of PAT

The 2D analysis helped to demonstrate that FPAT improves the plan quality by having more control points so on average the beamlet weight is lower, but the improvement in robustness was geometry dependent. The 2D nature has the advantage of simplicity – it does not need to consider the impact of the third dimension (heterogeneities and setup uncertainties) or non-coplanar beam angles, which are not vital factors for understanding the general trends of PAT characteristics. However, the limitation of using only coplanar beam angles is not ideal for the IMPT plans since it is common for IMPT plans to use non-coplanar beam angles. Therefore, the use of 2D analysis means that the IMPT plans might not be representative of the plan quality that is achievable clinically. Nevertheless, the use of the 2D analysis is enough to investigate the general principles of PAT and IMPT behaviours. To understand how PAT behaves in reality, the study must be carried out in 3D, which was the dimensionality Chapter 3 and 4 were in.

5.1.4 The value of FPAT

FPAT was an important step to gain a fundamental understanding of PAT as FPAT represents the full degrees of freedom in dose optimisation compared to any energy reduced PAT. In general, more control points mean better plan quality, so FPAT represents the highest possible plan quality and reduced PAT would only degrade it. This both supports the importance of FPAT and leads to the investigation of finding the balance of plan degradation and efficient delivery time in Chapter 3 and 4.

5.2 ELEANOR-PAT, an energy reduction strategy for proton arc therapy based on energy layer coverage abilities

Chapter 3 introduced ELEANOR-PAT as a novel energy selection strategy for PAT with the aim of reducing the beam-on time while conserving the plan quality (target dose conformality, OAR sparing and plan robustness). The ELEANOR-PAT algorithm assesses the target coverage abilities of candidate energy layers prior to dose optimisation, as a result of which the most efficient energy layers in terms of target dose coverage are selected. ELEANOR-PAT was shown to be effective for

eight different ependymoma geometries and successfully reduced the estimated beam-on times by 25% - 84%. This means that ELEANOR-PAT is independent of geometry to a certain extent (brain geometries) and can effectively push towards deliverable PAT plans that meet or exceed clinical requirements. The nature of the energy layer preselection meant faster dose optimisation than full-energy PAT (FPAT), which is an important advantage for effective clinical implementation. This section will discuss ELEANOR-PAT around four aspects: 5.2.1 Comparison to other energy selection/reduction strategies; 5.2.2 Potential treatment sites; 5.2.3 Assumptions set in Chapter 3; and 5.2.4 Room for further development.

5.2.1 Comparison to SPArc and PMAT

From the dosimetric aspects, SPArc and ELEANOR-PAT can both offer clinically acceptable plans for a range of geometries [5] - [12]. Although ELEANOR-PAT has been tested for a range of sizes, locations and geometries of tumours in the ependymoma cases examined, other sites such as the H&N and lung should be investigated as validation cases for ELEANOR-PAT in future studies. H&N sites are interesting due to their distinctive targets on either one side or both sides, and lung sites due to the challenge of producing robust ELEANOR-PAT plans. On the other hand, PMAT has limitations on the target geometry as it only places one energy layer at the centre of the target. This means that a minimum 180-degree arc is required for relatively symmetric targets and a larger arc must be used for general geometries.

From the algorithmic perspective, PMAT takes the shortest time to optimise and SPArc the longest (2 and 6 hours respectively for a lung and oropharyngeal carcinoma case in [5], which are about 8 and 10 times longer than IMPT optimisation time). The total optimisation time for PMAT and ELEANOR-PAT are longer than IMPT optimisation because PMAT and ELEANOR-PAT must select energy layers prior to dose optimisation. The time spent on energy selection by PMAT is considerably shorter than ELEANOR-PAT as the single energy that PMAT selects for each beam angle is directly known at the start from the water equivalent thickness of the target. ELEANOR-PAT takes longer on energy selection as it must loop through all target voxels. For the eight ependymoma

cases with energies selected using the ELEANOR-PAT approach, the time spent on energy selection ranges from 27 seconds to 9 minutes. The total optimisation time for ELEANOR-PAT ranges from 177 seconds to 19 minutes. Compared to the IMPT optimisation time of 55 seconds to 5 minutes, ELEANOR-PAT is about 3 to 4 times longer. PMAT and ELEANOR-PAT both take the pre-selection approach. This reduces the optimisation time very much. SPArc is the longest as it completely relies on the computational power to select, redistribute and remove energy layers based on the objective function values of the energy layers selected. Therefore, in terms of the optimisation time, PMAT and ELEANOR-PAT are more effective.

5.2.2 Potential treatment sites

ELEANOR-PAT was validated with eight different ependymoma geometries in Chapter 3 of this thesis. Ependymoma cases were chosen because they usually involve complex geometries (critical OAR near the target) and were relatively free from setup uncertainties, so the ELEANOR-PAT strategy is an important approach which was shown to improve the plan quality consistently, meaning better OAR sparing, skin sparing and target conformality. Moreover, these cases would be treated in shorter timeframes.

5.2.3 Assumptions

The main assumption set in the work described in Chapter 3 is the constant gantry rotation speed. The reason for this assumption was to avoid gantry acceleration or deceleration during the delivery of the arc as it can be difficult to achieve the planned angular precision considering the large mass of a proton gantry. However, as IMPT does not require gantry motion while the beam is active, routine QC of the delivery system does not test the accuracy of the reported gantry angles during acceleration of the gantry. For PAT delivery, an accuracy test for gantry rotation should be added to the QC program. Therefore, an accuracy test for rotating gantry is recommended. If it meets the desired accuracy, then the restriction on constant gantry rotation can be lifted.

5.2.4 Room for development

Energy layer preselection provides flexibility in terms of the assessment criteria for the selections. ELEANOR-PAT always ensures target coverage in the nominal scenario because each target voxel has at least one energy layer covering it. An additional assessment criterion added was the option of avoiding OARs, which proved effective in terms of OAR sparing for overlapping geometries. This flexibility means the additional criteria can be anything as long as it is understood how it translates to the plan quality. For example, linear energy transfer can be one of the criteria. Instead of assessing the OAR coverage, an LET-influence matrix can be calculated to avoid high LET regions in the OARs. Since the LET distribution requires recalculation of the optimised plan, direct optimisation of the LET requires linear fractional programming techniques [17]. Another method is to use LET surrogates, e.g., track end objectives as surrogates to push down the LET at the end of proton beam tracks [18]. The incorporation of LET or LET surrogate objectives generates comparable dose distributions to dose only objectives [17] but trade-offs between dose and LET are expected in IMPT plans [17]. With more proton spots in PAT, LET incorporated PAT optimisation is expected to push the LET within the target more than that in IMPT [19].

The beam angles and the arc range are selected manually by the planner, but this could be optimised to avoid beam angles passing through regions of high-density variations. This could be incorporated into ELEANOR-PAT to support beam off during an arc.

5.3 Assessment of proton arc therapy plans under continuous delivery emulation

In this thesis, PAT plans are currently planned with fixed angle beams which are closely spaced (< 10 degrees). However, PAT plans will be delivered with a continuously rotating gantry. Due to protons' sensitivity to different tissue density values along their delivered paths, the delivered PAT plan would be different to the fixed angle PAT plans. The aim of the study in Chapter 4 was to quantify these dose differences and to assess whether the delivered dose still met clinical dose

requirements. Due to the limited experimental equipment and time, experimental dose delivery is outside the scope, so the quantification of the dose distributions remained theoretical. The ‘delivered’ dose distribution was therefore estimated with an emulator which calculated the delivery time stamp of individual proton spot under the assumption of continuous gantry rotation. The study in Chapter 4 showed that the angular spacing and the number of energy layers planned per beam angle both affected the gamma pass rates between the plan and ‘delivery’, and that one energy layer planned per beam angle guaranteed all eight cases to pass clinical requirements under continuous gantry rotation. These findings are important because they show the considerations that must be taken when making a PAT plan in order for the plan to match its delivered dose distribution at a clinically acceptable level.

5.3.1 Limitations and future work

In reality, the PAT plans would be delivered with a rotating gantry, so a limitation of the work in Chapter 4 was that the emulated PAT plans were calculated based on the dose profiles of individual proton spots under fixed angle assumption. Under continuous gantry rotation, the profile of each proton spot may have a different shape to that under fixed beam irradiation as the time to deliver a proton spot is finite. Therefore, a natural future step would be to validate the spot profiles with experimental deliveries where the gantry would be continuously rotating. Although the beam characteristics have been measured for an IBA Proteus® One proton machine and shown to be very similar to those under fixed angle irradiation [10] (98% gamma pass rate for [3%, 3mm] criteria), there exists no publication which studies this for a Varian manufactured proton gantry, which is the equipment installed at the Christie proton therapy centre. Since the research room at the Christie proton therapy centre has a horizontal fixed angle beam line, it is not possible to rotate a gantry, but rather to rotate the phantom to simulate the relative rotation between the phantom and the gantry. There exists no phantom specifically designed for measuring PAT dose as PAT is such a new technique still under research and development, so a substitute needs to be carefully chosen as it must be able to measure the dose accurately at desired locations from 360 degrees. A potential choice is the ArcCHECK® phantom from Sun Nuclear corporation, which is a cylindrical phantom recommended for VMAT. Whether the ArcCHECK®

phantom can be used for PAT QA is currently under investigation at the Christie proton therapy centre.

Since the deformation of a spot profile is related to the time spent on delivering each spot, which is related to the gantry rotation speed, the faster the gantry rotates, the more difference in the spot profile there would be. If the resultant dose distribution is different to the planned dose distribution at a clinically unacceptable level, e.g., < 95% gamma pass rate with [3%, 3mm] criteria, it would be unacceptable to plan with the fixed spot profiles but deliver with a continuously rotating gantry. Therefore, if this is the case, it will be important to define these ‘deformed’ spot profiles prior to PAT treatment planning as a separate library of beam model specifically for PAT.

5.4 References

[1] Teoh, May, et al. "Volumetric modulated arc therapy: a review of current literature and clinical use in practice." The British journal of radiology 84.1007 (2011): 967-996.

[2] Seco, Joao, et al. "Proton arc reduces range uncertainty effects and improves conformality compared with photon volumetric modulated arc therapy in stereotactic body radiation therapy for non-small cell lung cancer." International Journal of Radiation Oncology* Biology* Physics 87.1 (2013): 188-194.

[3] Rah, Jeong-Eun, et al. "A treatment planning study of proton arc therapy for para-aortic lymph node tumors: dosimetric evaluation of conventional proton therapy, proton arc therapy, and intensity modulated radiotherapy." Radiation Oncology 11.1 (2016): 1-10.

[4] Lowe, Matthew, et al. "A robust optimisation approach accounting for the effect of fractionation on setup uncertainties." Physics in Medicine & Biology 62.20 (2017): 8178.

[5] Ding, Xuanfeng, et al. "Spot-scanning proton arc (SPArc) therapy: the first robust and delivery-efficient spot-scanning proton arc therapy." International Journal of Radiation Oncology* Biology* Physics 96.5 (2016): 1107-1116.

[6] Ding, Xuanfeng, et al. "Improving dosimetric outcome for hippocampus and cochlea sparing whole brain radiotherapy using spot-scanning proton arc therapy." Acta Oncologica 58.4 (2019): 483-490.

[7] Ding, Xuanfeng, et al. "Have we reached proton beam therapy dosimetric limitations?–A novel robust, delivery-efficient and continuous spot-scanning proton arc (SPArc) therapy is to improve the dosimetric outcome in treating prostate cancer." Acta Oncologica 57.3 (2018): 435-437.

[8] Chang, Sheng, et al. "Feasibility study: spot-scanning proton arc therapy (SPArc) for left-sided whole breast radiotherapy." Radiation Oncology 15.1 (2020): 1-11.

[9] Liu, Gang, et al. "Improve the dosimetric outcome in bilateral head and neck cancer (HNC) treatment using spot-scanning proton arc (SPArc) therapy: a feasibility study." Radiation Oncology 15.1 (2020): 1-11.

[10] Li, Xiaoqiang, et al. "The first prototype of spot-scanning proton arc treatment delivery." Radiotherapy and Oncology 137 (2019): 130-136.

[11] Liu, Gang, et al. "Lung stereotactic body radiotherapy (SBRT) using Spot-scanning Proton Arc (SPArc) therapy: A feasibility study." Frontiers in Oncology 11 (2021): 1245.

[12] Liu, Gang, et al. "Is proton beam therapy ready for single fraction spine SBRS?–a feasibility study to use spot-scanning proton arc (SPArc) therapy to improve the robustness and dosimetric plan quality." Acta Oncologica 60.5 (2021): 653-657.

[13] Sanchez-Parcerisa, Daniel, et al. "Range optimization for mono-and bi-energetic proton modulated arc therapy with pencil beam scanning." Physics in Medicine & Biology 61.21 (2016): N565.

[14] Toussaint, Laura, et al. "Towards proton arc therapy: physical and biologically equivalent doses with increasing number of beams in pediatric brain irradiation." Acta oncologica 58.10 (2019): 1451-1456.

[15] T. E. Merchant, C.-h. Hua, H. Shukla, X. Ying, S. Nill, U. Oelfke, Proton versus photon radiotherapy for common pediatric brain tumors: comparison of models of dose characteristics and their relationship to cognitive function, Pediatric blood & cancer 51 (1) (2008) 110–117.

[16] Tambas, Makbule, et al. "Current practice in proton therapy delivery in adult cancer patients across Europe." Radiotherapy and Oncology 167 (2022): 7-13.

[17] Cao, Wenhua, et al. "Linear energy transfer incorporated intensity modulated proton therapy optimization." Physics in Medicine & Biology 63.1 (2017): 015013.

[18] Ödén, J., and E. Traneus. "Introducing proton track-end objectives as a tool to mitigate the elevated relative biological effectiveness in critical structures." International Journal of Radiation Oncology, Biology, Physics 99.2 (2017): E705.

[19] Li, Xiaoqiang, et al. "Linear Energy Transfer Incorporated Spot-Scanning Proton Arc Therapy Optimization: A Feasibility Study." Frontiers in Oncology (2021): 2636.

Chapter 6. Conclusions

PAT has the potential to become the next technological evolution for proton therapy development, but whether PAT is a suitable treatment for brain and H&N cases and how PAT plans should be optimised or delivered were not completely understood at the start of this work. Chapter 2 of the thesis shows that PAT improves target coverage and OAR sparing for the brain and H&N cases studied. Since proton therapy is sensitive to treatment uncertainties, the robustness must also be evaluated for PAT plans. Chapter 2 of the thesis shows that the robustness of PAT was not always better and so must be evaluated on a case-by-case basis. However, PAT plans optimised with full energies (Chapter 2) require more time to deliver than those with reduced energy layers, so Chapter 3 then explores whether the plan quality and robustness can still be realised with reduced PAT. Chapter 3 of the thesis presents a new energy reduction strategy, ELEANOR-PAT, and demonstrates that this energy reduction strategy is generalisable to eight different ependymoma cases and that the plan quality, including robustness, is not degraded even when the total number of energy layers is reduced. Chapter 4 of the thesis then concerns the deliverability of PAT optimised with the ELEANOR-PAT strategy and concludes that the ELEANOR-PAT plans must be interpolated to one energy layer per finer beam angle for the delivered dose distribution to match the plan. The theoretically estimated times for delivery are shorter than 3 minutes for the eight ependymoma cases. Considering these PAT plans are intended to be delivered in one continuous arc, it eliminates the time spent on beam switching (at multi-room proton therapy centres) and intrafraction re-setup, so a single PAT treatment session is expected to be considerably shorter than a typical IMPT treatment session which usually lasts about 15-20 minutes.

At the time of writing this thesis, PAT is not in routine clinical use. This thesis has contributed towards deeper understandings about PAT's dosimetric characteristics and practical delivery, which are important steps towards the realisation of clinical PAT delivery. PAT is able to improve target conformality, OAR sparing, robustness as well as to shorten the treatment time. The next steps will be to experimentally

deliver the PAT plans to a phantom to practically assess the deliverability and then moving onto human trials to fully realise its clinical potential.